NTNU – Trondheim
Norwegian University of
Science and Technology

Mechanical behavior of laminated glass exposed to blast loading

Arne Ilseng

Mechanical Engineering
Submission date: June 2013
Supervisor: Arild Holm Clausen, KT
Co-supervisor: Tore Børvik, KT

Norwegian University of Science and Technology
Department of Structural Engineering

Institutt for konstruksjonsteknikk
Fakultet for ingeniørvitenskap og teknologi
NTNU- Norges teknisk- naturvitenskapelige universitet

TILGJENGELIGHET

Åpen

MASTEROPPGAVE 2013

FAGOMRÅDE:	DATO:	ANTALL SIDER:95
Beregningsmekanikk	10. juni, 2013	14+70+11

TITTEL:

Mekanisk oppførsel av laminert glass utsatt for eksplosjonslast

UTFØRT AV:

Arne Ilseng

SAMMENDRAG:
Laminert glass utnytter et mellomsjikt til å redusere risikoen for flyvende glassplinter ved eksplosjonslast. I denne masteroppgaven er eksperimentelle og numeriske studia gjennomført for å undersøke de mekaniske egenskapene til laminert glass.

Den eksperimentelle delen består av fem forskjellig tester. Bøye- og strekktester ble gjennomført for å undersøke egenskapene til glass, mellomsjikt og laminert komponent under kvasistatisk last. Gas kanon og eksplosjonsforsøk ble benyttet for å undersøke oppførselen til glass under dynamisk trykkbelastning.

I de numeriske studia ble elementmetodemodeller laget for å etterregne de eksperimentelle forsøkene. Stokastisk skadefordeling og nodesplitting ble definert i glass materialet. I modellen av eksplosjonsforsøket ble nodesplitting også innført i deler av mellomsjiktet for å muliggjøre plastiske deformasjoner.

Delaminering mellom glass og PVB ble funnet for de kvastistatiske eksperimentene, men kunne ikke påvises for de dynamiske testene. For 3-punkts bøyetest av laminert glass ble det funnet god overensstemmelse mellom simuleringsresultater og eksperimentelle observasjoner. For modellen av eksplosjonsforsøkene ser plastisk deformasjon av mellomsjiktet ut til å være vesentlig for å oppnå realistisk respons i platen.

Nøkkelord: Laminert glass, Eksplosjonslast, Nodesplitting, Stokastisk skadefordeling.

FAGLÆRER: Professor Arild Holm Clausen

VEILEDER(E): Professor Arild Holm Clausen, Professor Tore Børvik

UTFØRT VED: SIMLab, Konstuksjonsteknikk, NTNU

Institutt for konstruksjonsteknikk

FAKULTET FOR INGENIØRVITENSKAP OG TEKNOLOGI
NTNU – Norges teknisk-naturvitenskapelige universitet

MASTER THESIS 2013

Arne Ilseng

Mechanical behavior of laminated glass exposed to blast loading

(Mekanisk oppførsel av laminert glass utsatt for eksplosjonslast)

There is an increasing concern in the society for possible injuries on people caused by explosions and glass fragments. Different types of pressure-safe glasses have therefore been developed. A common solution is to apply laminated glasses consisting of two glass plates with an intermediate layer of polyvinylbutural (PVB).

The aim of this thesis is to study the response of such a laminated glass when it is subjected to an explosion loading. The candidate should approach this aim through a literature survey, material and component tests, and nonlinear numerical simulations.

Some keywords for activities related to this master thesis project may include:

- Literature: Properties of glass and PVB, fracture of glass, explosions.
- Material tests: Glass, PVB and laminated glass. In-house tests or literature results.
- Component tests: Gas gun and free-field explosion tests on laminated glass
- Calibration: Identification of the coefficients of material models.
- Numerical modeling: Simulation of tests with IMPETUS. Evaluation of the model.

The candidate may agree with the supervisors to pay particular attention to specific parts of the investigation, or include other aspects than those already mentioned.

The thesis is to be organized as a research report, recognizing the guidelines provided by Department of Structural Engineering.

Supervisors: Arild Holm Clausen and Tore Børvik

The report is to be handed in at Department of Structural Engineering not later than 10 June 2013.

NTNU, 14 January 2013

Arild Holm Clausen
Main supervisor

Abstract

For laminated glass, the adherent properties of an interlayer reduce the risk of airborne glass splinters in case of blast loading. In this thesis, experimental and numerical studies were performed to investigate the mechanical properties of laminated glass exposed to blast loading.

The experimental part consisted of five different experiments. Bend and tensions experiments were performed to investigate mechanical properties of glass, interlayer, and laminated components under quasi-static loading. While a compressed gas gun and free field explosions were used to study the behavior of pure and laminated glass under dynamic pressure loading.

For the numerical study, finite element models were built to predict the response of the experimental tests. Stochastic initial damage distribution and node splitting was defined for the glass material. In the blast model, node splitting was also introduced in the interlayer to enable plastic deformation.

Delamination between glass and interlayer was seen in quasi-static experiments, but could not be detected in dynamically loaded panes. For the case of 3-point bend loading of laminated glass, good correlation was found between numerical predictions and experimental observations. Enabling plastic deformation of the interlayer seems to be vital to predict a reasonable response of laminated glass under blast loading.

Keywords: Laminated glass, Blast loading, Node splitting, Stochastic initial damage.

Preface

The work presented in this M.Sc. thesis has been carried out at SIMLab (Structural Impact Laboratory) - Center for Research-based Innovation, which is hosted by Department of Structural Engineering at Norwegian University of Science and Technology (NTNU). The thesis was written in the period between 14^{th} of January and 10^{th} of June 2013. Professor Arild Holm Clausen and Professor Tore Børvik have supervised the work.

The following people are acknowledged for their contribution:

- Professor Arild Holm Clausen and Professor Tore Børvik for guidance and support throughout the project.
- Dr. Lars Olovsson (IMPETUS Afea AS) for guidance on the use of IMPETUS Afea Solver, and implementation of a new damage criterion.
- Dr. Egil Fagerholt (NTNU) for support with Digital Image Correlation.
- Dr. Ida Westermann (SINTEF) for fractography and dye penetrant inspection of tested specimens.
- Knut Ove Hauge (Norwegian Defense Estate Agency (NDEA)), Vidar Hjelmen (SINTEF) and Trond Auestad (NTNU) for support with experimental testing.
- Fellow students for providing an inspiring working environment.

Arne Ilseng
Trondheim, June 10^{th} 2013

Contents

List of Figures

List of Tables

Notation

The following list gives general notation used throughout the report. Be aware that some symbols are given multiple definitions, this is done to follow notation established in literature.

Abbreviations

DIC	Digital Image Correlation
DOF	Degree(s) of Freedom
DPI	Dye Penetrant Inspection
FE	Finite Element
FEA	Finite Element Analysis
FEM	Finite Element Method
FPS	Frames Per Second
LEFM	Linear Elastic Fracture Mechanics
NDEA	Norwegian Defence Estates Agency
PVB	Polyvinylbutyral

Mathematical symbols

[ ]	Rectangular matrix
{ }	Column vector
$\dot{a}$	Time differentiation of variable a
a_n	Values of variable a at time step n
$\hat{a}$	Statistical estimate of a
Δa	Change in a

Latin symbols

A	Cross sectional area
a	Half of crack length in fracture mechanics, DOF amplitude in DIC theory
b	Specimen width
c	Wave speed
[**C**]	Damping matrix
d	Specimen thickness
E	Young's modulus, also used for energy balance in FEM
{**D**}	Displacement vector
D	Damage in IMPETUS
G	Energy release rate
I	Image in DIC analysis, second moment of area in beam theory, impulse in explosion theory
K_I	Stress intensity factor, mode I
k	Loading factor in weakest link theory

L^e	Length of element in FEM mesh
l	Length of specimen
[**M**]	Mass matrix in FEM
m	Weibull modulus
N	Shape function in FEM
p_r	Reflected pressure
p_s	Side-on pressure
P	Point loading in beam theory
q	Load function in beam theory
$\{R^{ext}\}$	Vector of internal forces
$\{R^{int}\}$	Vector of internal forces
r	Distance to charge, explosion theory
T	Temperature
t	Time
W	Work in fracture mechanics, charge mass in kg TNT in explosion theory
w	Deformation function in beam theory
Z	Scaled distance for explosion theory

Greek symbols

β	Weibull scale parameter
ϵ	Strain
Γ	Adhesion glass-PVB
γ	Adiabatic index
γ_s	Surface energy
ν	Poisson's ratio
ω	Natural frequency
Π	Potential energy released by strain
ρ	Density
Σ_0	Area independent scale parameter for Weibull analysis
σ	Stress

1 Introduction

According to Smith [33], 80% of casualties related to historic city bombings were due to flying glass splinters. As a consequence, there is great interest in architectural glazing solutions where the risk of airborne glass splinters is reduced. One such solution is laminated glass. Laminated glass was first introduced in windshields of cars to avoid flying glass splinters in case of a collision. It normally consists of two layers of glass, with an interlayer of polyvinylbutyral (PVB). This thesis focus on the mechanical behavior of laminated glass exposed to blast loading.

In 1998 Norville et al. [26] presented a theoretical model for uncracked laminated glass based on beam theory. Wei et al. [40] presented in 2006 a 3D finite element (FE) model predicting the response of laminated glass up to glass fracture. In 2012 both Larcher et al. [20] and Hopper et al. [14] presented experimental results and FE models for laminated glass under blast loading. At SIMLab, the master thesis of Sandven [31] in 2009 investigated the behavior of glass windows exposed to blast loading, but no work was performed with laminated glass before this thesis.

In this thesis, bend and tension experiments were conducted on glass, PVB, and laminated components to investigate their mechanical behavior under quasi-static loading. To study the behavior of pure and laminated glass under dynamic pressure loading, the compressed gas gun facility at SIMLab and free field explosions were used. The results from the experiments were used as validation of explicit FE computations. Full 3D models were built, stochastic initial damage was introduced in the glass, and node splitting was used for the crack development.

The layout of the report is as follows:

- Section 2 - Theory. A brief discussion of the theory applied throughout this report, emphasis on fracture mechanics in brittle materials, theory of blast loading, and finite element method calculations.
- Section 3 - Previous work. Presentation of previous work on laminated glass, emphasis on material models used for glass and PVB.
- Section 4 - Experimental setup. Setup and test procedure for the experiments performed in the project.
- Section 5 - Experimental results. Results from the experiments are presented and discussed.
- Section 6 - FEM modeling. Setup of FE models are described.
- Section 7 - FEM results. Results from FE simulations are presented and discussed.
- Section 8 - Concluding remarks. Central results found in the thesis is summarized.
- Section 9 - Further work. A list of further work proposed by the author.

Software used in this thesis is IMPETUS Afea Solver (IMPETUS) by IMPETUS Afea AS, the numerical computing environment MATLAB by MathWorks, and an in-house digital image correlation (DIC) software developed by Egil Fagerholt. All FE simulations were performed in IMPETUS, while MATLAB was used for all processing of experimental data.

2 Theory

In this section, some of the theory relevant for this thesis is briefly presented. A more comprehensive discussion of each topic can be found in the references. The topics that will be discussed is the general behavior of laminated glass, fracture mechanics of brittle materials, the theory of blast loading, formulation of the finite element method, concepts of DIC, and theory on bend testing.

2.1 Laminated glass

A typical layout of laminated glass can be seen in Figure 1. Laminated glass consists of two layers of glass and one interlayer normally made out of polyvinylbutyral (PVB).

Glass. Normal architectural glazing is made out of soda-lime glass. Soda-lime glass is an amorphous ceramic with brittle material behavior. Its main constituents is 70-72% SiO_2, 12-13%Na_2O , 9-10%CaO and 5-7%MgO.

PVB. PVB is a polymer with the molecular formula $(C_8H_{14}O_2)_n$. The main application of PVB is as an interlayer material for laminated glass. It is normally produced in 0.76 mm thick foils, and for standard laminated glass two layers of PVB are used to create a 1.52 mm thick interlayer. The lamination of glass and PVB is done through appliance of heat and pressure. For the samples used in the experimental part of this thesis, the total process lasted for nine hours and the temperature reached 124 °C. Through the lamination process the PVB layers changes from opaque to transparent. This indicates that the mechanical properties might also change through the lamination process.

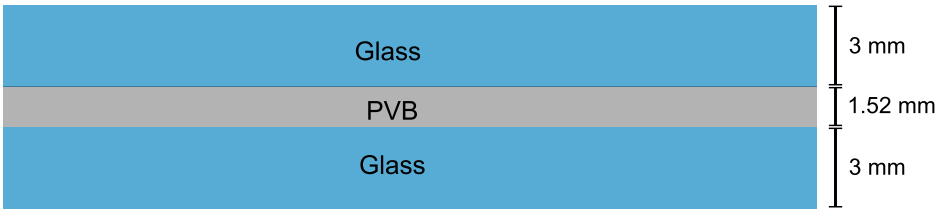

Figure 1: *Typical layout of laminated glass.*

For architectural purpose laminated glass has a clear advantage compared with single glass panes in two ways:

1. The adherent properties of PVB reduce risk of flying glass splinters in case of glass breakage. This increase safety for building occupants.
2. The ductility of PVB leads to retained strength after glass breakage. This reduces the risk of overhead glazing etc.

This thesis will focus on the mechanical behavior of laminated glass exposed to blast pressure.

The quasi-static behavior of laminated glass exposed to a uniform pressure load is schematically shown in Figure 2. The failure of a laminated pane consists of four phases:

1. D_0-D_1: Laminated pane is intact and deformed elastically. Glass ply on unloaded side (maximum tension) fails at D_1.
2. D_1-D_2: Glass ply at loading side still intact and dominates global behavior, it fails at D_2.
3. D_2-D_3: Both glass ply has failed, interlayer is still intact and deform elastically.
4. D_3-D_4: Interlayer deforms plastically, and fails at D_4.

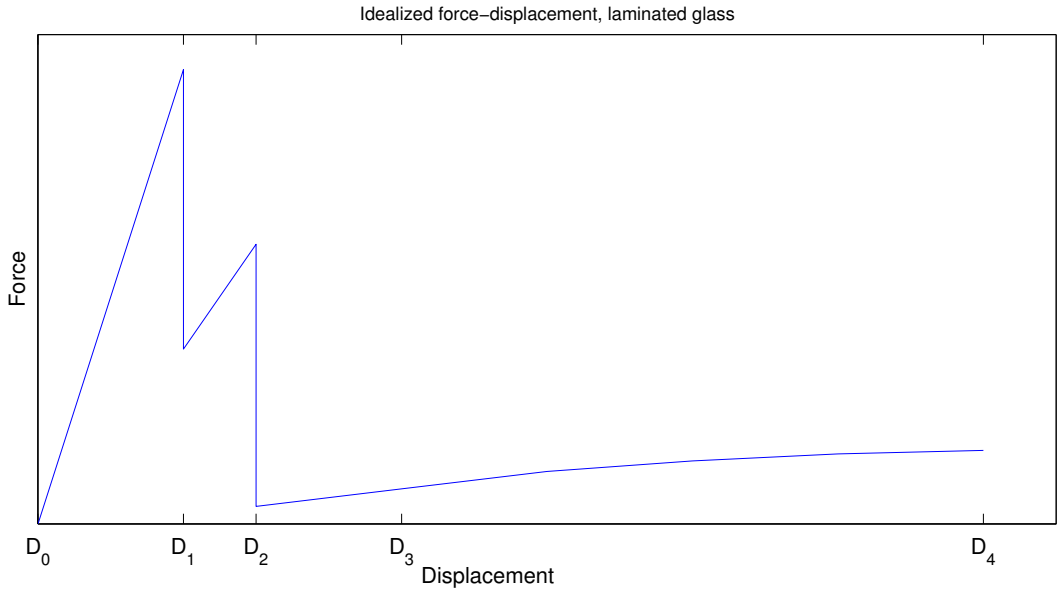

Figure 2: *Idealized force-displacement curve for quasi-static behavior of laminated glass. Figure adapted from [20].*

2.2 Fracture mechanics

Fracture of a material occurs if the tension stress at atomic level exceeds the attractive forces holding the atoms together. At equilibrium distance between atoms x_0 the attractive and repelling forces are balanced. The cohesive strength σ_c can be calculated based on Young's modulus E, the surface energy of the material γ_s, and x_0:

$$\sigma_c = \left(\frac{E\gamma_s}{x_0} \right)^{\frac{1}{2}}. \tag{1}$$

Equation 1 gives the theoretical strength, but experiments show that for brittle materials the fracture stress is normally three to four times lower [1]. To understand this fact, a closer look into the theory of fracture mechanics is needed. Since glass do not experience plasticity prior to breakage, the discussion will be limited to linear elastic fracture mechanics (LEFM). Also statistics for failure in brittle materials will be discussed and a derivation of the weakest link theory will be outlined. The theory in this subsection is adapted from [1] and [38].

LEFM

In the 1920's Griffith [12] did research on glass to explain the difference in the theoretical strength

of inter atomic bonds and the experienced strength. Assuming no or little plastic behavior prior to breakage, Griffith applied the first law of thermodynamics. This law states that the energy in a system will decrease as the system goes from a nonequilibrium to an equilibrium condition. A consequence of this law is that a crack will grow only if the elastic energy released upon crack growth is greater than or equal to the energy required to create the new crack surfaces. Mathematically this means that for a crack to grow:

$$\frac{d\Pi}{dA} + \frac{dW_s}{dA} \geq 0, \tag{2}$$

where Π is the potential energy released by strain energy and external forces, and W_s is the work required to create the new crack surfaces. For an infinitely sharp through thickness crack, in an infinitely wide plate configuration, as shown in Figure 3, the following equation applies for the potential energy release:

$$\Pi = \Pi_0 - \frac{\pi\sigma^2 a^2 d}{E}, \tag{3}$$

where Π_0 is the potential energy of a crack free plate. The work required to create new surfaces is given by:

$$W_s = 4ad\gamma_s. \tag{4}$$

By inserting Equations 3 and 4 into Equation 2 the following can be obtained for the fracture stress:

$$\sigma_f = \left(\frac{2E\gamma_s}{\pi a}\right)^{\frac{1}{2}}. \tag{5}$$

With Equation 5 Griffith obtained good agreement for the fracture strength of glass. It can be seen that the fracture stress is a function of the crack size, and since glass is a material containing natural intrinsic flaws, this explains the difference in theoretical and experimental fracture strength.

Since the stress needed for crack growth decrease as the size of the crack increase, growth due to a constant stress level will continue until the whole section is broken. It should be noted that in a glass pane the local critical stress in a flaw can be reached at a point not coinciding with the point of maximum global stress.

In 1956 Irwin proposed an energy release rate G defined as:

$$G = -\frac{d\Pi}{dA}. \tag{6}$$

The energy release rate is based on the work of Griffith, and G can be interpreted as the energy available for an increment of crack extension. By combining Equations 2, 3 and 6 a critical value G_c, being the fracture toughness of the material, can be found:

$$G_c = \frac{\pi\sigma_c^2 a}{E} = \frac{dW_s}{dA} = 2\gamma_s. \tag{7}$$

This approach of defining a critical value for crack growth is convenient for solving typical engineering fracture problems.

While G is a global fracture parameter, the stress intensity factor K defines a local fracture parameter. The stress intensity approach defines three different modes of crack loading, as shown in Figure 4.

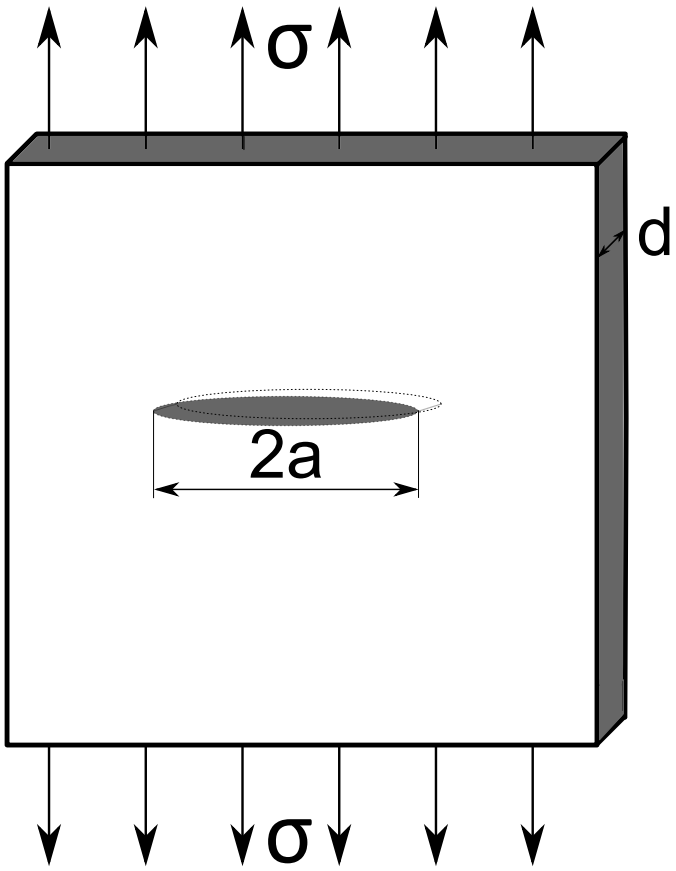

Figure 3: *Schematic of through thickness crack in infinitely long plate. Figure adapted from [1].*

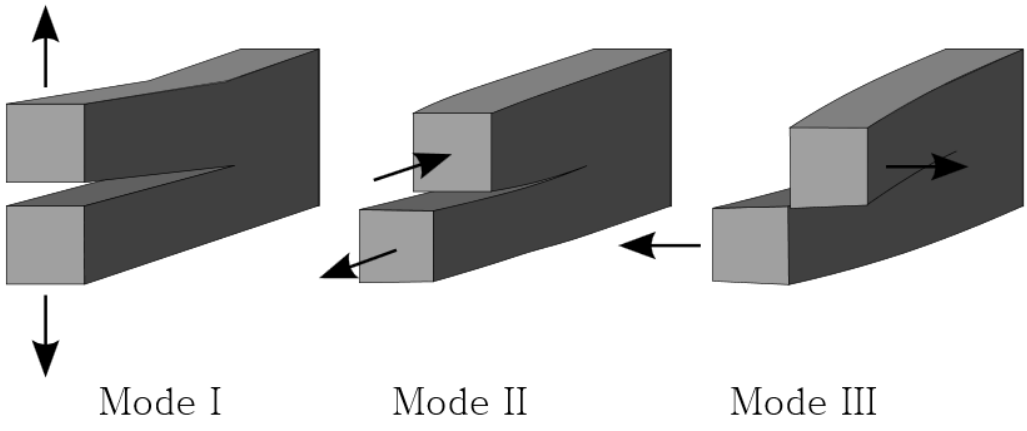

Figure 4: *Schematic of the three fracture modes. Figure taken from [16].*

The stress intensity for the different modes are labeled K_I, K_{II}, and K_{III} referring to mode 1,2 and 3. Mode 1 is normally assumed being the critical fracture mode. For the plate configuration shown in Figure 3, the expression for K_I was found by Westergaard as:

$$K_I = \sigma\sqrt{\pi a}. \tag{8}$$

As for the fracture toughness approach, crack growth will occur when K_I reach the critical stress intensity factor K_{Ic}. By comparing Equations 7 and 22, the following relation between the stress intensity factor K_I and energy release rate G can be found:

$$G = \frac{K_I^2}{E} \tag{9}$$

Statistics of brittle fracture

Since the fracture of glass is dependent on the size and location of the natural surface flaws the maximum obtained strength will vary in a series of intentionally similar tests. To gain useful information from fracture strength testing on glass, statistical methods must be applied. The Weibull distribution[1] is commonly used for statistics on glass. The probability density function of a Weibull distribution with random variable x is given by [9]:

$$f(x) = \begin{cases} \frac{m}{\beta}\left(\frac{x}{\beta}\right)^{m-1} exp\left[-\left(\frac{x}{\beta}\right)^{m}\right], & x > 0, \\ 0, & \text{elsewhere}, \end{cases} \tag{10}$$

where m and β is the Weibull modulus and a scale parameter respectively, both holding a value larger than zero. The cumulative distribution is given by:

$$F(x) = 1 - exp\left[-\left(\frac{x}{\beta}\right)^{m}\right], \quad for\ x \geq 0 \tag{11}$$

Figure 5 show probability density function and cumulative distribution of the Weibull distribution, for β being equal to one and varying values of m.

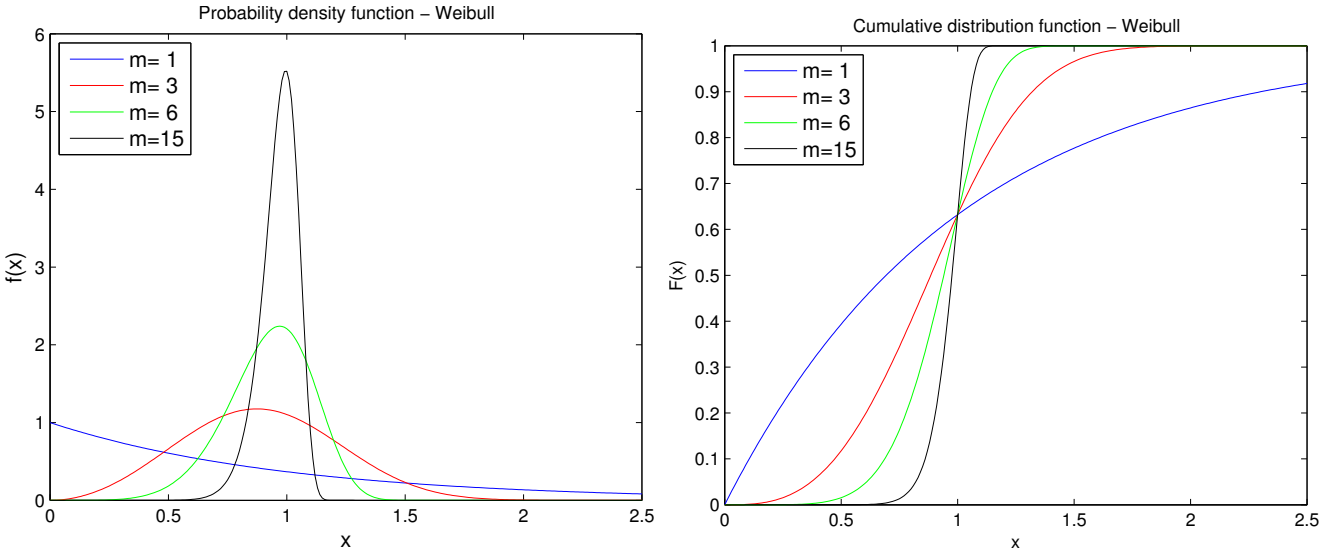

(a) *Probability density functions* (b) *Cumulative distribution*

Figure 5: *Weibull distribution for* $\beta = 1$.

[1]Introduced by Waloddi Weibull in 1939

It should be noted that the parameter m change the shape of the probability function significantly. For large values of m the cumulative distribution function goes from 0 to 1 over a very short span of x. For a set of failure tests this would mean relatively similar fracture strength for all tests. For small values of m the cumulative distribution changes from 0 to 1 in a wide span of x values. For a failure test this would mean a large scatter of strength results. A change in the value of β does not affect the shape of the curves in Figure 5, but will move them along the x-axis.

For the application of Weibull distribution to failure strength in brittle materials, the distribution parameter x and scale parameter β is set to the stress level σ and the characteristic strength σ_0 respectively. By substituting these parameters into Equation 11, the following is found for the probability of failure:

$$P_f(\sigma) = 1 - exp\left[-\left(\frac{\sigma}{\sigma_0}\right)^m\right]. \tag{12}$$

Approximations to the parameters σ_0 and m can relatively easily be found through analysis of test data[2]. But since failure in glass initiate at flaws at the surface, and a larger surface area has larger probability of containing flaws of critical size, it can be argued that the probability of fracture will have a area dependency. Therefore σ_0 will be dependent on specimen size and test method. To find a general material parameter a weakest link approach must be applied.

Weakest link theory. In the weakest link theory the specimen is divided into n elements with area δA, all exposed to a stress σ. It is assumed that failure in a single element of the specimen leads to failure of the whole specimen. For an homogeneous material the probability of each of the n elements failing would be equal and noted P_f. By use of $\delta A = \frac{A}{n}$ the total probability of specimen *survival* can be written as:

$$1 - P_f(\sigma, A) = [1 - P_f(\sigma, \delta A)]^n = \left[1 - \frac{A}{n}\frac{P_f(\sigma, \delta A)}{\delta A}\right]^n = \left[1 - \frac{A}{n}\phi(\sigma)\right]^n. \tag{13}$$

$\phi(\sigma)$ was assumed by Weibull [41] to be defined as:

$$\lim_{n\to\infty}\left(\frac{P_f(\sigma, \delta A)}{\delta A}\right) = \phi(\sigma) = \left(\frac{\sigma}{\Sigma_0}\right)^m, \tag{14}$$

where Σ_0 is a scale parameter for a unite area. By use of the mathematical rule:

$$\lim_{n\to\infty}\left(1 - \frac{x}{n}\right)^n = exp(-x), \tag{15}$$

and Equation 14 the probability of *failure* can be from Equation 13 as:

$$P_f(\sigma, A) = 1 - \lim_{n\to\infty}\left[1 - \frac{A}{n}\phi(\sigma)\right]^n = 1 - exp\left[-A\left(\frac{\sigma}{\Sigma_0}\right)^m\right]. \tag{16}$$

Area dependence. For Equation 16 it is assumed that the whole specimen is subject to the same level of stress. For a bend test this is not the case, and loading factor k must be introduced. The stress in the specimen can be given as the maximum stress times a function of point in space:

$$\sigma(r) = \sigma_{max} g(r), \tag{17}$$

[2]For a good Weibull approximation at least 30 experiments should be included in the data set.

where g(r) gives the shape of the stress curve and equals one at the point of maximum stress. By combining Equations 16 and 17 the probability of failure for a specimen under varying loading condition can be expressed as:

$$P_f(\sigma, A) = 1 - exp\left[-\left(\frac{\sigma_{max}}{\Sigma_0}\right)^m \int_A g^m(r)dA\right]. \tag{18}$$

The loading factor can be defined as:

$$k = \frac{1}{A}\int_A g^m(r)dA, \tag{19}$$

so that Equation 54 simplifies to:

$$P_f(\sigma, A) = 1 - exp\left[-kA\left(\frac{\sigma_{max}}{\Sigma_0}\right)^m\right]. \tag{20}$$

kA represents the effective area and would be the area of a specimen yielding the same probability of failure in uniform tension. By comparing Equations 12 and 20, the relation between Σ_0 and σ_0 is:

$$\Sigma_0 = (kA)^{\frac{1}{m}}\sigma_0. \tag{21}$$

For a four point bend test with specimen thickness d, width b, distance between supporting cylinders L, and distance between loading cylinders L/2, k can be shown to be [38]:

$$k = \frac{m+2}{4(m+1)^2}\frac{b(m+1)+d}{w+d}. \tag{22}$$

By substituting Equation 22 and A=2L(b+d) into Equation 21, the final expression for Σ_0 is found:

$$\Sigma_0 = \sigma_0\left[L\left(\frac{d}{m+1}+b\right)\left(\frac{\frac{1}{2}m+1}{m+1}\right)\right]^{\frac{1}{m}}. \tag{23}$$

It should be noted that the parameters m and Σ_0 are the true values for the material which would be found if an infinite number of tests were performed. For a limited number of tests only an estimate to the real material parameters can be found and these are noted $\hat{m}$ and $\hat{\Sigma}_0$.

Note that all derivations until now assumes no time dependency for the fracture. In glass this is strictly not the case since a certain time is needed for flaws to develop into macro cracks.

Initial damage distribution in IMPETUS

A new algorithm *INITAL_DAMAGE_SURFACE_ RANDOM was implemented in IMPETUS during the work of this thesis. An expression for the failure stress of each integration point can be found from Equation 20:

$$\sigma = \Sigma_0\left(\frac{-ln(1-P_f)}{A}\right)^{1/m}. \tag{24}$$

Here P_f is a number following $0<P_f<1$ and randomly distributed to all integrations points. In IMPETUS the initial damage of an element D_0 is given by:

$$D_0 = 1 - \frac{\sigma}{\sigma_{max}}, \tag{25}$$

where σ is the failure stress of an integration point and σ_{max} is the maximum failure stress obtained in the material. By combining Equations 24 and 25 the following is found:

$$D_0 = 1 - \frac{\Sigma_0}{\sigma_{max}} \left(\frac{-ln(1-P_f)}{A} \right)^{1/m} = 1 - \Delta_0 \left(\frac{-ln(1-P_f)}{A} \right)^{1/m} \tag{26}$$

The new damage criterion in IMPETUS is based on Equation 26. A is the area represented by the integration point at hand, and damage is distributed to integration points close to the surface only. Figure 6 shows the relation between D_0 and P_f, the effect of a change in area represented by the integration point is indicated by dotted lines.

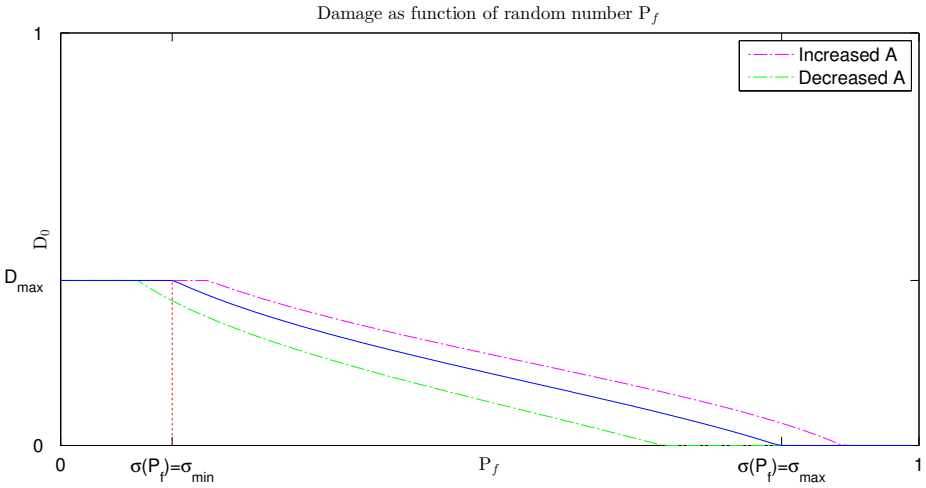

Figure 6: *Schematic of D_0 vs P_f for new damage criterion, the area dependence is indicated by dotted lines.*

2.3 Blast loading

In this section central concepts of blast loading is presented. First the general physics of blast loading is explained, then the relation between side-on and reflected pressure is discussed, and at last parameter scaling is presented. Note that all concepts are presented for spherical symmetric charges. The theory in this subsection is adapted from [10] and [30].

Physics of blast loading

With the detonation of explosives large amounts of energy is released in a very small volume through an increase of temperature. Since the gases related to the explosion are heated they will expand and force surrounding air away from the point of detonation. This leads to a layer of compressed air containing the main part of the detonation energy that will form around the expanding gases. This symmetric layer of compressed air is called the wave front, and it travels away from the point of detonation at supersonic velocity.

The pressure felt in a point in space x some distance r from the explosion center would be close to an ideal pressure curve for free field explosions. Such a curve is schematically shown in Figure 7. Since the velocity of the wave front increase with pressure the peak pressure will arrive first at point x. This will happen after an arrival time t_1-t_0, and lead to an instantaneous pressure rise

from p_0 to $p_0+p_s^+$. After the instantaneous peak the pressure will gradually decay back towards the ambient pressure. Due to the momentum of the molecules, gases behind the wave front will over expand. This leads the pressure to drop below ambient level, to a value of $p_0+p_s^-$. The period of time with pressure above the ambient level is called positive phase, and the integral of pressure with respect to time is the positive impulse I. Mathematically this is given by:

$$I = \int_{t_1}^{t_2} (p(t) - p_0)\mathrm{dt}. \tag{27}$$

In the same manner the time of pressure below ambient level is called the negative phase, and the integral of pressure values over time is the negative impulse. The form of the pressure curve shown in Figure 7 can be described by the modified Frielander equation:

$$p(t) = p_0 + p_{max}\left(1 - \frac{t}{t_d}\right)^{-\frac{bt}{t_d}}, \tag{28}$$

where b describes the decay of the curve, and t_d is the time of a positive over pressure (e.g. t_2-t_1 in Figure 7).

As the distance to the charge r is increased the peak pressure would decrease, while the time period of the positive phase would increase.

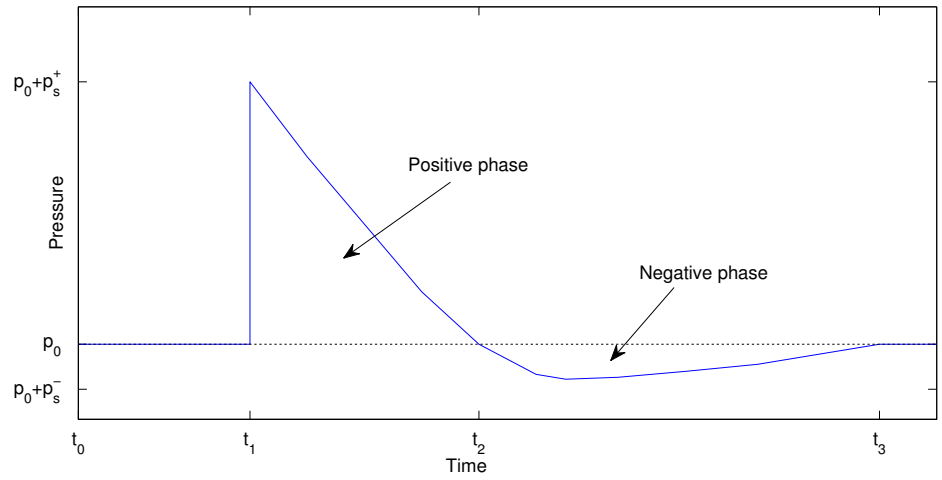

Figure 7: *Idealized curve for blast pressure. Figure adapted from [20].*

Side-on vs reflected pressure

The over pressure discussed up to here p_s is also called the side-on pressure. This is the pressure that would load a rigid plate with a shock front traveling with velocity direction parallel to the wall, as shown in Figure 8. For structures exposed to blast loading though, the reflected pressure is normally of most interest. The reflected overpressure arise when a shock front travel with velocity normal to a rigid plate, as shown in Figure 9. When the shock front reach the rigid wall the velocity of the molecules in the wave front will be arrested, and the wall will be loaded with a reflected overpressure p_r.

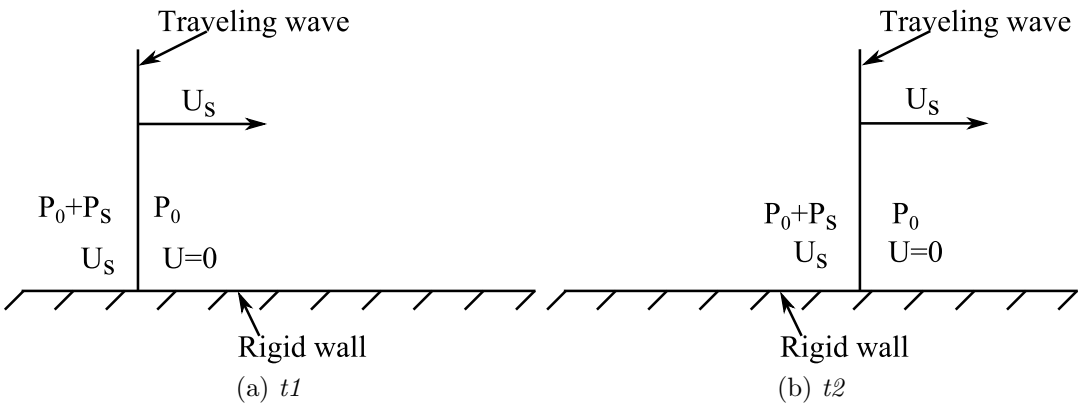

(a) *t1* (b) *t2*

Figure 8: *State variables for side-on pressure. Figure adapted from [10].*

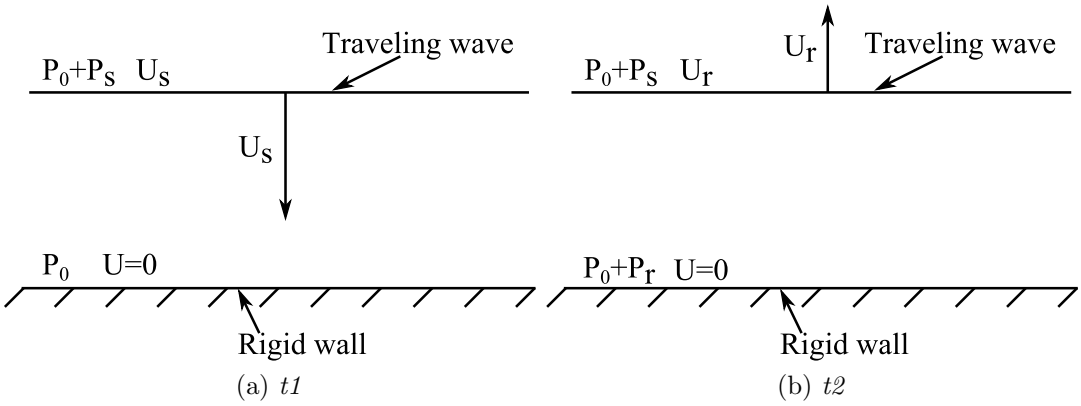

(a) *t1* (b) *t2*

Figure 9: *State variables for reflected pressure. Figure adapted from [10].*

For a perfect gas the relation between p_s and p_r is given as:

$$p_r = 2p_s + \frac{(\gamma+1)p_s^2}{(\gamma-1)p_s + 2\gamma p_0}. \tag{29}$$

For weak explosions (p_s^2 is close to zero) a relation of p_r=2p_s can be obtained. By assuming γ to be constant at 1.4 (air under normal conditions) a relation p_r=8p_s is found. During large explosion though air is not behaving like a perfect gas and Equation 29 is not valid. An exact relation between p_r and p_s for large explosions in air is not known, but theoretical calculations suggest it to be as high as p_r=20p_s [10].

Note that the situation shown in Figures 8 and 9 is for a completely rigid wall which will normally not be the case in practice. If a pressure front interacts with a pane of laminated glass, significant deformations of the pane will occur. The deformations in the pane will lead to changes of the pressure wave, which in turn will change the deformation and so on. This gives rise to the need of an iterative solution technique (e.g. full fluid-structure interaction simulations) if the problem is to be solved as correct as possible with numerical methods. For small deformations of the structure though, the pressure and the deformation is normally decoupled for simplicity. This means that the pressure that would be measured on a rigid surface is applied to the deformable structure. This disregards the effect the deformation has on the pressure front, but simplifies the calculations considerably.

Scaling of parameters

By use of a scaling law, an estimate for the state variables resulting from an explosion can be found. The most used form of scaling in blast loading is the ratio of distance r (in meters) to the cube root of the charge mass W (in kg TNT). This is called Hopkinson[3] or "cube-root" scaling:

$$Z = \frac{r}{\sqrt[3]{W}}. \tag{30}$$

Figure 10 shows how different explosion parameters is affected by the scaled distance Z. It should be noted that for other than the peak pressure and the velocity, the parameters are given per unite weight of explosive. This means that for equal Z values, only peak pressure and velocity would be constant, while for example the positive impulse would depend on charge weight. When scaling charge weight down, care should be taken that if explosives are placed too close to the target, there will be a localized pressure hitting the surface first since the shock wave expands in a spherical manner.

The effect of explosives is normally related through equivalent kilos trinitrotoluene (TNT). Table 1 shows a comparison of different high explosives.

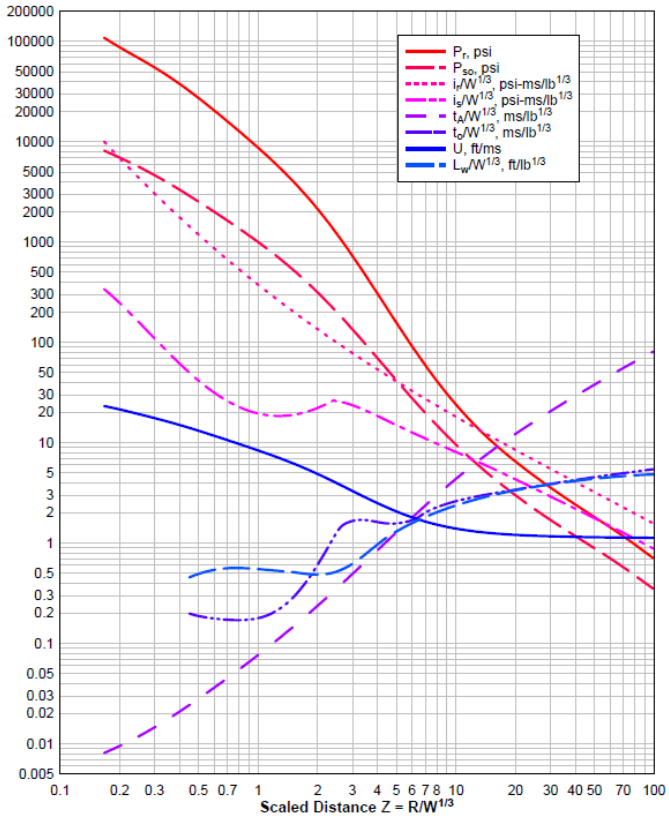

Figure 10: *Graphical representation of explosion parameters with respect to scaled distance Z for spherical charges. Figure taken from [36].*

[3]After the British engineer Betram Hopkinson who formulated the law in 1915

Explosive	Mass specific energy [kJ/kg]	TNT equivalent
TNT	4520	1
Torpex	7540	1.667
Semtex 1A	4980	1.102
C4	6057	1.34

Table 1: *TNT equivalents for different explosives [23].*

2.4 Finite Element Method (FEM)

FEM is a numerical method used to solve field problems described by differential equations. FEM can be applied to a variety of problems, and is extensively used in the field of structural mechanics. In this thesis FEM will be used to simulate the response of both quasi-static and dynamic experiments. In the following, explicit FEM and some of the features of the commercial software IMPETUS will be discussed. The theory in this subsection is adapted from [7], [24] and [37].

Mathematic formulation
For a general structural problem, the equilibrium equation on discrete form given at time step n is:

$$[\mathbf{M}]\{\ddot{\mathbf{D}}\}_{\mathbf{n}} + [\mathbf{C}]\{\dot{\mathbf{D}}\}_n + \{\mathbf{R}\}_n^{int} = \{\mathbf{R}\}_n^{ext}. \tag{31}$$

Here $[\mathbf{M}]$ is the mass matrix, $[\mathbf{C}]$ the damping matrix, $\{\mathbf{D}\}_n$ the nodal displacements, $\{\mathbf{R}\}_n^{ext}$ is the external nodal forces, while $\{\mathbf{R}\}_n^{int}$ is the internal nodal forces at time step n. All information before and including time step n is assumed known.

Nonlinearities in structural mechanics are normally divided in three types. Blast loading on laminated glass experiences every type of nonlinearity:

1. Material nonlinearity: Glass experience fracture and PVB experience plasticity.
2. Boundary condition nonlinearity: The applied force (blast pressure) varies with time.
3. Geometric nonlinearity: Large deformations of PVB.

To solve the equilibrium equation in time, two different time integrating methods can be used:

- Implicit method: Equilibrium is established through iterations for each time step.
- Explicit method: No equilibrium check, each time step performed directly.

With explicit time integration, Equation 31 can be solved with use of the half step method by the following procedure:

1. Calculate mean velocity

$$\{\dot{\mathbf{D}}\}_{n+\frac{1}{2}} = \{\dot{\mathbf{D}}\}_{n-\frac{1}{2}} + \frac{1}{2}\left(\Delta t_{n+1} + \Delta t_n\right)\{\ddot{\mathbf{D}}\}_n. \tag{32}$$

2. Enforce constraints on the mean velocity (e.g. boundary conditions).

3. Calculate displacement
$$\{\mathbf{D}\}_{n+1} = \{\mathbf{D}\}_n + \Delta t_{n+1}\{\dot{\mathbf{D}}\}_{n+\frac{1}{2}}. \tag{33}$$

4. Calculate current position.

5. Compute effective forces
$$\{\mathbf{R}\}^{eff}_{n+1} = \{\mathbf{R}\}^{ext}_{n+1} - [\mathbf{C}]\{\dot{\mathbf{D}}\}_{n+\frac{1}{2}} - \{\mathbf{R}\}^{int}_{n+1}. \tag{34}$$

6. Calculate new acceleration
$$\{\ddot{\mathbf{D}}\}_{n+1} = [\mathbf{M}]^{-1}\{\mathbf{R}\}^{eff}_{n+1}. \tag{35}$$

7. Enforce constraints on acceleration, set n=n+1 and go back to step 1.

If **[M]** is diagonal, i.e. all mass lumped to nodes, no equation solving is needed for the time integration. This leads to very low computational costs for each step in time of the explicit method.

The drawback with the explicit method is the fact that it is only conditionally stable, imposing a stability limit on the time step. The physical meaning of the critical time step is that information in the system cannot propagate further than the smallest adjacent distance between two nodes in one time step. If this condition is violated the solution will blow up in time and be useless. Mathematically the stability limit is given by:

$$\Delta t \leq \frac{2}{\omega_{max}}, \tag{36}$$

where ω_{max} is the highest natural frequency in the discrete system. To avoid calculating the highest natural frequency of the deformed system at every increment, a conservative estimate is normally used:

$$\omega_{max} \approx \frac{2c}{L^e} = \frac{2}{L^e}\sqrt{\frac{E}{\rho}}. \tag{37}$$

Substituting the estimate of ω_{max} into Equation 36 yields:

$$\Delta t \leq \frac{L^e}{c} = L^e\sqrt{\frac{\rho}{E}}. \tag{38}$$

This means that the critical time step will depend on the smallest element in the mesh, in addition to the density and stiffness of the material. Most commercial FEM software has a built in algorithm that automatically chose the optimal time step for an explicit calculation.

The stability limit imposes a clear drawback of the explicit method compared to the implicit method, since the wanted simulation period must be divided in more time steps. But when total simulation time is short, and small time steps are needed to capture all effects, e.g. changing boundary conditions, the explicit method is normally superior. Since no equilibrium check is performed in the explicit integration scheme the total energy of the simulation must be checked to see if the solution is stable, e.g. conservation of energy is satisfied. The total energy of the entire FE model should be constant, this can be written as:

$$E_{internal} + E_{viscous} + E_{frictional} + E_{kinetic} - E_{work} = E_{tot} = constant, \tag{39}$$

where $E_{internal}$ is internal energy, $E_{viscous}$ is viscous energy dissipated, $E_{frictional}$ is energy dissipated by friction, $E_{kinetic}$ is kinetic energy, and E_{work} is work done by applied loads.

IMPETUS

IMPETUS is a general purpose FEM software for nonlinear computational mechanics. Its focus is on accurate solutions and user friendliness. Therefore the number of user specified numerical parameters are kept at a minimum, and only fully integrated solid elements are provided. Three types of hexahedron solid elements are available in IMPETUS:

1. Linear elements with 8 nodes.
2. Quadratic elements with 26 nodes.
3. Cubic elements with 64 nodes.

Figure 11 show nodal locations for the cubic element.

An explicit method is used for the time integration in IMPETUS and the time step is by default set to 90% of the critical time step. Explicit integration in combination with higher order solid elements leads to high computational cost. To lower computation time IMPETUS is optimized to utilize the computers graphics processing unit (GPU) in addition to the central processing unit (CPU) to increase computational speed.

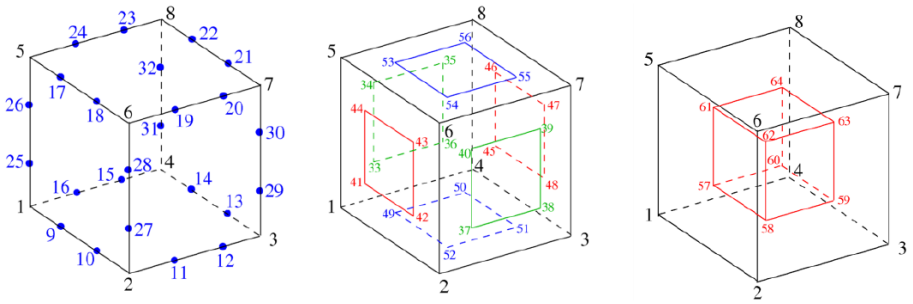

Figure 11: *Nodal location for cubic element in IMPETUS. Figure taken from [37].*

An attractive feature in IMPETUS for this thesis is the fracture technique using node splitting. The most used way of modeling fracture in FEM software is element erosion. With element erosion elements are deleted (eroded) when their stress level exceeds a critical value. For brittle material experiencing significant cracking, element erosion will normally lead to an unphysical response as a large part of the material will be deleted from the analysis, violating conservation of energy and mass. With node splitting the element boundaries will open up, allowing a crack to form or grow. This will happen when a predefined damage parameter reaches a value of unity. By changing the parameter *erode* in IMPETUS, nodes can be split such that the crack plane is orthogonal either to the maximum principal strain or the maximum principal stress. Node splitting is a relatively new technique and not as well tested as element erosion techniques. A drawback with node splitting is increased computation cost compared with element erosion.

2.5 Digital Image Correlation (DIC)

DIC is a powerful measuring tool used in experimental solid mechanics. In this thesis DIC is used as a measuring technique for both 3-point bend and tension tests on laminated glass. Therefore a brief discussion of the technique will be given here. The theory in this subsection is adapted from [11] and [27]. In this thesis, in-house DIC software developed by Fagerholt [11] is used.

Basic concepts

The basic concept of DIC is that pictures taken throughout an experiment can be compared to calculate the deformation of the specimen. DIC can be divided into three parts (1) specimen preparation, (2) image recording during experiment, and (3) image processing with computer algorithms. The specimen preparation is normally to apply a random speckle pattern to the surface of the specimen. This speckle pattern carries the information of the deformation and can be applied by use of black and white spray paint. During the experiment cameras are used to track the deformation of the speckle pattern. By the use of one camera aligned normally on the surface of interest, a 2D strain field can be calculated. With the use of two cameras in angle $\pm\alpha$ to the normal of the surface a 3D strain field can be calculated. In the DIC algorithms the speckle pattern at current (deformed) configuration is compared to a reference (undeformed or deformed) configuration to calculate the strain in the material. This is normally done by either the subset or the finite element based method. Due to its ease of implementation the subset based method is the most used approach for the deformation calculations. However, the FE based DIC method is more convenient when the results are compared with results from FEA. Therefore the FE based method will be presented and used herein.

Finite element based DIC

In FE based DIC computations a mesh of Q4 elements is used to define a global correlation problem. Each element in the mesh covers m×m pixels (in this project approximately 25*25 pixels are used in one element), and all four nodes of an element has two degrees of freedom (u,v). The deformations are found by optimizing the nodal displacements such that the grayscale value of an element is equal in reference and current configuration. This grayscale similarity can be given mathematically as:

$$I_c(X + u(X)) = I_r(X), \tag{40}$$

where I_c is the image in current configuration, while I_r is image in reference configuration. It is assumed that the displacement from reference configuration u(X) can be divided into an already known part u'(X) and a small unknown part Δu such that:

$$u(X) = u'(X) + \Delta u(X), \tag{41}$$

where u'(X)=0 for the very first iteration. Shape functions are used to describe the unknown displacement of an element as:

$$\Delta u^e(X) = \sum_{\alpha} \sum_{m} a_{\alpha m} N_m(X) e_\alpha, \tag{42}$$

where a is the DOF amplitude, α denotes a particular axis, N_m is the shape function of node m, and e_α is a unite vector along axis α. By combining Equations 40, 41, and 42 and minimizing the difference in grayscale values between current and reference configuration, a global equation system with the compact form:

$$[\mathbf{M}]\{\mathbf{a}\} = \{\mathbf{b}\}, \tag{43}$$

can be derived (see [11] for full derivation). By solving Equation 43 with respect to $\{\mathbf{a}\}$, the unknown displacements can be found from Equation 42. To increase accuracy for nonlinear problems an iterative process is carried out, updating the known part u'(X) between each iteration.

2.6 Bend testing

Both three and four point bend tests is performed in this thesis. The basis of a bend test is that a simply supported beam is loaded between two supports, forcing it to bend. The force and displacement is logged through the test, and Euler-Bernoulli beam theory is used to find mechanical properties of the test specimen. Beam theory is therefore an essential part of bend testing and the assumptions and limitations of the theory is presented here. In the last paragraph the application of bend tests to laminated glass is discussed. The theory in this subsection is adapted from [3] and [26].

Euler-Bernoulli beam theory
The fundamental equation of beam theory is the relation between the deformation field w and the applied load q:

$$\frac{d^2}{dx^2}\left(EI\frac{d^2w}{dx^2}\right) = q(x). \tag{44}$$

By assuming uniform cross section with centroid at y=z=0, the second moment of area I is defined by:

$$I = \iint z^2 dy\, dz = \frac{bd^3}{12} \tag{45}$$

For a uniform cross section E and I is constant with respect to x, and Equation 44 can be written as:

$$EI\left(\frac{d^4w}{dx^4}\right) = q(x). \tag{46}$$

By use of boundary conditions (simply supported and point load), Equation 46 can be solved to find the deflection of the midpoint. With deformation of midpoint and applied force logged through an experiment, E can be calculated from the linear part of the force-displacement curve. For 3-point bending E is given by:

$$E = \frac{L^3\Delta P}{48I\Delta w}. \tag{47}$$

With force data known, also the stress level in the specimen can be found. The tensile stress in a beam is given by:

$$\sigma = \frac{Mz}{I} = -zE\frac{d^2w}{dx^2}, \tag{48}$$

where M is the effective moment, and z is the coordinate for the thickness of the beam going from z=-d/2 to z=d/2. The mid section of the beam z=0 is called the neutral axis, having a tensile stress of zero. Above the neutral axis the specimen will be in compression, and below the neutral axis it will be in tension. For symmetric 3-point bend the stress will be given by:

$$\sigma = \frac{PLz}{4I}. \tag{49}$$

The assumptions made for Equations 47 and 49 are:

- Specimen having a uniform cross section.
- Simply supported specimen.

- Point loading.
- Plane sections remain plane and normal to the beam axis (no shear).

Application to laminated glass.
The behavior of laminated glass under bending is assumed to be in between an upper and lower bound:

- Upper bound: Linear stress distribution, neutral axis in PVB.
- Lower bound: Non-linear stress distribution, neutral axis in middle of both glass plies.

For the upper bound the neutral axis will be placed in the middle of the PVB layer and the laminated plate will follow beam theory. The upper ply will experience compression only while the lower glass ply will be in tension. The PVB layer is close to the neutral axis and will have low levels of strain compared to the glass layers. The total second moment of area for the component can be approximated as:

$$I_{upper} = \frac{b}{12}\left(d_{tot}^3 - d_{PVB}^3\right), \tag{50}$$

where d_{tot} is the total thickness of the pane and d_{PVB} is the thickness of the PVB layer.

For the lower bound the PVB layer only separates the two glass panes, and beam theory applies to the two glass plies separately. Significantly shear is expected in the PVB and the total second moment of area for the component can be approximated as:

$$I_{lower} = 2 \cdot \frac{b d_{glass}^3}{12}, \tag{51}$$

where d_{glass} is the thickness of one glass layer. Figure 12 shows the difference in bending mode and stress distribution for upper and lower bound.

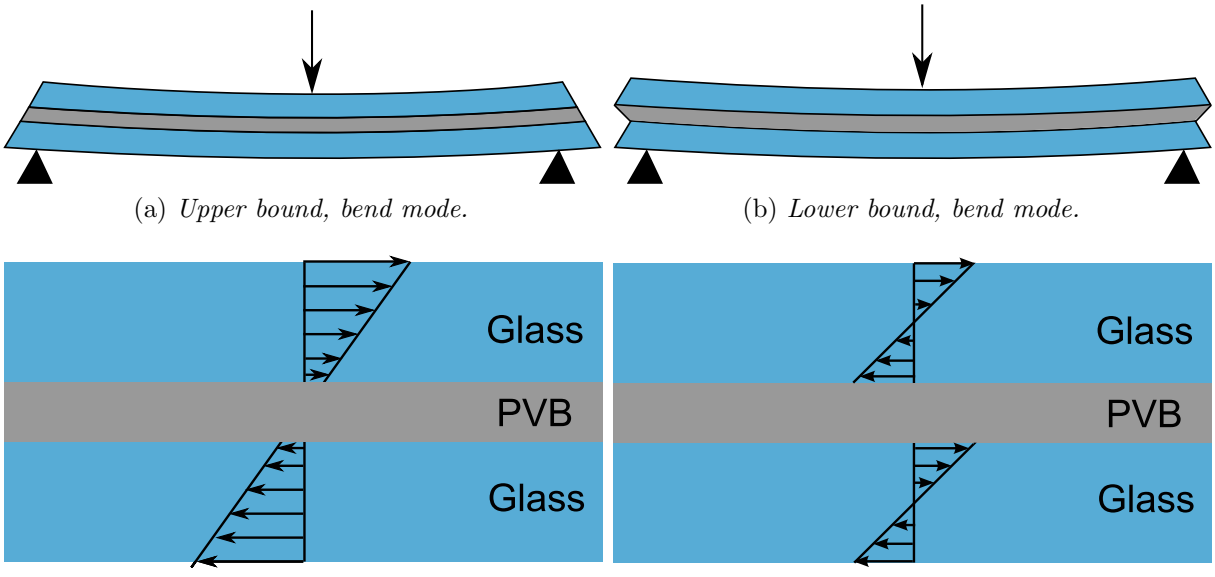

(a) *Upper bound, bend mode.* (b) *Lower bound, bend mode.*

(c) *Upper bound, linear stress distribution.* (d) *Lower bound, nonlinear stress distribution.*

Figure 12: *Bend mode and stress distribution through thickness of laminated glass. Stress in PVB is orders of magnitude lower than those in glass. Figure adapted from [26].*

3 Previous work

In this section previous work in the field of dynamic loading on laminated glass is presented. Emphasize will be on studies on laminated glass for architectural use exposed to blast pressure, but also work on windshields exposed to impact will be presented. An important difference in the studies done in the literature is found in the material modeling. The following subsection will therefore present the findings in this area.

Material models
Different material models for both glass and PVB are found in the literature, and Table 2 provide an overview of different material models used.

Main author	Glass	σ_f glass	PVB
Zhang [42]	JH2 - rate dependent	Rate dependent	Rate dependent plastic[2]
Larcher [20]	Elastic	84 MPa	Elasto-plastic
Hooper precrack [14]	Elastic	80 MPa	Generalized maxwell
Hooper postcrack [14]	-	-	JC
Timmel[1] [35]	Elastic	105 MPa	Hyperelastic
Sun[1] [34]	Elastic	Not given	Elastic / Mooney-Rivlin

Table 2: *Overview of material models used for glass and PVB in literature.*

Glass. As can be seen from Table 2 most authors used an elastic material model for glass, and this is normally combined with a brittle failure criterion. The Young's modulus E varies from 70-72 GPa, and strength σ_f from 80-105 MPa. Since intrinsic flaws in glass needs time to escalate into macro cracks, the failure strength of glass is known to be depending on the strain rate. Peroni et al. [28] did research on the strain rate dependency of glass for use in laminated panes. Under tensile loading an increase in strength of approximately 30 MPa (from 60-90 MPa) was found when test speed increased with six orders of magnitude (from approximately $1{\cdot}10^{-5}$ to $1{\cdot}10^{1}$ m/s), clear strain rate dependency was not found in compression. Zhang et al. included the strain rate dependency by use of a strain rate dependent Johnsen-Holmquist ceramic material model.

To model glass failure, Timmel et al. and Zhang et al. used element erosion. In the work by Larcher et al., the tension stress in a glass element was set to zero when critical loading was reached. Hooper et al. used a precrack model until critical loading was reached in glass, the simulation was then restarted with a postcrack model where glass stiffness was set to 1 Pa.

PVB. For the constitutive modeling of PVB, a number of different models are used. Some authors, e.g. Iwasaki et al. [13] and Morrison [25] have performed experiments for the mechanical properties of PVB without stating clearly if the tested PVB has been through the process of lamination. Since the lamination process expose PVB to high temperature and pressure, which

[1]Research on windshields
[2]MAT-STRAIN-RATE-DEPENDENT-PLASTICITY in LS-Dyna

clearly changes its optical characteristics, it should be expected that also the mechanical properties changes. The mechanical properties of PVB are shown to be strongly strain rate dependent. For small strain rates PVB behave in a hyperelastic manner [13], while for the large strain rates which should be expected during blast loading, an elastic-plastic behavior is reported [14].

In the studies done by Timmel et al. and Sun et al., the material values for PVB exposed to low strain rates were used. Larcher et al. included the fact that PVB behave elastic-plastic under high strain rates, while Hopper et al. and Zhang et al. also included rate dependency in the elastic-plastic model. Hooper et al. performed high strain rate experiments on post-lamination PVB, by tensile tests on precracked specimens. Figure 13 shows the resulting stress-strain data for Hooper's experiments. A Johnsen-Cook plasticity model including strain rate effects shows good consistency with the experimental results. A great challenge with strain rate dependency of PVB is the fact that prior to glass cracking the strain rate in the PVB layer is rather low, while after glass cracking significant strain rate is expected. Hooper et al. solved this problem by dividing the calculations into pre- and postcrack models. In the precrack model a generalized maxwell law was applied for a viscoelastic description of the PVB, while for the postcrack model a Johnsen-Cook plasticity model was employed.

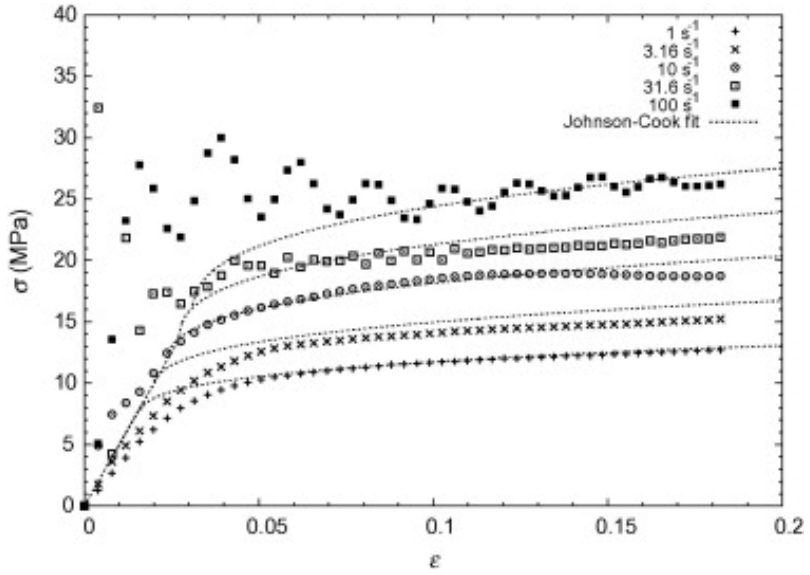

Figure 13: *Results found by Hooper et al. for laminated PVB at different strain rates. Figure taken from [14].*

Delamination. To be able of predicting the postcrack behavior of laminated glass, the delamination process between glass and PVB is important to understand. Larcher et al. argued that adhesive forces between glass and PVB are relative high, and delamination was therefore not considered in their work. Hooper et al. on the other hand used a stiffness of 1 Pa for glass in the postcrack model, approximately equaling a situation where the whole area between PVB and glass delaminates at the beginning of glass cracking. Butchart and Overend [4] argued that the work used for delamination can be found through an energy balance as follows:

$$F\delta = W_{delam} + W_{strain} + W_{visco}, \tag{52}$$

where F is applied force, δ the displacement, W_{strain} the energy stored as strain in the interlayer, W_{visco} the energy dissipated by viscous deformation, and W_{delam} the energy used for delamination. If tests are performed where W_{strain} and W_{visco} can be calculated, W_{delam} can be determined from the energy balance. The adhesion Γ of the PVB-glass interface can then be found from:

$$\Gamma = \frac{W_{delam}}{A}, \tag{53}$$

where A is the total area of delaminated interface. Through their calculations Butchart and Overend found that interfacial adhesion varied with testing rate. According to Larcher et al. [21] delamination has never been observed in blast experiments, while Zhang et al. [42] observed glass debonding in impact tests on laminated glass.

4 Experimental setup

Five different experiments were carried out in this project:

1. 4-point bending tests of glass to find Weibull parameters for the statistical distribution of fracture stress.
2. Tension tests of precracked laminated glass specimens to find material properties of PVB.
3. 3-point bending tests of laminated glass as validation for numerical model.
4. Gas gun tests to investigate behavior of pure and laminated glass under pressure loading.
5. Blast experiments with laminated glass exposed to C4 explosion.

This section gives an overview of the setup for the experimental tests. For the compressed gas gun and free field explosions also measured pressure data is given. All results from the experiments are given in Section 5.

The 4-point bend, tension, and 3-point bend test were performed by Vidar Hjelmen at SINTEF. Trond Auestad performed the experiments in the compressed gas gun at NTNU, while the free field explosions were performed by Knut Ove Hauge (NDEA) at Nammo Raufoss Test Center. Pressure measurements for both gas gun and blast experiments were performed by Hauge in 2009. All glass used in this project were delivered by the local supplier "Larsen Mesterglass". The laminated panes were produced by "Sikkerhetsglass Norge".[4]

Due to delays in glass delivery and waiting time for lab equipment, material testing did not start before middle of April.

4.1 4-point bend - Glass

Setup
The ASTM standard for mechanical testing of ceramics [8] was used as a basis for the test setup, which can be seen in Figure 14. The test fixture had freely rotating bearings with diameter of 4.7 mm and a loading span of 20 mm. The support span was 40 mm, and inner dimension of the fixture was 45.94 mm. Displacement was measured by three pins located directly under the specimen. A 200 kg load cell was used for loading. The upper part of the fixture had a weight of 286.8 g and was placed freely on the glass. This weight must therefore be added to the logged force. The loading speed was 0.5 mm/min for the first 45 tests, while for the last 15 tests the maximum machine speed of 1.9 mm/min was used. Because of the small dimensions of both specimen and fixture, it was hard to align the specimens perfectly in the middle of the fixture.

Specimens
The local supplier was not able to meet all specimen specifications in the ASTM standard. The width of the specimens was therefore increased from 4 to 10 mm, the tolerances were set to ± 1 mm instead of ± 0.13 mm, and edge grinding was not performed. 60 specimens with dimensions $45 \times 10 \times 3$ mm and 30 specimens with dimensions $45 \times 10 \times 1.7$ mm were ordered.

[4] Exact chemical composition of delivered components was not known by the supplier.

It turned out that 86 out of 90 specimens were too long to fit in the fixture with inner dimension 45.94 mm. In addition about half of the specimens had edge cracks visible to the naked eye, as shown in Figure 15. Therefore a "Struers LaboPol-21" grinding machine with P320 paper was used to reduce the length of the specimens and grind the edges.

In total 60 specimens were tested. Prior to testing all specimen dimensions were measured by use of a slide gauge. Typical dimensions can be seen in Table 3, while the full list of measured data is given in Appendix C.

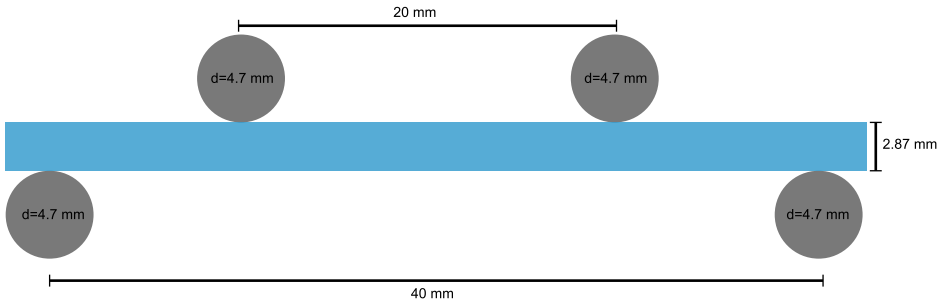

(a) *Dimensions*

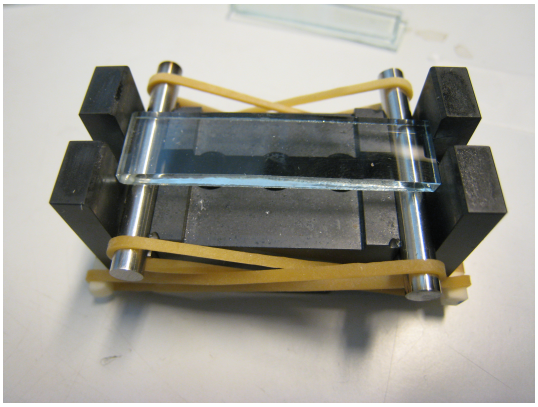

(b) *Glass in fixture*

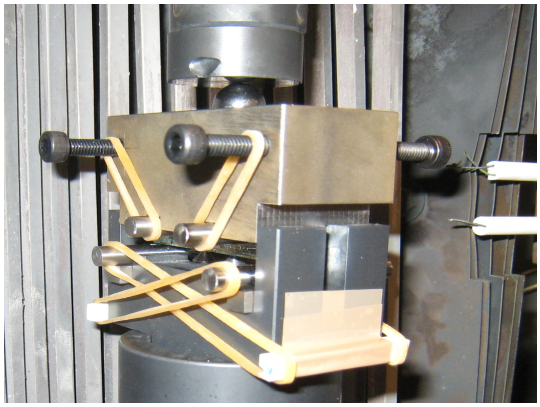

(c) *Fixture in machine*

Figure 14: *Setup for 4-point bend test of glass specimens. Note that some of the specimens were 2.06 mm thick, the other setup dimensions were similar.*

	Length (l)	Width (b)	Thickness (d)
Mean	45.70	11.34	2.06/2.86
Max	45.93	11.90	2.07/2.87
Min	44.94	9.61	2.06/2.86

Table 3: *Overview of specimen dimension for 4-point bend test. Full list of measured dimensions given in Appendix C. All dimensions in mm.*

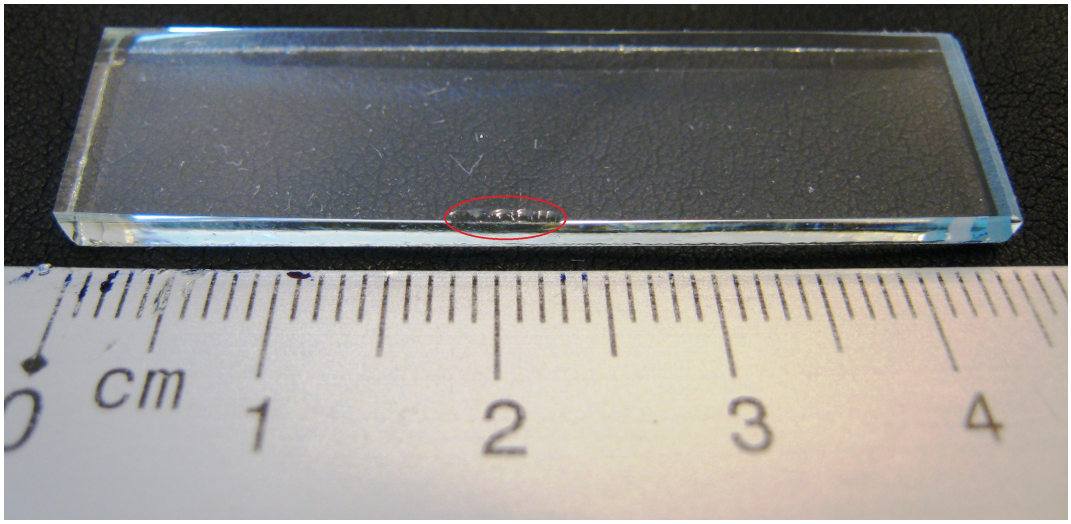

Figure 15: *Example of macro crack in 4-point-bend specimen.*

4.2 Tension - PVB

Setup

Tension tests of precracked laminated plates with dimensions 200×40×7.52 mm were conducted in an attempt to find the mechanical properties of post lamination PVB. Due to the large difference in Young's modulus, all deformation was expected to occur in the free PVB. The test was performed in a Zwick/Roell Z030 30 kN test machine, and pneumatic clamps were used to fix the specimen. 13 specimens were tested with elongation rate varying from 10 mm/s to the machine maximum of 500 mm/s. Force and displacement were logged by the test machine. Two cameras were used in the first four testes, one normal to the width (200×40 mm face) of the specimen to track glass deformation, and one normal to the thickness (200×7.52 mm face) to track deformation of PVB. For the two camera setup a frame rate of 1 frame per second (FPS) was used for each camera. For the last 9 experiments only the camera normal to the thickness of the specimen was used, and the frame rate was increased to 15 FPS. Figure 16 shows the tension specimen in the fixture.

Specimens

For the use of DIC calculations all specimens were painted with black and white spray paint to produce a gray scale speckle pattern. All specimen dimensions were measured prior to testing, and Table 4 shows typical dimensions. The full list of measured data is given in Appendix C. Thickness of the three layers and the width of the precrack were measured by use of a microscope, while the specimen width was measured with a slide gauge.

	Thickness			
	Width	Glass	PVB	Initial crack width
Mean	40.76	2.85	1.55	0.024
Max	41.5	3.12	1.85	0.037
Min	40	2.53	1.4	0.017

Table 4: *Overview of specimen dimension for tension test. Full list of measured dimensions given in Appendix C. All dimensions in mm.*

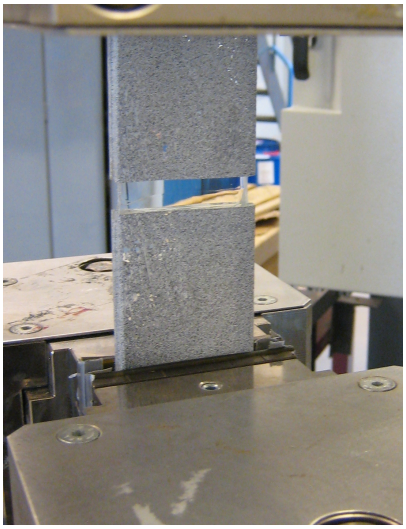

Figure 16: *Placing of tension specimen in fixture. PVB in area of pre-cracked glass is elongated under loading.*

4.3 3-point bend - Laminate

Setup

Laminated glass panes with dimension 200×40×7.52 mm were tested in 3-point bending as a validation test for the numerical model of laminated glass. The tests were performed in a Zwick/Roell Z030 30 kN test machine. The dimensions of the setup can be seen in Figure 17. A total of 7 tests were performed and deformation speeds varied from 0.01 mm/s to 0.5 mm/s. Force and displacement were logged by the machine. For DIC analysis one camera normal to the 200×7.52 mm side of the specimen was used with a frame rate of 4 FPS.

Specimens

All specimens were measured prior to testing, and a gray scale pattern was painted on the 200×7.52 face. The outer dimensions were measured with a slide gauge, and a microscope was used to find the thickness of the three layers. Table 5 shows typical specimen dimensions, while the full list of measured data is given in Appendix C.

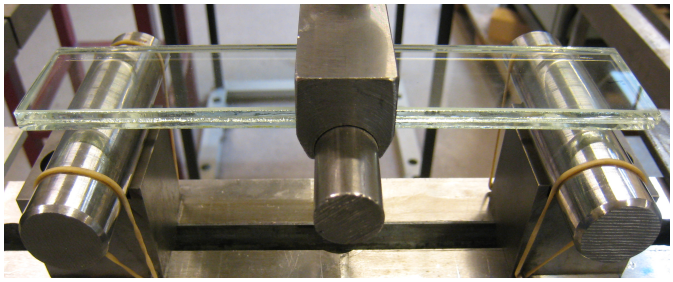

(a) *Setup*

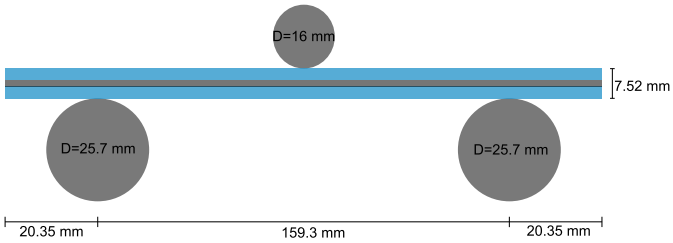

(b) *Dimensions*

Figure 17: *Setup geometry for 3-point bend test of laminated plates. Note that there is some variation in thickness between the specimens.*

		Thickness	
	Width	Glass	PVB
Mean	40.57	2.89	1.49
Max	41.36	3.00	1.55
Min	40.00	1.55	1.37

Table 5: *Overview of specimen dimension for 3-point bend test. Full list of measured dimensions given in Appendix C. All dimensions in mm.*

4.4 Gas gun experiment

As a preliminary test of glass exposed to pressure load, the gas gun facility of SIMLab was used. An overview of the gas gun setup is shown in Figure 18. The original purpose of the gas gun is to investigate ballistic penetration. The four main parts of the gas gun is the 20 L pressure tank, the firing section, a 10 m long barrel of 50 mm diameter and a 16 m^3 impact chamber. When performing an experiment, the pressure tank, firing section, and barrel is initially separated by mylar membranes. The pressure tank is then filled to a pressure p, while the firing section is filled to p/2. Due to its small volume the pressure in the firing section can be released quickly. When this is done, the pressure gradient between the pressure tank and the firing section doubles in a short time, leading to rupture of the membrane. If ammunition is not used, the second membrane separating the firing section and the barrel will experience approximately the same pressure gradient and rupture as well. The released air pressure will travel down the barrel and load the target. A throughout description of the gas gun is given by Børvik et al. [5].

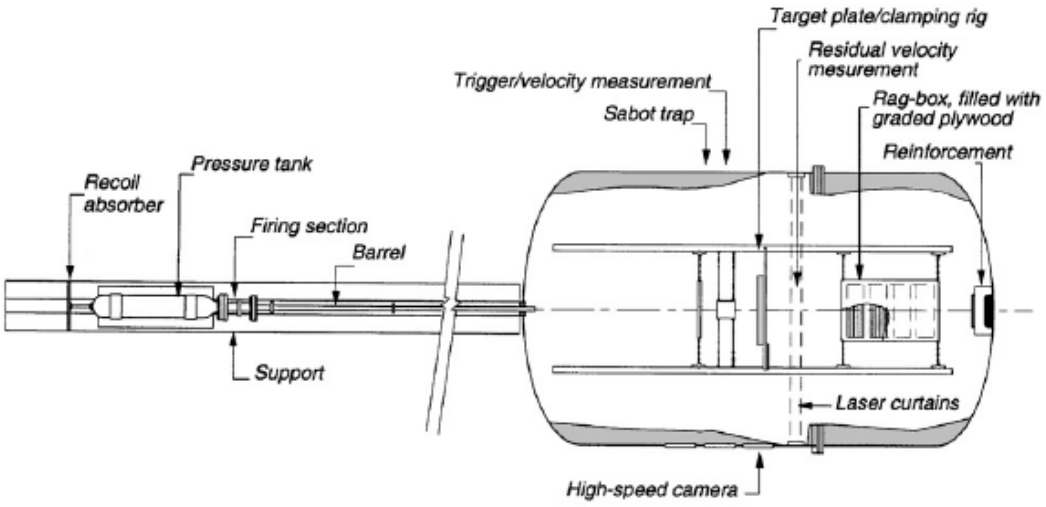

Figure 18: *Sketch of gas gun layout. Figure taken from [5].*

Setup

The glass panes of 400×400 mm were mounted 290 mm from the barrel outlet. A rubber strip of 7.5 mm width were glued to the backside of the panes, and placed in contact with a close to rigid frame with inner dimension 300×300 mm. Clamps were used in the corners to ensure the plane stayed in place. A picture of the setup taken from barrel outlet side can be seen in Figure 19.

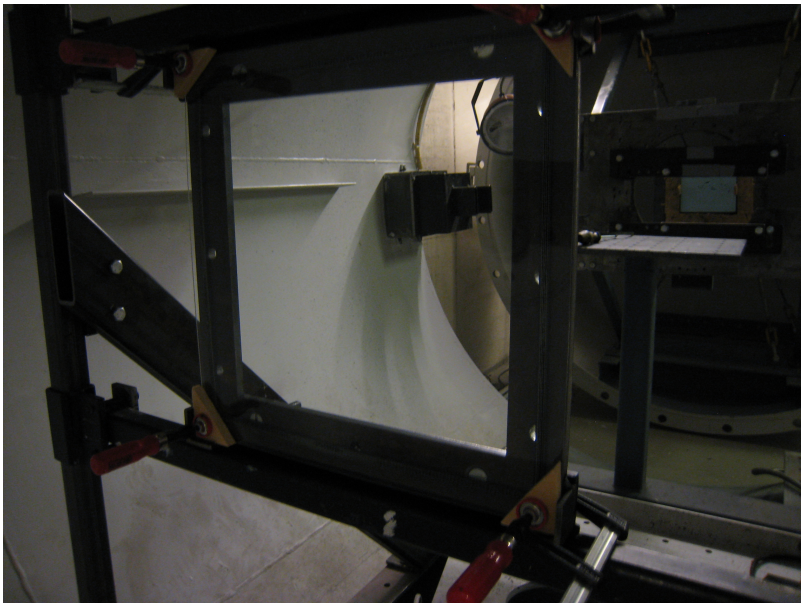

Figure 19: *Glass pane in compressed gas gun.*

A total of nine panes were tested, seven of pure glass with thickness of 2.87 mm, and two panes of laminated glass with total thickness of 4.92 mm. A high speed camera taking 20 000 FPS was used to capture the resulting fragmentation.

Pressure measurement

The gas gun has been used for pressure loading experiments in master theses at NTNU previously, among others by Rakvåg [30]. A known problem with the gas gun is the limitations in peak pressure. In an attempt to reduce the pressure loss in the impact chamber, a funnel between the outlet of the barrel and the target was introduced this year. Through pressure measurements it was found that the funnel did not work as planned. The peak pressure did not increase, the pressure situation was highly antisymmetric, and significant noise was experienced in the measurements. Therefore the use of the funnel was disregarded for the experiments in this thesis. The measurements performed by Hauge in 2009 are therefore used in the further analysis. To ease readability the unit of bar is used for the tank pressure while kPa is used for the pressure loading the plate.

Filtering. 13 pressure transducers were used for the measurement. They were mounted on a close to rigid plate in the manner shown in Figure 20. Slot number 5, 10 and 15 were not used. Logging of the pressure started when firing the gas gun and lasted for half a second. The raw data from the test setup is influenced by relatively large oscillations. It is sensible to assume turbulence in front of the rigid plate, and numerous reflections between the plate and the wall of the impact chamber. Also the membrane on the pressure transducers can flutter, creating unphysical oscillations. The logging of the data is therefore complex, and it is hard to distinguish measuring noise from the actual physics. To reduce oscillations the raw data was filtered in MATLAB with a Butterworth lowpas filter of second order with normalized frequency of Wn=0.001. Figure 21 shows the relation between raw and filtered data for sensor 1 at 20 bar tank pressure.

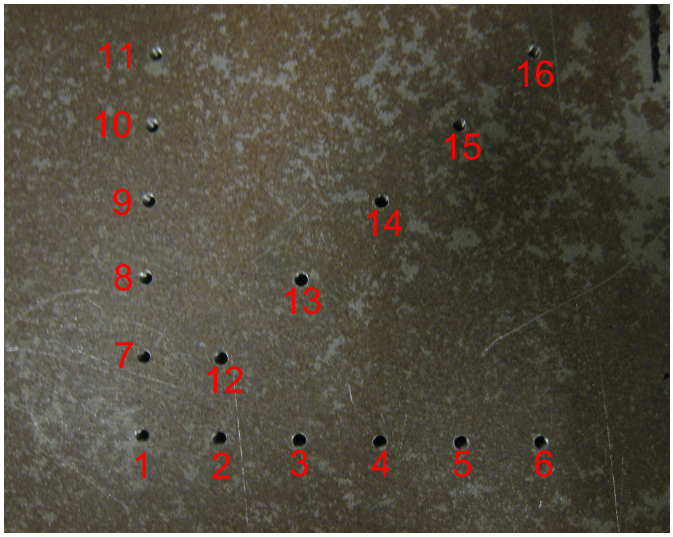

Figure 20: *Location of pressure transducers. Slot 5, 10 and 15 were not used.*

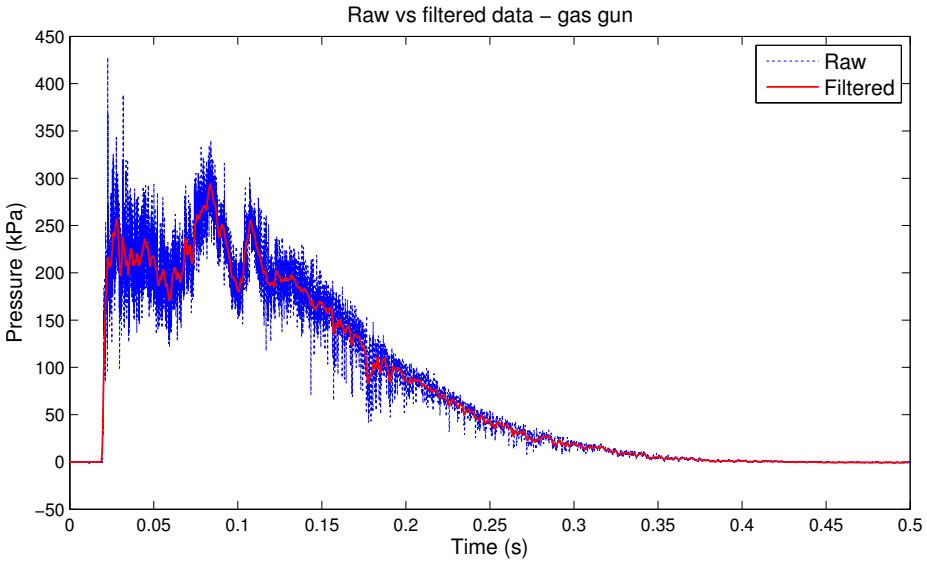

Figure 21: *Raw vs filtered data from gas gun. Data from sensor 1 and 20 bar tank pressure.*

Repeatability. To test the repeatability of the gas gun three shots were performed at both 5 and 20 bar. Figure 22 shows the filtered data for sensor 1. Both shape and peak values are very similar for all three shots at both pressure levels. The experimental test is therefore assumed repeatable, and the measurements from 2009 are used for the experiments performed in this project.

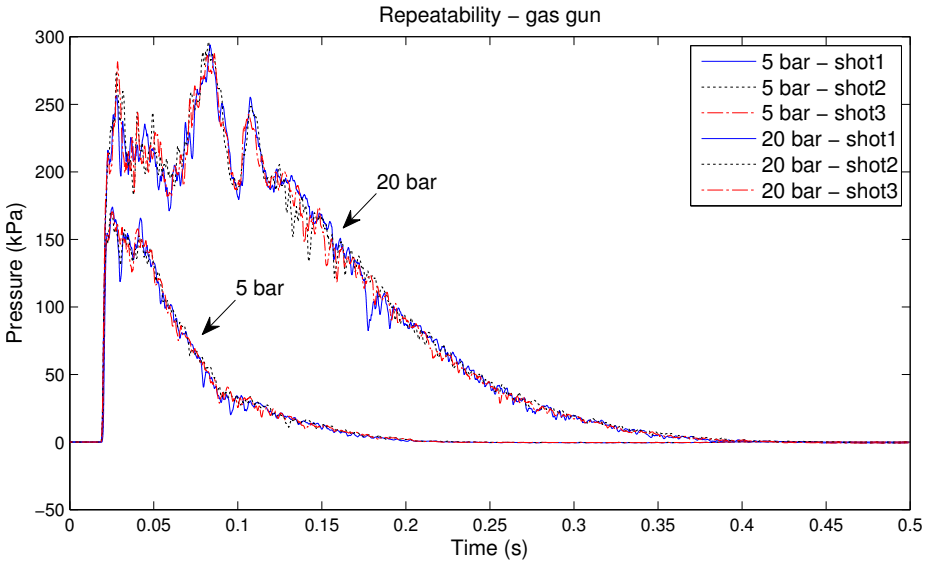

Figure 22: *Repeatability of gas gun, sensor 1. Filtered data.*

Effect of tank pressure. The resulting pressure on the plate was measured for a tank pressure varying from 5 to 40 bar. The effect of a change in tank pressure for the load in sensor 1 can be seen in Figure 23. For a change in tank pressure form 5 to 10 bar the peak pressure rise from 174 kPa to 306 kPa, in addition to an elongation of the positive phase. A change in tank pressure from

10 bar to 40 bar delays the pressure peak and elongate the positive phase, but does not increase the value of the peak pressure.

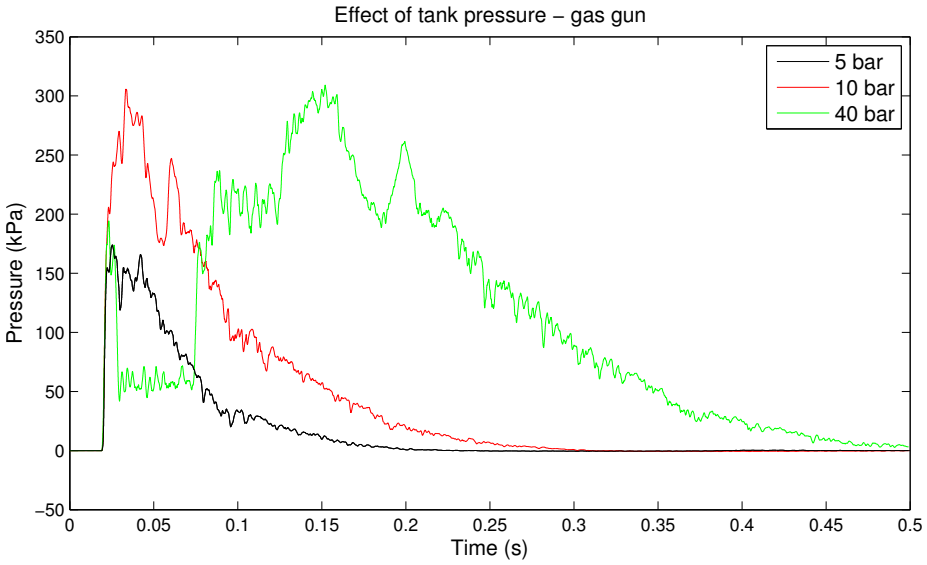

Figure 23: *Effect of tank pressure in sensor 1. Filtered data.*

Symmetry. For a perfectly symmetric setup, the plate would be symmetrically loaded. This means that the pressure and impulse should be equal in two transducers with equal distance to the center of the plate. For filtered data Table 6 list maximum peak pressure p_{max} and positive impulse I[5]. From this table it is clear that the measured pressure situation is not perfectly symmetric. Especially sensor 3 and 8 both a distance 50 mm from the center differ significantly in peak value for 20 bar tank pressure, with 135 kPa and 190 kPa respectively. This is probably due to asymmetries in the setup, e.g. the plate not being perfectly centered in front of the barrel outlet or the barrel outlet not being perfectly circular. Despite incorrect, symmetry is assumed for simplicity and only the horizontal pressure transducers are used for the further calculations. Figure 24 shows the filtered pressure-time history for horizontal pressure transducers at 20 bar.

It is important to notice that due to its low peak value, long positive phase, lack of negative impulse, and centralization of peak pressure on target the pressure load in the gas gun differ significantly from blast loading.

[5]Impulse was found through numerical integration by use of the built-in MATLAB function *trapz*

Distance (mm)	Sensor	5 bar p_{max}	5 bar I	20 bar p_{max}	20 bar I
0	1	174	9	294	39
25	2	115	6	279	32
25	7	102	3	290	23
35.4	12	62	3	272	21
50	3	28	1	135	6
50	8	30	1	190	8
70.7	13	7	0	28	1
75	4	13	0	29	0
75	9	6	0	17	-1
106.1	14	4	0	12	0
125	6	7	0	25	0
125	11	3	0	14	1
176.8	16	4	0	19	1

Table 6: *Maximum pressure (kPa) and positive impulse (kPa*s) for 5 and 20 bar. Sorted after distance to center.*

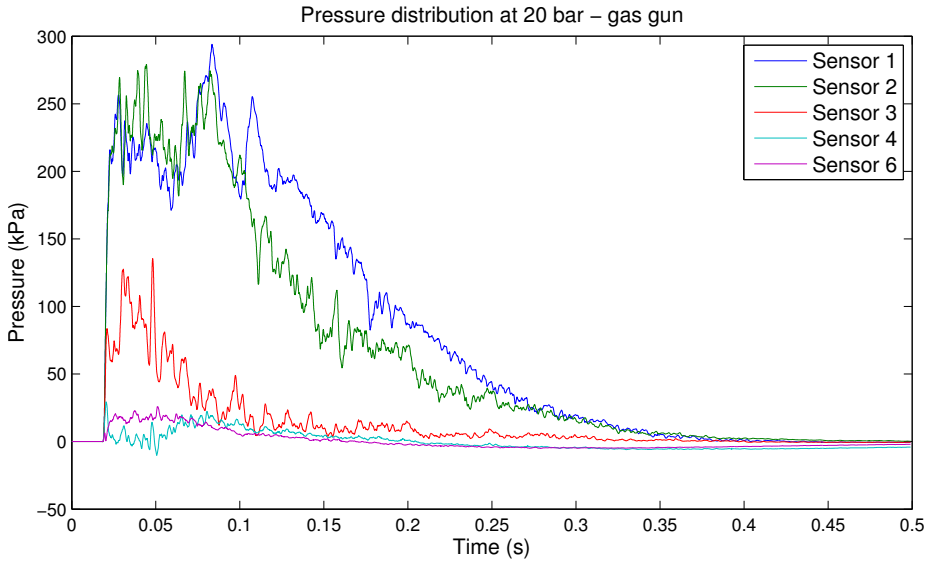

Figure 24: *Horizontal pressure sensors for 20 bar tank pressure. Filtered data.*

4.5 Blast experiment

In collaboration with NDEA, experiments with C4 explosives were carried out on laminated glass. In 2009 pressure measurements were performed related to experiments with steel plates. To reuse the pressure measurements, the same charge geometry and stand-off distances were used for the experiments in this thesis.

Setup

The setup for the experiments can be seen in Figure 25. The setup mainly consisted of the laminated glass pane in a close to rigid frame, the C4 charge, and one pressure transducer at 1 m stand-off. Dimension for the laminated panes were 400×400 mm, while the frame had inner dimension of 300×300 mm. To avoid creating holes in the glass panes bolts were used only in the lower and left part of the frame. The glass panes were placed on the lower bolts and against the left bolts, before the bolts were tightened.

The pressure transducer was only for safety reasons to assure that all explosives were detonated, and the measurements were not saved. A cylindrical charge with diameter 30 mm and length 130 mm was used. It contained 143 gram C4, and its center was located 70 cm above ground. The tests were performed on a concrete platform and Figure 26 shows a picture of the explosion. Table 7 list the 5 unique combinations of plate thickness and stand-off distance that were used, all combinations were tested twice giving a total of 10 experiments. Due to equipment limitations it was not possible to measure the displacement in the plate during loading. A clear improvement of the experiment would be to include high speed camera and DIC measurements to get deformations and progress of the fracture pattern.

Plate thickness	Stand-off	Z ($m/kg^{1/3}$)
1.7 - 1.52 -1.7 mm	75 cm	1.3
1.7 - 1.52 - 1.7 mm	125 cm	2.17
3 - 1.52 - 3 mm	60 cm	1.04
3 - 1.52 - 3 mm	75 cm	1.3
3 - 1.52 - 3 mm	125 cm	2.17

Table 7: *Plate thickness and stand-off distance for blast experiments, all combinations tested twice.*

Pressure data

Head-on pressure measurements were not possible to perform for this experiment due to equipment limitations. Therefore the pressure measurement from 2009 is used as a basis. A 143 gram cylindrical C4 charge with length 130 mm and diameter 30 mm was placed on the ground, and 8 side-on pressure transducers were put in the ground at distances from 60 to 215 cm. It is important to notice that significant ground effects can take place in these measurements, and the measured pressure might therefore differ from the pressure in the free field experiment conducted in this project. Also the reflected pressure that will load the laminated plate is significantly higher than the measured side-on pressure, as discussed in Section 2.3.

Figure 27 shows the measured pressure for one explosion at 60, 75 and 125 cm stand-off distance. Increasing stand-off distance from 60 cm to 125 cm gave a significant reduction in peak pressure from 1296 kPa to 286 kPa.

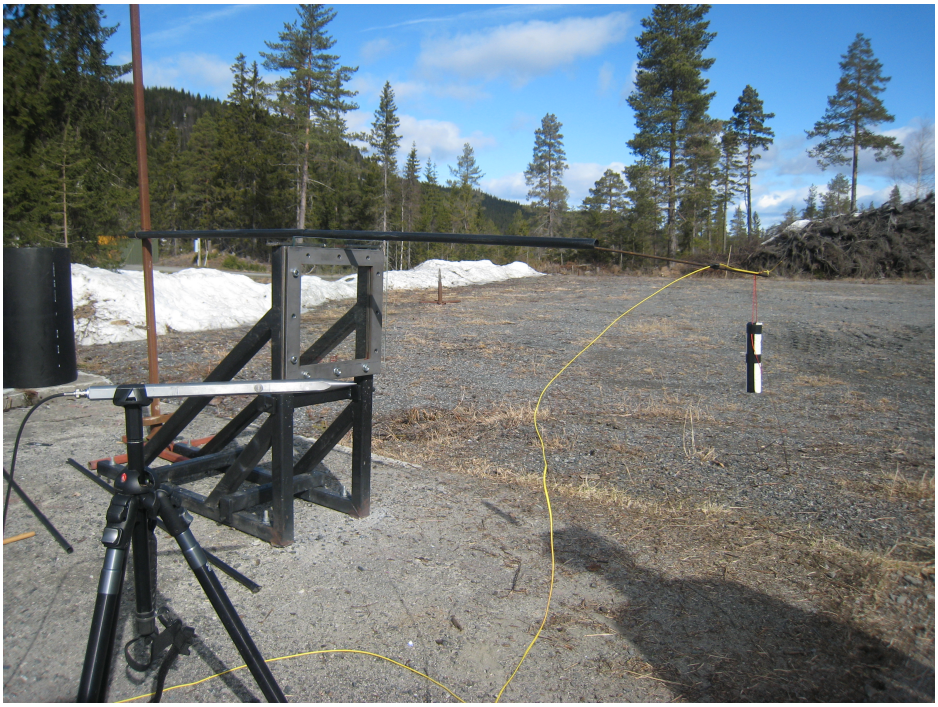

Figure 25: *Setup for blast experiments. Window, C4 charge and pressure transducer.*

(a) *Before explosion.* (b) *Explosion.*

Figure 26: *Explosion of 143 gram C4.*

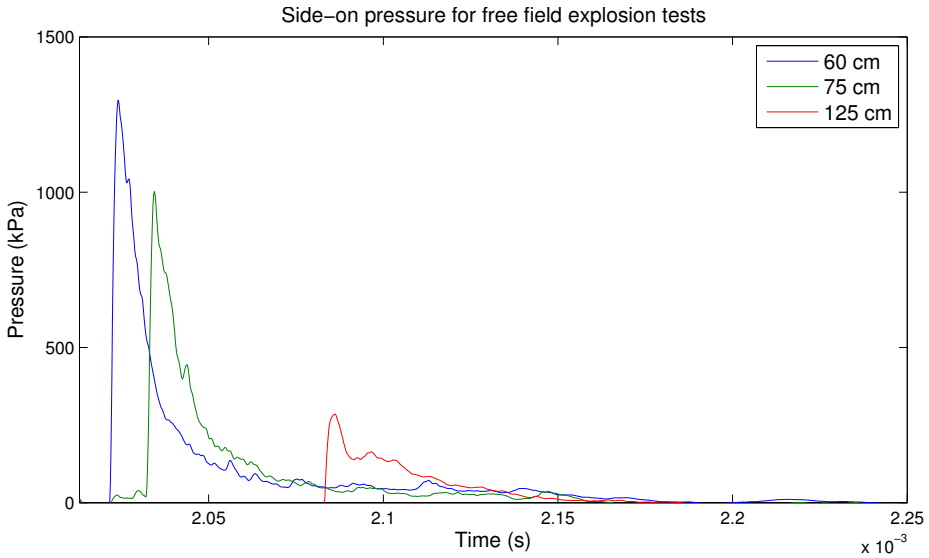

Figure 27: *Measured side-on pressure for test with explosives.*

Four repetitions of the measurements were performed and Figure 28 shows the four curves obtained at 75 cm stand-off. The maximum pressure varies from 919 kPa to 1047 kPa, while the shape of the curve is similar for all tests. The experiments are therefore assumed repeatable.

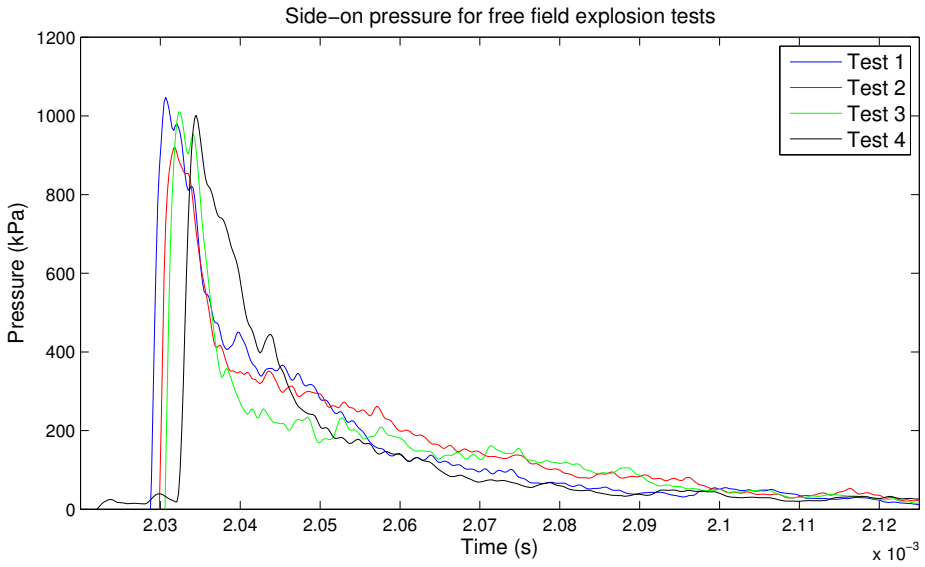

Figure 28: *Repeatability of pressure measurements. Test 1-4 at 75 cm stand-off distance.*

Note the significant difference in time scale and peak pressure between C4 explosions and gas gun testing. With 20 bar tank pressure the positive load in the gas gun lasts for about 0.3 s, while for an explosion with 75 cm stand-off the duration is approximately $1{\cdot}10^{-4}$ s.

5 Experimental results

In this section results from all experiments are presented and discussed.

5.1 4-point bend - Glass

Force - displacement
Figure 29 shows the resulting force-displacement curves for the 60 4-point bend experiments on pure glass. Some of the force-displacement curves show clearly unphysical nonlinear behavior.

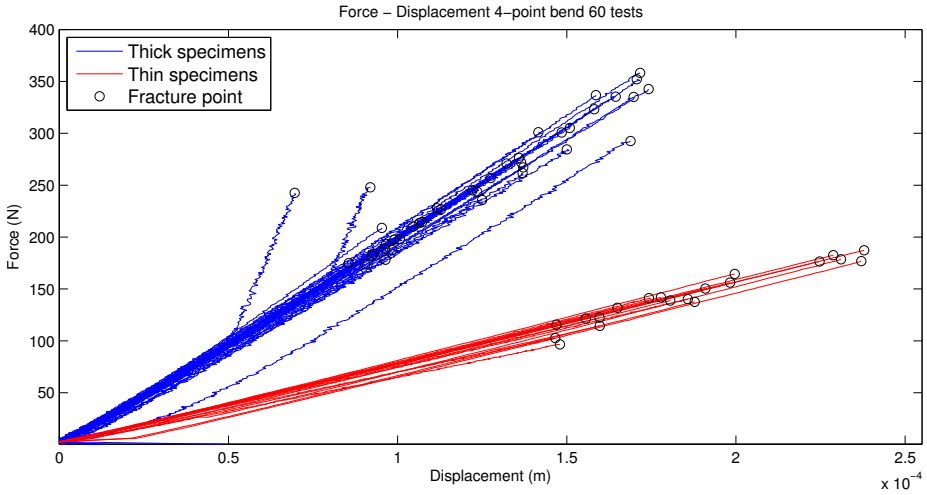

Figure 29: *Force - displacement curves for all 4-point bend tests.*

Fracture stress and Young's modulus
Beam theory was assumed valid for the 4-point bend test and E and σ was found from force displacement data by use of the equations given in Section 2.6. For the calculation of E, 60 percent of the logged points were used to find Δforce and Δdisplacement so that initial and end effects were not included. Table 8 list results for E and σ for all 60 tests, 33 tests used for a Weibull analysis in the following paragraph, and the 15 tests with deformation rate of 1.9 mm/min.

	E (GPa)			σ_f (MPa)		
	All 60	Weibull	Fast	All 60	Weibull	Fast
Mean	89.17	88.66	82.2	84.08	83.34	93.37
Max	133	98.23	87.6	116.3	114.57	116.3
Min	71.26	75.82	71.26	57.57	57.57	68.14

Table 8: *Results from 4-point bend. E and fracture stress given for all 60 tests, the 33 tests used for Weibull analysis and the 15 tests with deformation rate 1.9 mm/min.*

From Table 8 it can be seen that for all 60 experiments, calculated E has a mean value almost 20 GPa higher than what is reported in literature (70-72 GPa Section 3). Also a great variation in

the calculated E values is found, with a difference of 61 GPa between max and min value. The Young's modulus in a material like glass is given by the atomic bonds and is not expected to vary within specimens of the same chemical composition. A possible source of error is friction between the specimen and the side walls of the fixture. This is though expected to give a clearly nonlinear force-displacement curve which was not the case for the majority of these tests. Another possible source of error is the logging of force and displacement. An error here will give significant error in max stress, but for the calculation of E only Δ values were used, and a linear shift in force or displacement will not affect the result. A third possible error is in the calculation of second moment of area I, which assumes rectangular specimens. The width varied along the length of each specimen and an average value was used for the calculation. This can explain the variations in E, but does not explain the high mean value. After discussions with supervisors and test personnel at SINTEF, a good explanation for the E to yield so high and varying results was not found.

With a mean of 84.08 MPa for all 60 tests, the values calculated for the fracture stress is in better relation with values given in literature (80-105 MPa). The mean fracture stress for the 15 specimens tested with higher loading rates is seen to be 12 % (10 MPa) higher than the mean value for the 33 tests used for the Weibull analysis. This gives an indication of the rate dependency of glass fracture, as discussed in Section 3.

Weibull analysis

33 tests[6] with grinded edges, linear foce-displacement plots and thickness 2.86-2.87 mm were used for a Weibull fit. Figure 30 show resulting stress-strain curves for the 33 tests. Through the use of a linear regression technique the parameters $\hat{m}$ and $\hat{\sigma}_0$ was found. p_f was found by Equation 54 and the resulting regression can be seen in Figure 31.

$$p_f(i) = \frac{i - 0.5}{n}. \tag{54}$$

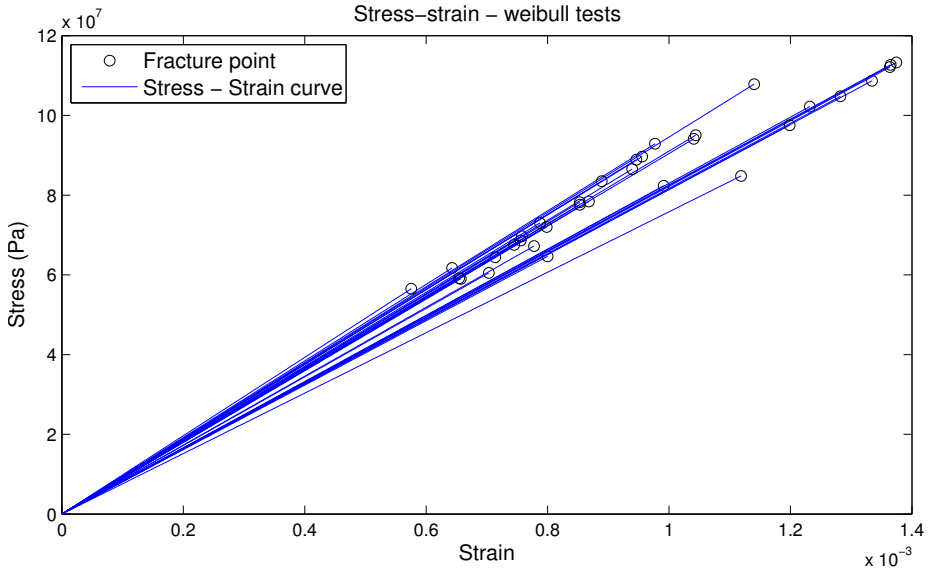

Figure 30: *Stress-strain curves for 33 tests used in Weibull estimate.*

[6]Specimen number 7-14,16,19-30 and 34-45

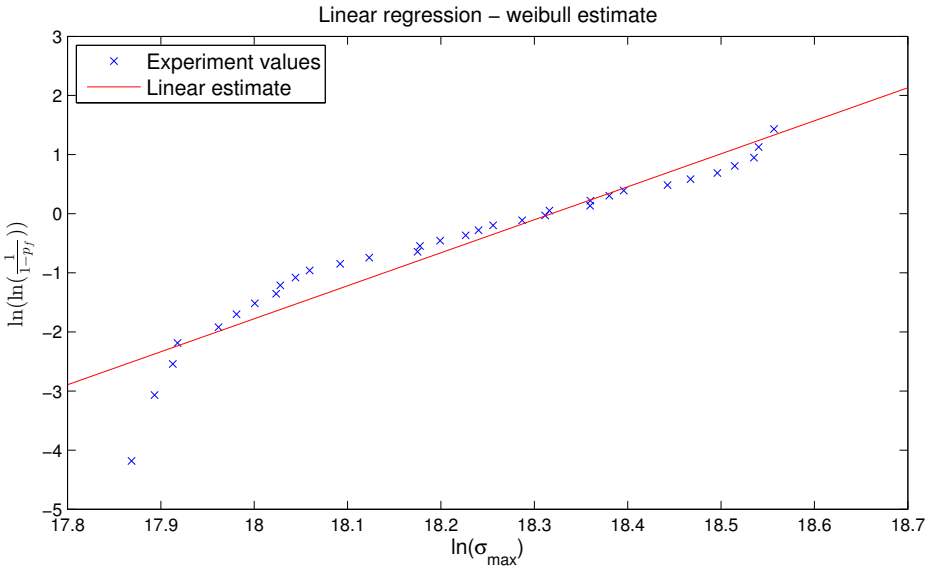

Figure 31: *Weibull estimate for 33 tests using regression. $\hat{m}$=5.58 and $\hat{\sigma}_0$=90.2 MPa.*

The resulting Weibull parameters were:

- $\hat{m}$=5.58
- $\hat{\sigma}_0$=90.2 MPa
- $\hat{\Sigma}_0$=46.0 MPa

Comparison of Weibull estimate and experimental data can be seen in Figure 32. It is clear from the probability density function that there is no perfect match between the experimental values and the Weibull theory. The extreme values were far to frequent compared to the middle values of the experiment. Since the calculation of E and σ_{max} was based on the same fundamental beam theory, it is expected that the unphysical variation that was found in calculated E-values is also present in the values of σ_{max}. This gives a second contribution to the variation in σ_{max}, in addition to the distribution of size and location of inherent flaws, and might explain the low accuracy of the Weibull fit.

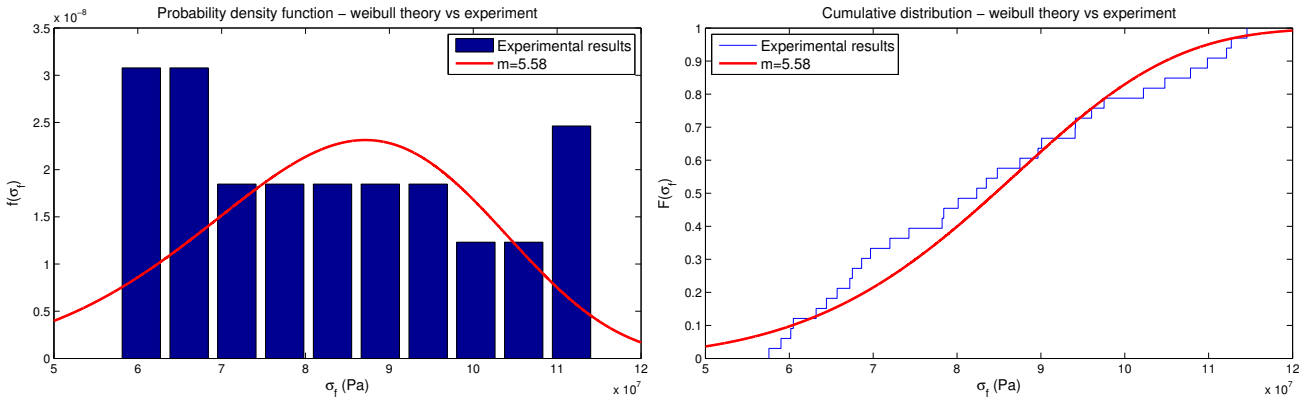

(a) *Density function.* (b) *Cumulative distribution.*

Figure 32: *Weibull estimate vs experimental values.*

5.2 Tension - PVB

Deformation of glass

DIC measurements of the glass were performed on the first 4 tests. Analysis of this data showed the maximum first principal strain level in the glass to be 0.01. Strain in the glass is therefore disregarded in the further analysis.

Delamination

Figure 33 shows how the first principal strain calculated with DIC develops through the test. A part of the 200×7.52 mm face is shown with a Q4 mesh assigned to the PVB interlayer. The color scale is equal in all pictures with blue indicating zero strains and deep red indicating a first principal strain level of one. In Figure 33a it can be seen that the initial deformation was skewed, this is due to the precracks in the two glass panes was not perfectly aligned. The fact that elements originally not located in the precrack get significant level of straining must be due to delamination. In Figure 33h clear delamination can also be seen by the open space between PVB layer and glass on right hand side.

The progress of first principal strain in element 50 in Test 6 (position indicated in Figure 33) is compared with machine force in Figure 34. It is seen that the strain rate in element 50 dropped significantly at 5 mm machine displacement. Due to the dominating delamination, an approximately constant force level of 0.31 kN was needed to elongate the specimen from 20 to 55 mm.

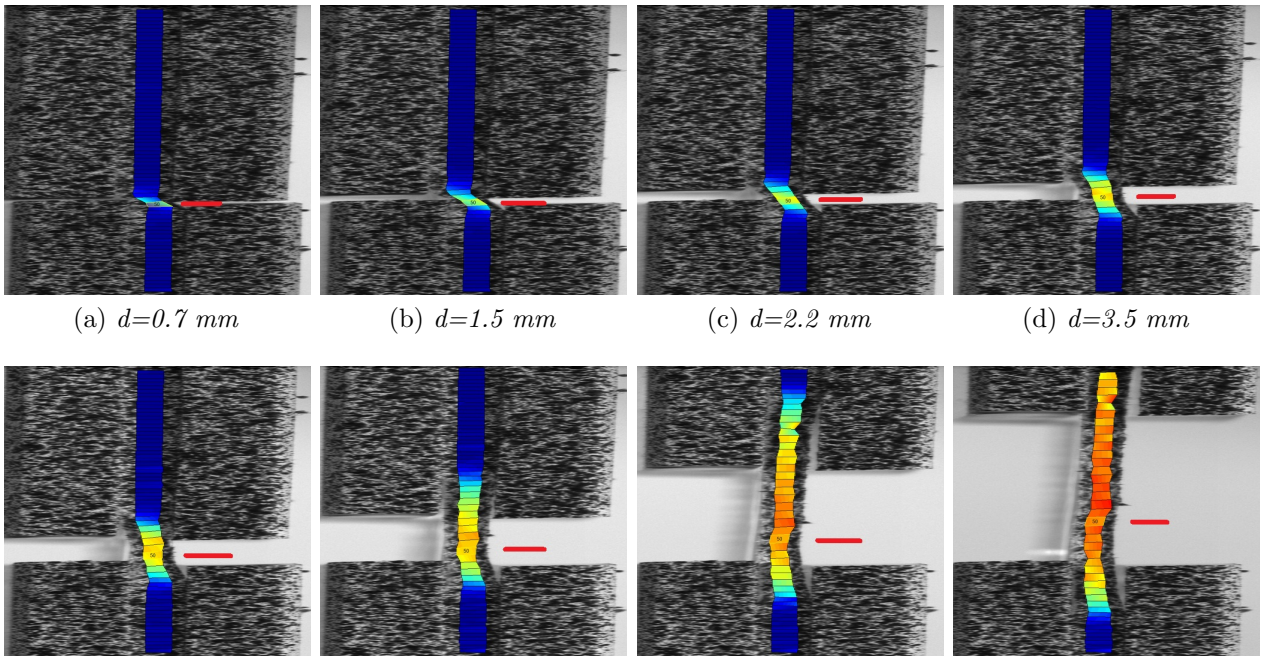

(a) *d=0.7 mm* (b) *d=1.5 mm* (c) *d=2.2 mm* (d) *d=3.5 mm*

(e) *d=4.8 mm* (f) *d=8.6 mm* (g) *d=17.1 mm* (h) *d=26.7 mm*

Figure 33: *Delamination process for Test 6. Blue indicate 0 strain and deep red a 1.principal strain of 1. Machine displacement is given for each figure. Vertical position of element 50 is indicated by red line.*

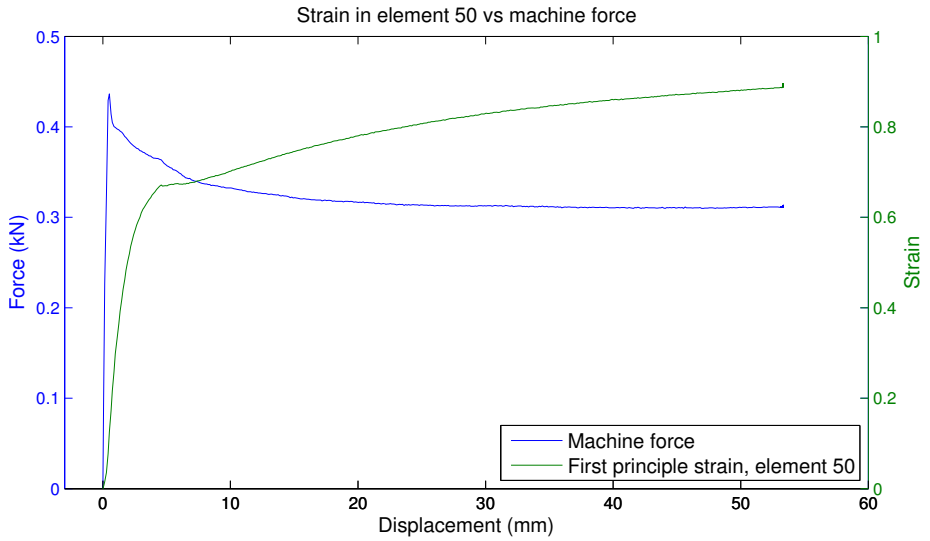

Figure 34: *Progress of first principal strain in element 50 Test 6 (see Figure 33) compared with force-displacement.*

Force-displacement

Force-displacement curves for Tests 2, 4, 6, 9 and 13 can be seen in Figure 35[7]. Due to dominating delamination between PVB and glass in all thirteen tests, material properties of PVB could not be found from this experiment.

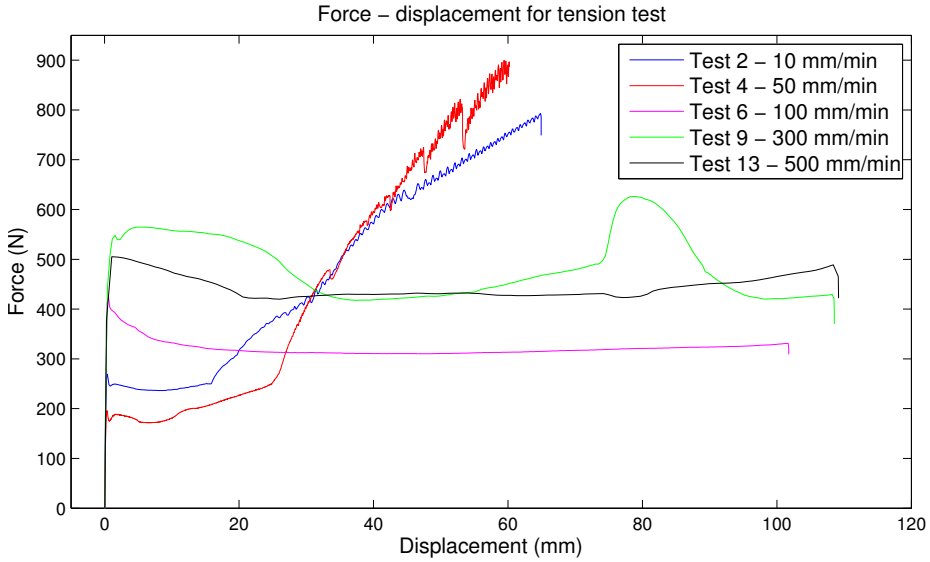

Figure 35: *Force-displacement for tension test of precracked laminated glass.*

[7]Force-displacement curves for all thirteen tests is included in Appendix A

5.3 3-point bend - Laminate

Force-displacement

Force-displacement curves for the seven 3-point bend tests are shown in Figure 36. Two different fracture behaviors can be observed. For Test 1, 6 and 7 two local force peaks can be seen. This is due to the upper glass ply fracturing at a larger deformation than the lower plate. For the four other tests, both glass plies broke at same deformation, leading to only one force peak. Table 9 summarizes results for all seven tests. The listed Young's modulus was calculated from the lower bound beam behavior, as discussed in Section 2.6. E is found to vary from 73 to 82 GPa with mean of 79 GPa. This is significantly lower than the mean value for E found in the 4-point bend test. For calculations with the upper bound beam assumption, E varies from 94 to 107 GPa with mean value 100.5 GPa. With literature values for E of 70-72 GPa, this indicates that the behavior of laminated pane in quasi static 3-point bending is close to the lower bound, with significant shear straining in PVB. It cannot be seen any clear effect of deformation rate on fracture force.

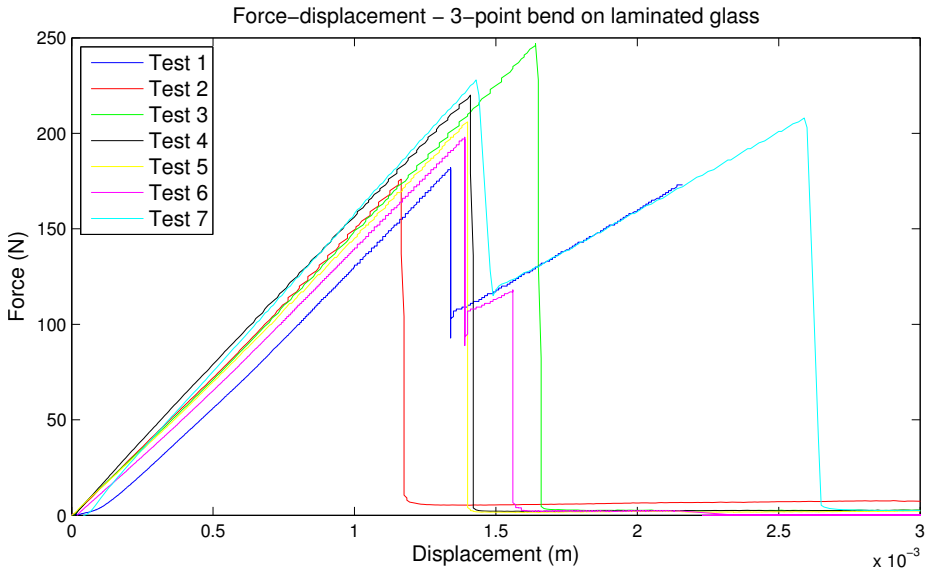

Figure 36: *Force displacement curves for 3-point bend test. Note that Test 1 ended before upper glass plate fractured.*

Deformation rate (mm/s)	First fracture (N)	E (GPa)	Separate glass fracture	Test
0.01	182	73	√	1
0.01	198	74	√	6
0.05	206	78	÷	5
0.1	176	77	÷	2
0.1	247	82	÷	3
0.1	220	82	÷	4
0.5	228	79	√	7

Table 9: *Results from all 3-point bend tests. E was calculated based on lower bound laminate behavior.*

DIC measurements

Due to its low deformation rate, Test 6 was used for DIC analysis. An interesting finding from the DIC measurement is the difference in first principal strain between the glass and the PVB layer at both sides of the loading point, as seen in Figure 37. The first principal strain in three elements on "Element line A" in Figure 37 is plotted in Figure 38. The elements are situated in upper glass plate, PVB, and lower glass plate. From Figure 39 it can be seen that, for the displacement span where the strain difference between glass and PVB is high, there is a significant difference in horizontal displacement for upper and lower node of PVB. This gives a clear indication that the relatively large first principal strain in PVB, which can be seen for this element in Figures 37 and 38, is dominated by shear strain. This is another indication that the behavior of laminated glass under quasi-static 3-point bend loading is close to the lower bound.

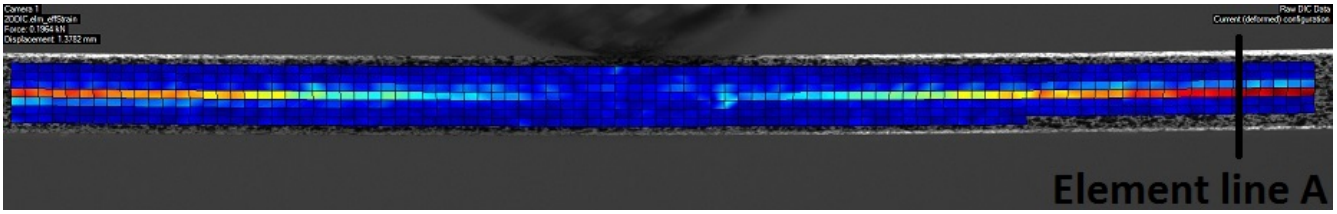

Figure 37: *Strain difference between glass and PVB for 3-point bend test. Blue indicates 0 strain while deep red indicates first principal strain of more than 0.05. Element line A indicates location of elements used in Figures 38 and 39.*

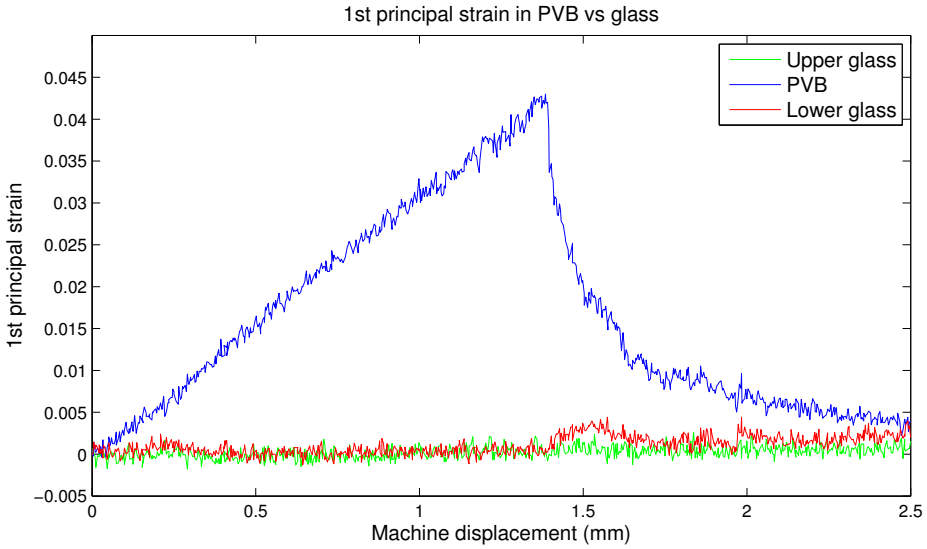

Figure 38: *Plot of first principal strain for glass and PVB layer in 3-point bend test. Data taken from elements located in "Element line A" in Figure 37. Glass fracture happens at 1.4 mm machine deformation.*

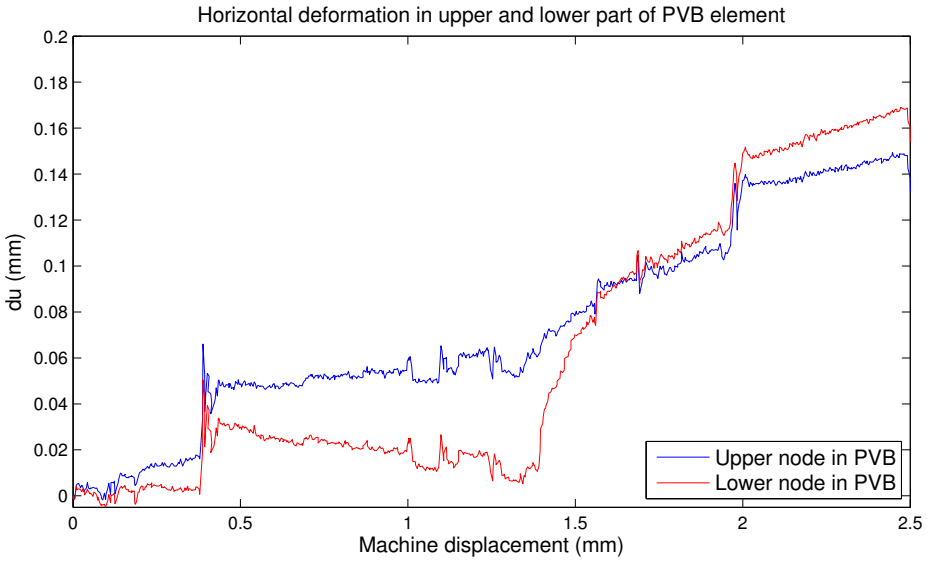

Figure 39: *Horizontal deformation in upper and lower node of PVB in "Element line A" in Figure 37. The difference in displacement between 0.5 and 1.5 mm machine displacement gives a clear indication of shear straining of PVB.*

Delamination

By use of Dye Penetration Inspection (DPI) the level of delamination in the 3-point bend test was investigated by Ida Westermann (SINTEF). The result for Test 4 can be seen in Figure 40 which shows a part of the 200×40 mm face of the specimen. The dye adhered to the gray scale pattern used for the DIC measurements as seen at the lower edge. Delamination can be seen along the cracks in the glass.

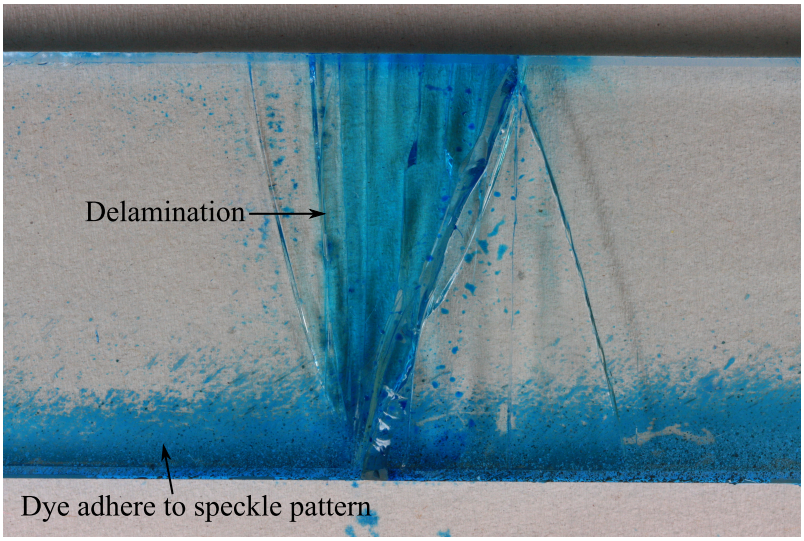

Figure 40: *DPI of 3-point bend specimen. At lower edge of dye adhered to paint used for DIC. Delamination can be seen along glass cracks.*

5.4 Gas gun experiment

Results - pure glass
A total of 7 panes of pure glass were tested in the compressed gas gun. All panes were tested to fracture and the pressure history can be seen in Table 10.

Thickness (mm)	Tank pressure (Bar)
2.87	10 - 15
2.87	10 - 20
2.87	10 - 20
2.87	15 - 20
2.87	20
2.87	20
2.87	20

Table 10: *Pressure history at breakage for glass tested in compressed gas gun.*

Based on the experimental results a conclusion can be drawn that the fracture limit for a standard 2.87 mm glass pane is situated between 10 and 20 bar tank pressure. The fracture of the panes seemed to initiate in two different manners. Two of the panes broke by initiating macro cracks in the middle of the pane where the largest pressure was applied, while five panes initiated fracture by edge cracks growing into the pane. Examples of initiation and final crack pattern can be seen in Figure 41. It can be seen that cracks initiating in the middle of the pane produce a structured crack pattern symmetric around the middle, while the pattern from edge cracks is more chaotic. It is assumed that the cracks initiating from the edges of the pane is due to edge cracks from the production and handling of the panes.

The picture sequence in Figure 42 gives a sense of the time span for crack growth with fracture initiating in the middle. t=0 is set to be the last frame before cracks can be observed, and the glass is totally scattered after about 2.5 ms.

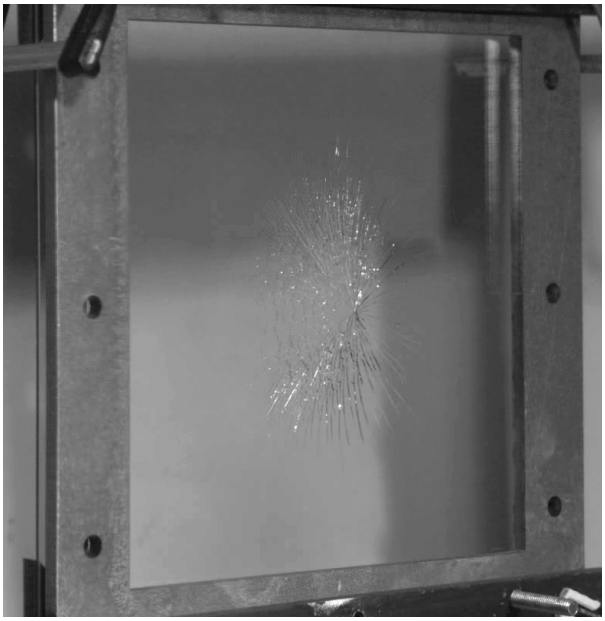

(a) *Cracks initiating in the middle*

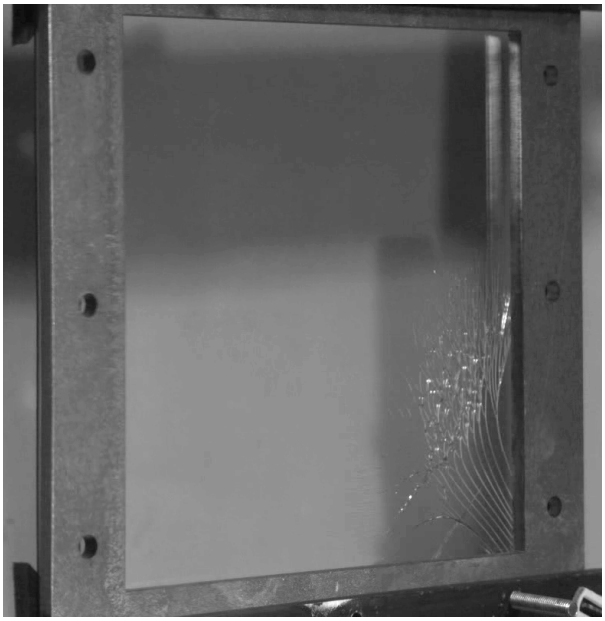

(b) *Cracks initiating from edge*

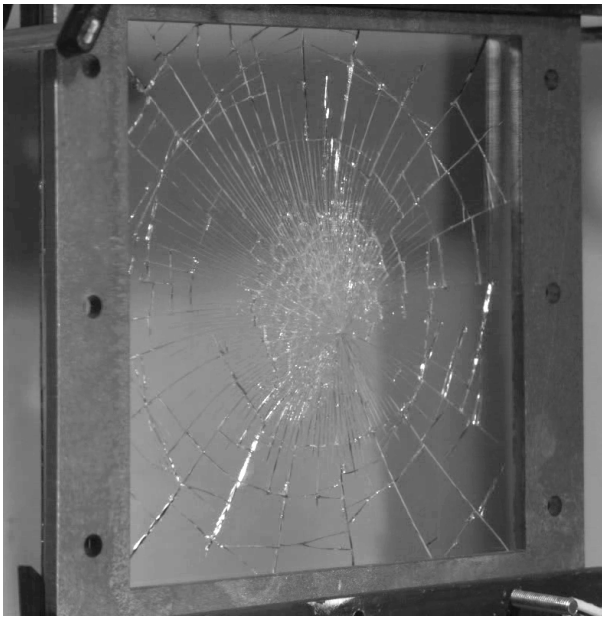

(c) *Crack pattern, initiation at middle*

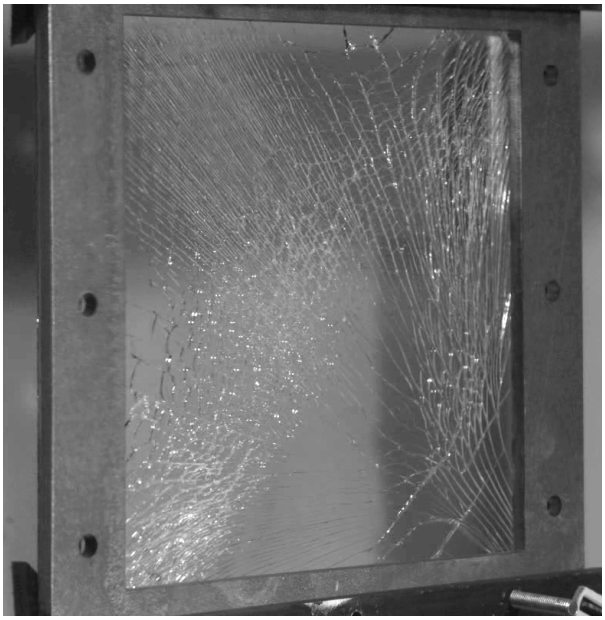

(d) *Crack pattern, initiation at edge*

Figure 41: *Fracture pattern in glass panes with crack initiation in the middle or at the edge.*

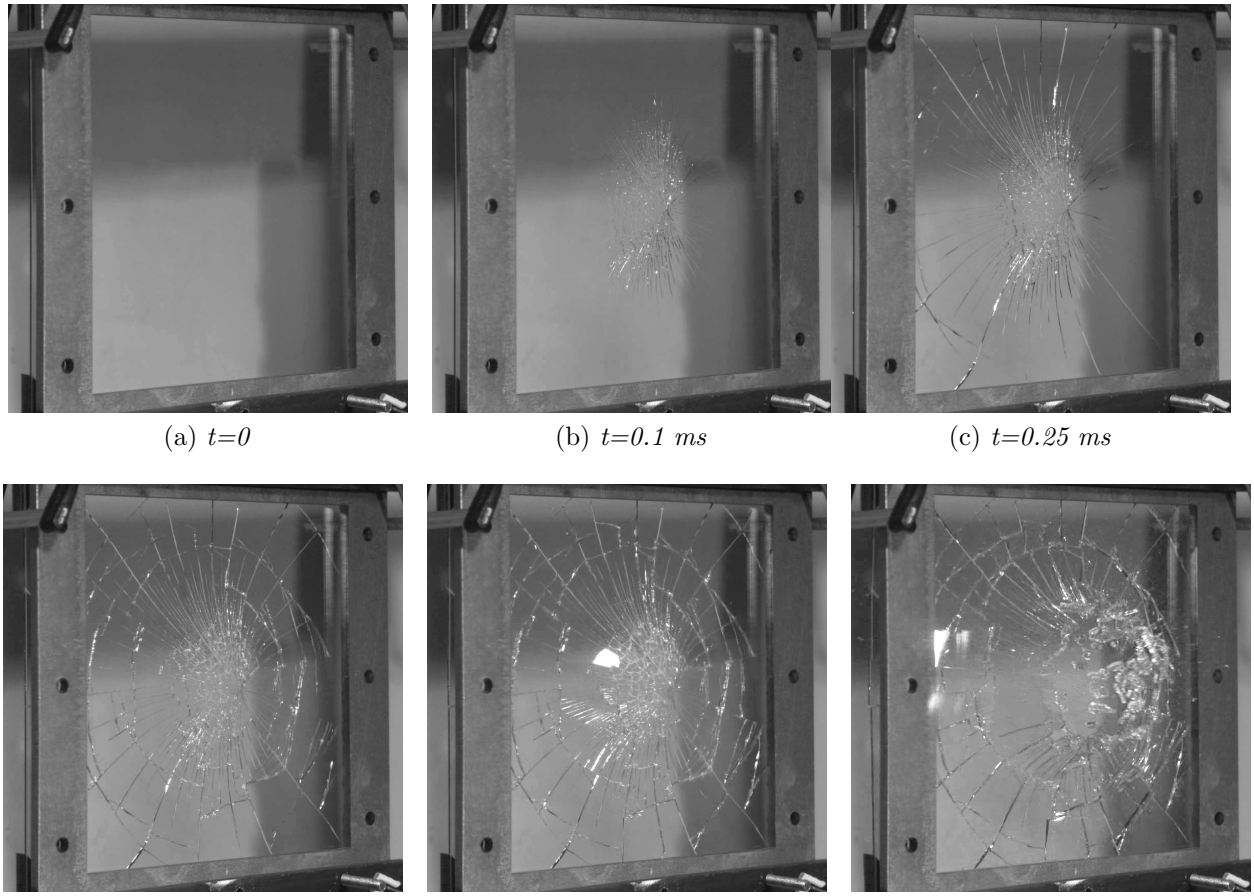

(a) *t=0* (b) *t=0.1 ms* (c) *t=0.25 ms*

(d) *t=0.45 ms* (e) *t=0.9 ms* (f) *t=2.5 ms*

Figure 42: *Time span for crack growth, initiation in middle.*

Results - laminate

Table 11 list pressure history for the two laminated panes tested in the compressed gas gun. The first of the two laminated panes fractured directly at 30 bar tank pressure. Only the glass pane on tension side fractured and the PVB layer kept all glass pieces in place. Figure 43 shows the resulting fracture pattern. The second pane was exposed to shots at 20, 30 and 40 bar tank pressure without fracturing.

Thickness	Tank pressure	Fracture in glass
4.92 mm	30 bar	$\surd$
4.92 mm	20-30-40 bar	$\div$

Table 11: *Pressure history for laminated glass tested in compressed gas gun.*

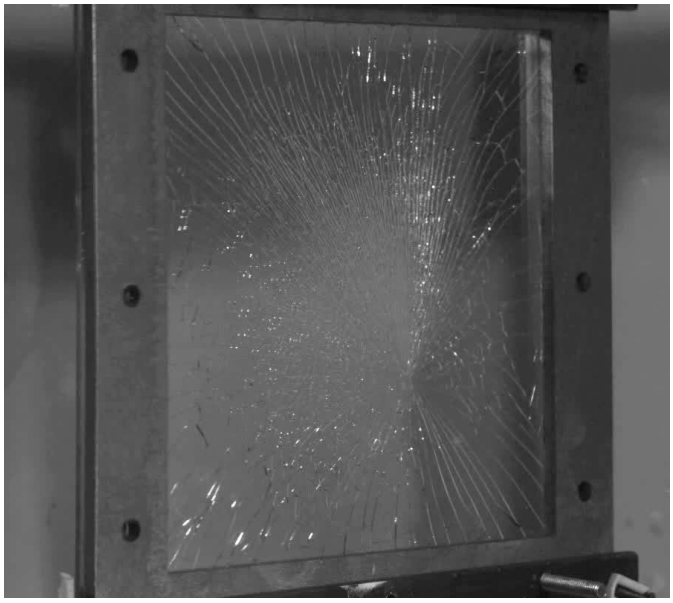

Figure 43: *Fracture pattern of laminated glass.*

Delamination. The laminated plate that fractured in the gas gun experiment was examined with DPI by Ida Westermann (SINTEF). A circular part (diameter=34 mm) of the midsection was taken out form the plate for inspection. Vacuum was used to force intrusion of the contrast dye. As seen in Figure 44, no delamination could be found.

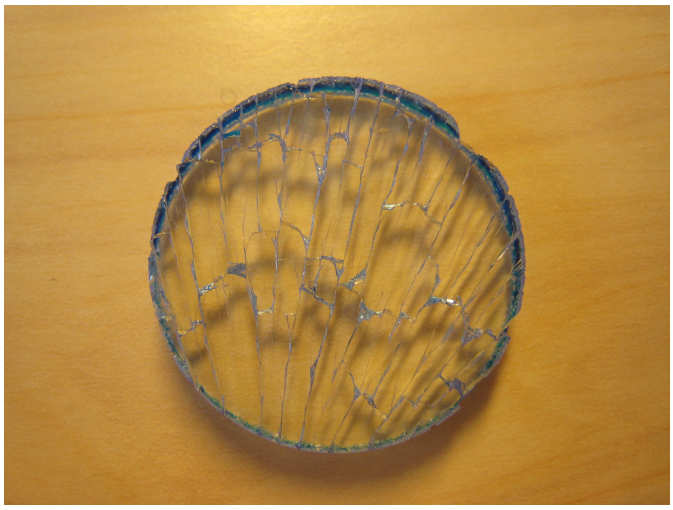

Figure 44: *Sample used for dye penetrant inspection, no delamination can be seen.*

5.5 Blast experiment

Results

Figure 47 show resulting crack patterns for the ten experiments with five different combinations of plate thickness and stand-off. For all ten blast experiments significant glass fracture was observed.

No rupture of PVB or delamination could be found by visual inspection. About the same level of fracture can be seen for similar plate thickness and stand-off distance.

For 125 cm stand-off there was no permanent deformation of the pane, and a nice symmetric pattern can be seen, particularly in Figure 47a. For 60 and 75 cm stand-off, permanent deformations occurred as seen in Figure 45. The permanent deformation is due to plastic deformation of the PVB layer. Small pieces of glass detached from the pane for 75 and 60 cm stand-off as can be seen from Figure 46. From visual inspection it is assumed that this glass is not delaminated from the PVB, but rather that small pieces of glass broke free from the glass pane due to extreme deformation. In the first experiment with 60 cm stand-off (Figure 47i), the plate detached from the frame along left edge.

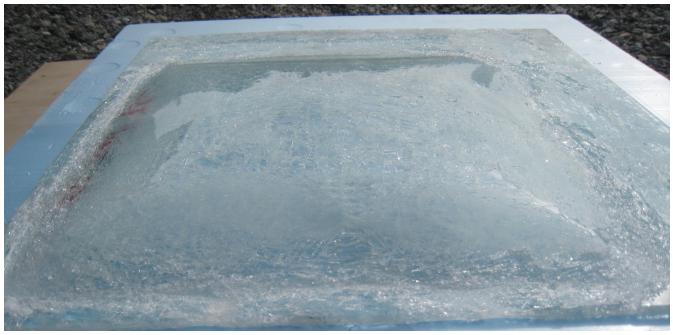

Figure 45: *Permanent deformation of laminated pane, 75 cm stand-off on thick plate.*

Figure 46: *Glass pieces on frame after explosion on thin plate with 75 cm stand-off.*

(a) *125 cm stand-off, thin plate 1.*

(b) *125 cm stand-off, thin plate 2.*

(c) *125 cm stand-off, thick plate 1.*

(d) *125 cm stand-off, thick plate 2.*

(e) *75 cm stand-off, thin plate 1.*

(f) *75 cm stand-off, thin plate 2.*

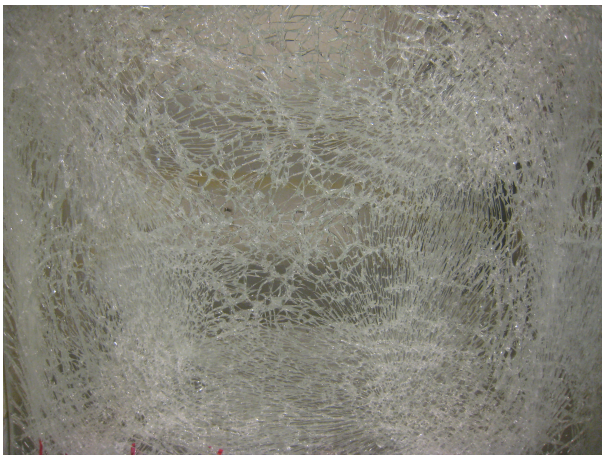

(g) *75 cm stand-off, thick plate 1.*

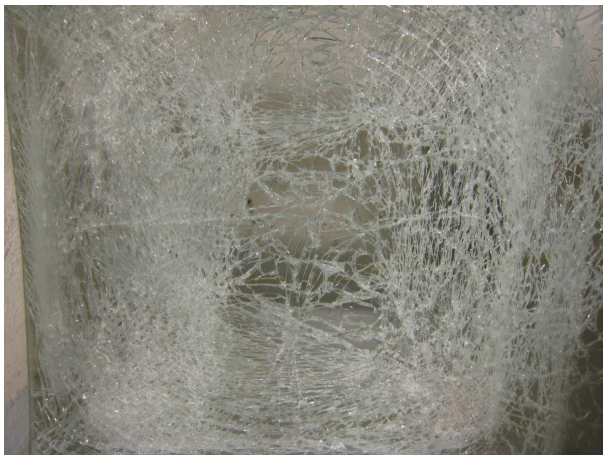

(h) *75 cm stand-off, thick plate 2.*

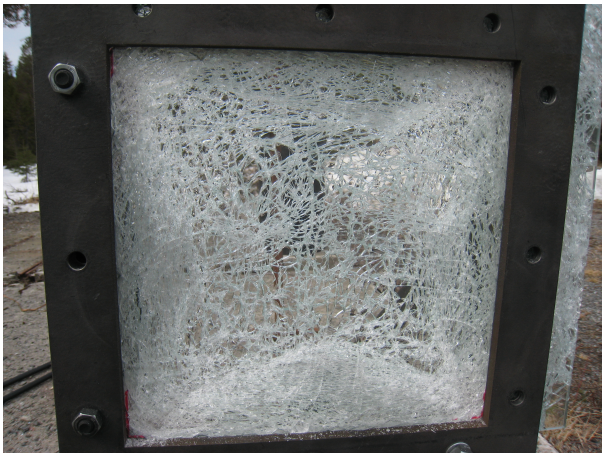

(i) *60 cm stand-off, thick plate 1.*

(j) *60 cm stand-off, thick plate 2.*

Figure 47: *Resulting crack patterns from blast experiments. Pictures for 75 cm stand-off on thick plates were taken after transport back to NTNU, due to low quality of test pictures.*

6 FEM modeling

All FEM simulations were carried out by use of IMPETUS. Due to the simple geometries at hand, all preprocessing was done directly in the input script. In the following subsections the numerical models for 4-point bend on pure glass, 3-point bend on laminated panes, compressed gas gun experiments on pure glass, and the blast experiment is explained. The tension test on precracked laminated glass was not modeled due to the dominating delamination. Input files can be found in Appendix D.1.

6.1 4-point bend - Glass

Setup. The setup of the numerical model of the 4-point bend test can be seen in Figure 48. All geometries were taken from the experimental setup in Figure 14a. In Figure 48 an element size of 1.4×1.1 mm, and two elements over the thickness was used.

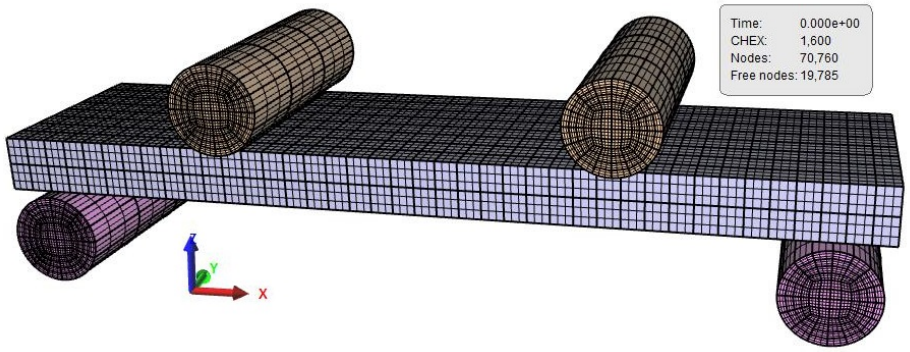

Figure 48: *Model of 4-point bend test used for FEM simulation. Total of 1600 3.order elements.*

Boundary conditions. The two supporting cylinders had all DOF fixed, while the two loading cylinders had z-translation free and rest of DOF fixed. The displacement was set by use of the built in function *smooth_v* in IMPETUS, giving a smooth velocity curve. Thereby the acceleration of the test machine was taken into account, and unwanted dynamic effects were avoided. The punch velocity was scaled so that fracture occurred after 20 ms, compared to 10-20 s in the experiment.

Glass. For glass elastic material behavior, randomly distributed initial damage, and a brittle fracture criterion was defined. The input parameters for glass are given in Table 12. Due to the small dimensions of the 4-point bend test, the new damage algorithm did not give any significant initial damage. To resemble the fracture force in the experimental tests, the maximum stress was lowered from 115 MPa, as found in 4-point bend experiments, to 70 MPa. This affect input values of Δ_0 and D_{max}.

Cylinders. The cylinders were modeled as rigid with density of 7800 kg/m^3.

E^a [14] GPa	ν^a [14] -	ρ^a [14] kg/m^3	m^b -	Δ_0^c -	D_{max}^c -	K_{Ic}^a[2] MPa$\sqrt{m}$	t_c^c -	α_c^c -
72	0.22	2530	5.58	0.657	0.171	0.75	1e-5	1

Table 12: *Material parameters used for glass in 3 and 4-point bend test. Superscript: a - Found in literature, b - calculated from experiments, c - approximated to match experimental response.*

6.2 3-point bend - Laminate

Setup. The setup of the model used to simulate the 3-point bend test on laminated glass can be seen in Figure 49. All geometries were similar to the experiment and shown in Figure 17. The model in Figure 49 has 1680 second order elements with size 5×5 mm, and one element over the thickness of each layer.

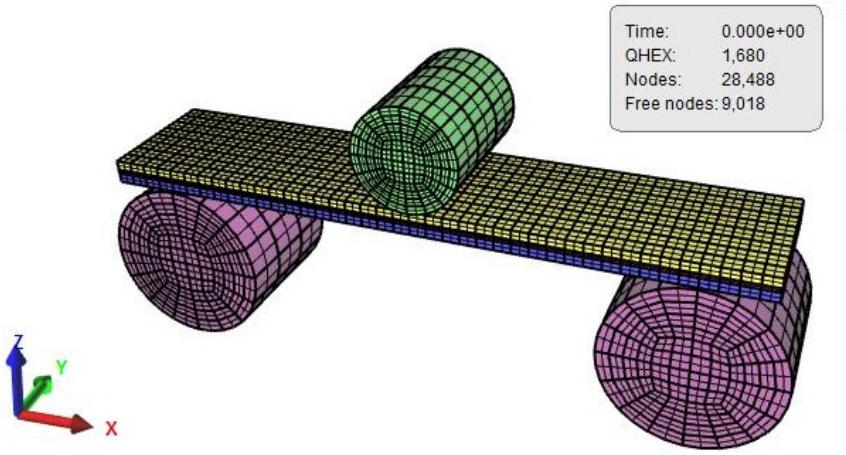

Figure 49: *Model of 3-point bend test used for FEM simulation. Total of 1680 second order elements.*

Boundary conditions. The boundary conditions for support and load cylinders were equal as those of the 4-point bend model. The punch velocity was scaled so that the critical deformation was done in 15 ms, compared to 3-140 seconds for the experimental tests.

Glass. For glass the same parameters as in the 4-point bend model was used, see Table 12.

PVB. Due to the quasi-static loading and relatively short test period, the rate dependency and viscoelastic effects of PVB were neglected. An elastic material behavior was thereby assumed, and input values are given in Table 13.

E[29]	ν[14]	ρ [14]
1.56 MPa	0.485	1100 kg/m^3

Table 13: *Material parameters used for elastic PVB behavior. All parameters found in literature.*

Cylinders. The cylinders were modeled as rigid with density of 7800 kg/m^3.

6.3 Gas gun experiment

Setup. A model of the glass plate used in the gas gun experiments was built up of 4 608 third order elements with size of 6.25×6.25 mm and one element in thickness. The rubber strip used in the experiments was modeled on the backside of the glass pane and merged to the glass nodes.

Boundary conditions. The back surface of the rubber strip was restrained in z-direction, approximating the contact with the close to rigid frame in the experimental setup. Figure 50 shows the rubber strip on the backside of the plate.

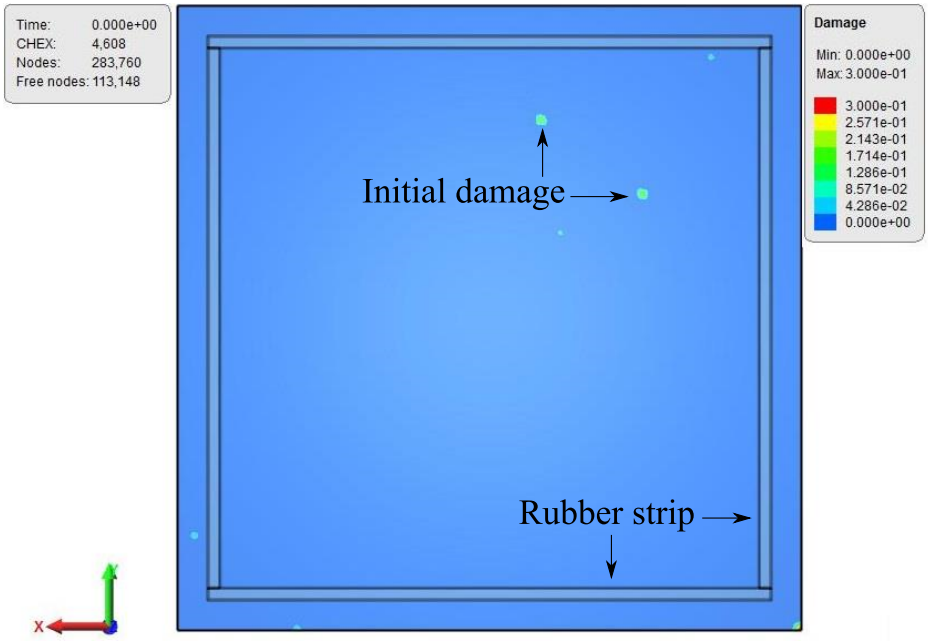

Figure 50: *Rubber strip on backside of glass pane and initial damage.*

Pressure. For the appliance of pressure, the plate was divided into five sections. Figure 51 shows the pressure areas for one quarter of the plate. Only data from the horizontal pressure transducers was used. Pressure data from sensor one was applied to the red area, data from sensor 2 to the blue area and so on. The change from one data set to the next happened at half distance between sensor points. The green field in Figure 51 is relatively large since the last measuring point in the horizontal direction was 125 mm from the center, while the length of 1/4 of the pane is 200 mm. Filtered pressure data was used, and the arrival time for the pressure was removed to reduce computation cost.

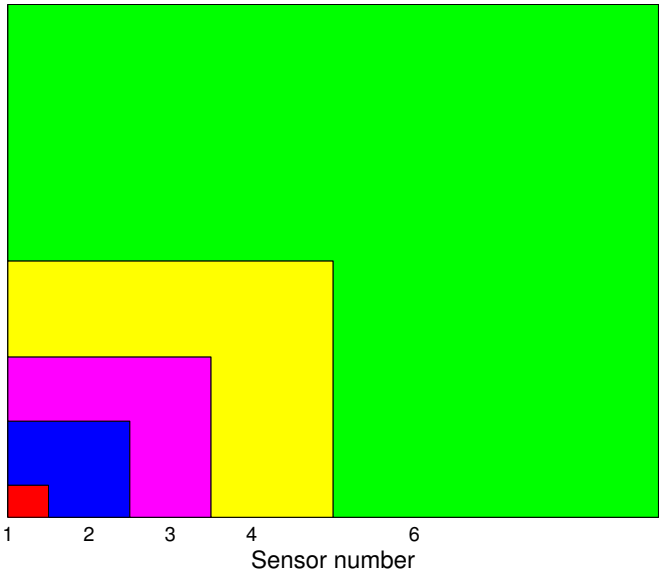

Figure 51: *Distribution of pressure data on 1/4 of plate. Sensor number 5 was not used in the measurement.*

Glass. The rate dependency of glass indicated in previous sections was neglected, and almost the same parameters as for the bend test models were used for the glass in the gas gun model. Due to greater specimen size, initial damage was distributed with use of the calculated values for Δ_0 and D_{max}. The resulting values are given in Table 14. Figure 50 shows distributed initial damage.

E^a [14] GPa	ν^a[14] -	ρ^a[14] kg/m^3	m^b -	Δ_0^b -	D_{max}^b -	K_{Ic}^a[2] MPa$\sqrt{m}$	t_c^c -	α_c^c -
72	0.22	2530	5.58	0.4	0.496	0.75	1e-5	1

Table 14: *Material parameters used for glass in gas gun and blast model. Superscript: a - Found from literature, b - calculated from experiments, c - approximated to match experimental response.*

Rubber strip. The rubber strip behavior was assumed elastic with E of 10 MPa, ν of 0.49 and ρ of 1522 kg/m^3.

6.4 Blast experiment

A model of the blast experiment was built with 12 200 2.order elements. An element size of 6.67×6.67 mm and one element in thickness was used for the laminated pane. The model can be seen in Figure 52. Only the response of thick plates (2.9 - 1.4 - 2.9 mm) was simulated.

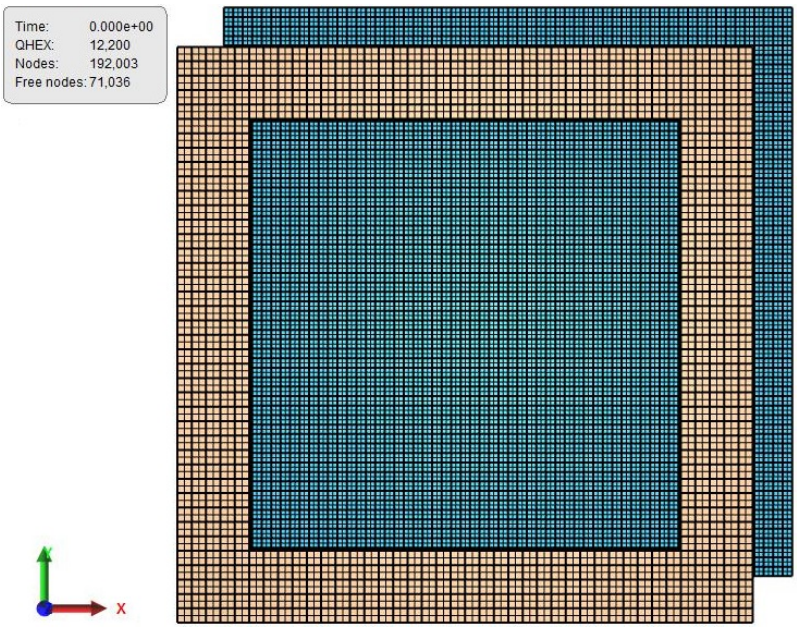

Figure 52: *Numerical model for blast experiment. The frame was assumed rigid and got all DOF fixed. Total of 12 200 2.order elements*

Boundary conditions. All DOF of the rigid frame were fixed. The glass plies were merged to the frame so that overlapping nodes had the same displacement. The blast loading for 125 cm and 75 cm was introduced in two different manners. First the measured side-on pressure presented in Section 4.5 was applied uniformly to the front of the pane. To account for the difference between side-on and reflected pressure, the side-on pressure was multiplied by a factor 7. Secondly the built-in IMPETUS functions *PBLAST was used to calculate the load from the C4 explosives used in the experiment. In *PBLAST the cylindrical C4 charge and surrounding air is defined by particles. With detonation, the C4 particles are given an impulse which is transferred to the air particles by collision. A throughout description of *PBLAST is given in [6].

Material parameters. For glass the same material parameters as for the gas gun model was used, see Table 14. For PVB the strain rate sensitivity was assumed to be dominant. Therefore the Johnson-Cook (JC) material parameters found by Hooper et al. [14] were used. The input parameters for the JC model are given in Table 15. The frame was modeled as a rigid material with density of 7 800 kg/m^3.

E	A	B	C	n
0.53 GPa	6.72 MPa	10.6 MPa	0.248	0.303

Table 15: *Material parameters for JC model of PVB. All parameters found in [14].*

Plastic straining of PVB. As reported in Section 5.5 permanent deformations occurred in the laminated plates for 60 and 75 cm stand-off. To be able of predicting permanent deformations of laminated panes in the numerical model, special care must be taken. The situation of glass and

PVB merged together, and node splitting only allowed in the glass layer is shown in Figure 53a. The lower nodes of the two glass elements are connected in the common PVB node, and the glass elements can therefore not separate completely. The behavior of the total pane will therefore be purely elastic, dominated by the glass behavior. But if the node in the PVB layer is allowed to split, as shown in Figure 53b, the two glass elements can separate completely, and plastic straining of the PVB is enabled. To investigate the effect of node splitting in a thin layer of PVB, both 75 cm and 125 cm stand-off calculations were performed with and without node splitting in PVB.

It should be noted that micro cracking of PVB is not documented from the physical tests, but is merely a theory on how the plastic straining of PVB is possible.

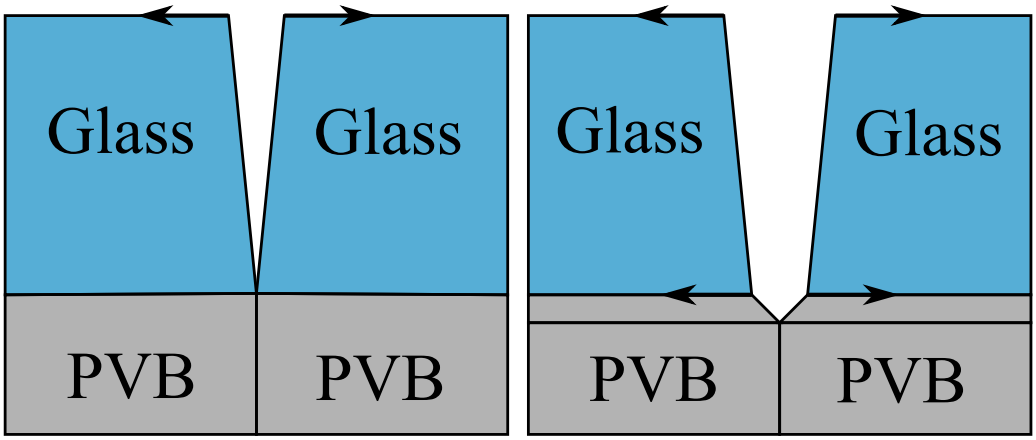

(a) *Node splitting only in glass*

(b) *Node splitting in glass and thin layer of PVB*

Figure 53: *Illustration of node splitting of thin PVB layer to allow plastic straining of PVB layer. Arrow indicates node splitting.*

7 FEM results

The results from the FEM models presented in the preceding section are presented and discussed herein. For the 3-point bend test the results from a sensitivity study of mesh density, time scaling, and element order are included.

7.1 4-point bend - Glass

Force-displacement
The resulting force-displacement curve for the 4-point bend model can be seen in Figure 54. The fracture displacement for the FEM model equals the average fracture displacement for the experimental tests. The stress-strain results from experiments and numerical simulation are seen in Figure 55. Here the difference in Young's Modulus between numerical model and experimental results can be seen clearly.

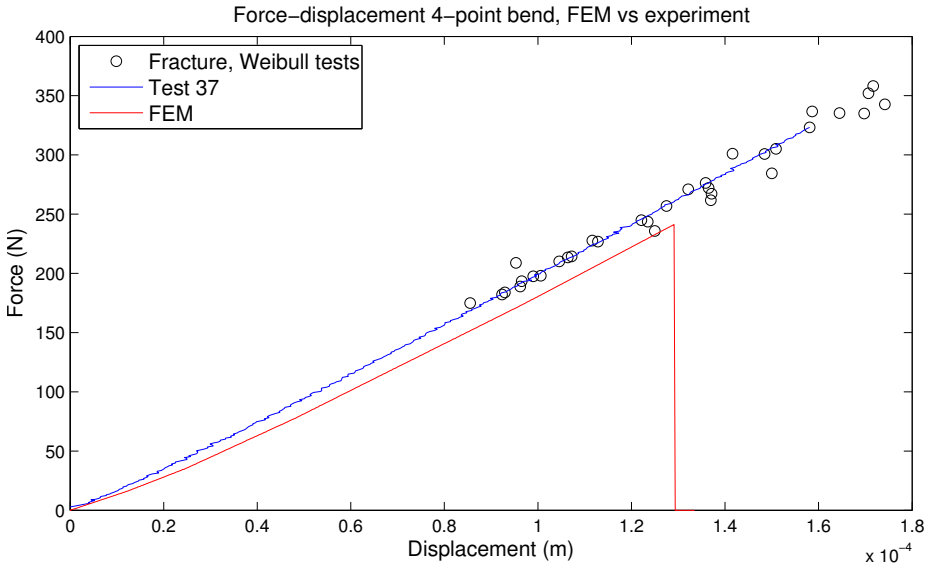

Figure 54: *Force-displacement for 4-point bend simulation, compared with curve for test 37 and fracture point for all tests used for Weibull fit.*

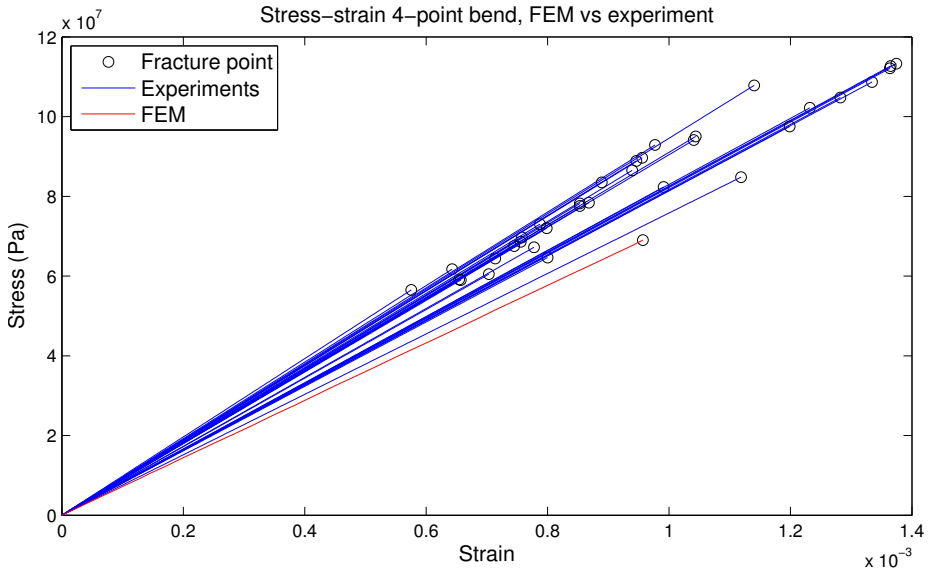

Figure 55: *Stress-strain for 4-point bend simulation compared with results in tests used for Weibull fit.*

7.2 3-point bend - Laminate

Sensitivity study
A sensitivity study of the laminated model for 3-point bend was performed to study the sensitivity to mesh size, time scaling, and element order. The setup presented in the preceding section was taken as a basis model and one parameter was increased or decreased in succeeding simulations, leading to a total of 6 additional models.

Mesh sensitivity. The mesh was changed from 1680 to 855 and 2880 second order elements and resulting force-displacement plots can be seen in Figure 56. The number of elements does not influence the stiffness of the model, but with 855 elements an unphysical sudden increase of force can be seen in relation to breakage of the glass panes. There is only a slight difference in fracture point between 1680 and 2880 elements models. Based on the three simulations the model does not seem to have any significant mesh dependency, and 1680 second order elements is a good trade-off between accuracy and computational cost[8].

[8]Computation time with Intel i5-450M CPU for mesh sensitivity study was 55m - 2h 34m - 4h 54m.

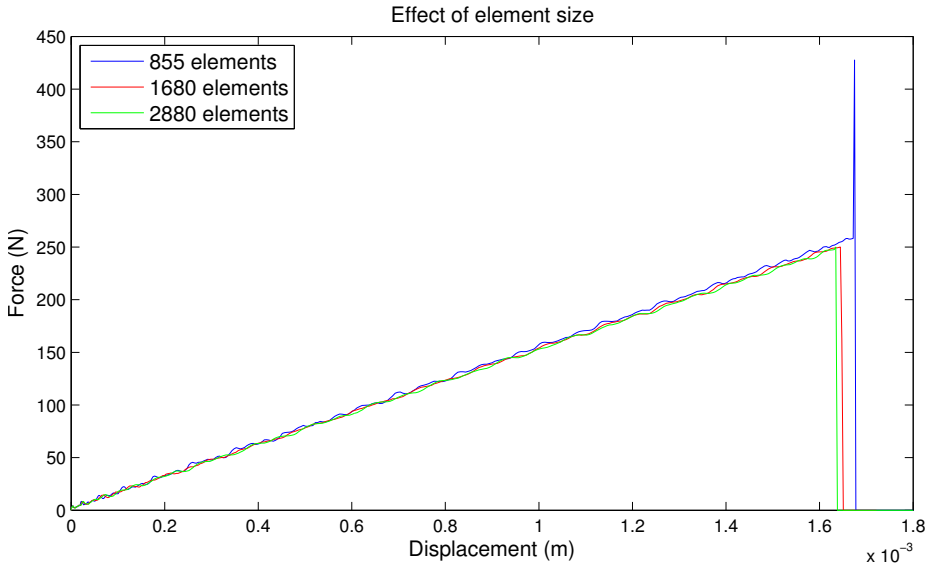

Figure 56: *Mesh sensitivity of 3-point bend model.*

Time scaling. For the effect of time scaling, simulations with total time of 5 and 50 ms were performed in addition to the 15 ms basis model. The resulting force-displacement plots can be seen in Figure 57. Due to increased inertia effects, oscillations in the force level can be seen to increase for shorter simulation time. The difference from 15 to 50 ms is small, and 15 ms seems to be a good trade-off between accuracy and computational cost[9].

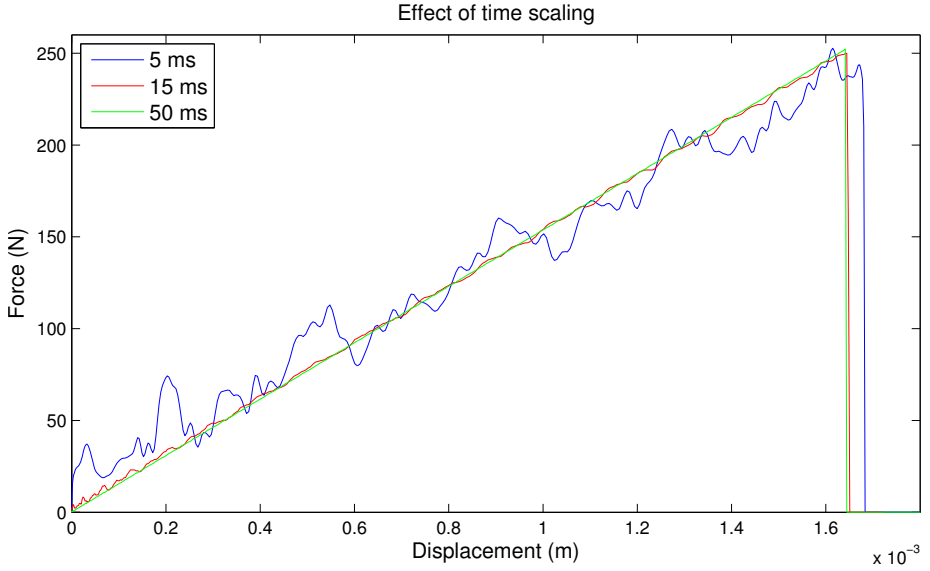

Figure 57: *Time scaling sensitivity, 3-point bend model.*

Element order. Resulting force-displacement plots for changed element order can be seen in Figure 58. It can be seen from Figure 58 that the first order elements are overly stiff compared

[9]Computation with Intel i5-450M CPU for time scaling study was 50m - 2h 34m - 8h 16m

with second and third order elements. Second and third order elements is seen to have the same stiffness, but third order elements led to fracture at a force 15 % (38 N) lower than for the second order elements. Due to the significantly lower fracture force, third order elements are seen as best-practice despite higher computational cost[10].

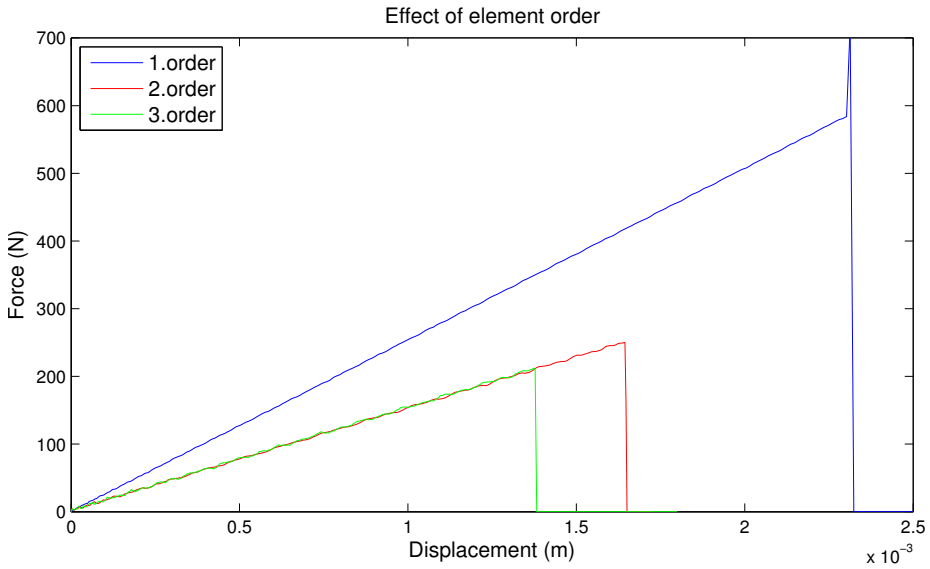

Figure 58: *Effect of element order, 3-point bend model.*

Results - best model
A total of 1600 third order elements and a time scaling to 15 ms simulation time was found to be best-practice for modeling of the 3-point bend problem.

Force-displacement. In Figure 59 the force-displacement from best-practice simulation and experimental data is compared. To enhance readability only the curve for Test 4 is shown, while point of first fracture is indicated for the other tests. It is seen that the FEM model predicts the force-displacement behavior of Test 4 with good accuracy.

[10]Computation time with Intel i5-450M CPU for element order study was 15 m - 2h 34m - 5h 3m.

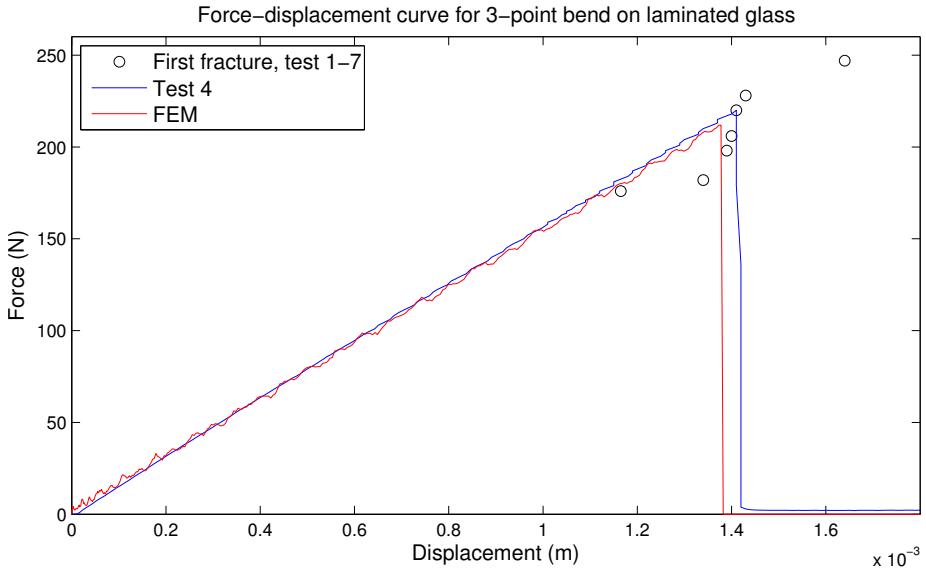

Figure 59: *Force-displacement curve for experiment and simulation, 3-point bend.*

Strain level. Figure 60 shows the distribution of shear strain in the FEM model. The shear strain is symmetric around loading point, and a clear resemblance with DIC measurements (Figure 37) can be seen. The shear strain from "Element line B" in Figure 60 is plotted in Figure 61. Similarity with first principal strain calculated from DIC measurements (Figure 38) can be seen, with both plots having a maximum close to 0.04.

Figure 60: *Distribution of shear strain (ϵ_{xz}) from FEM simulation. Strain from element line B is plotted in Figure 61. Experimental results seen in Figure 37.*

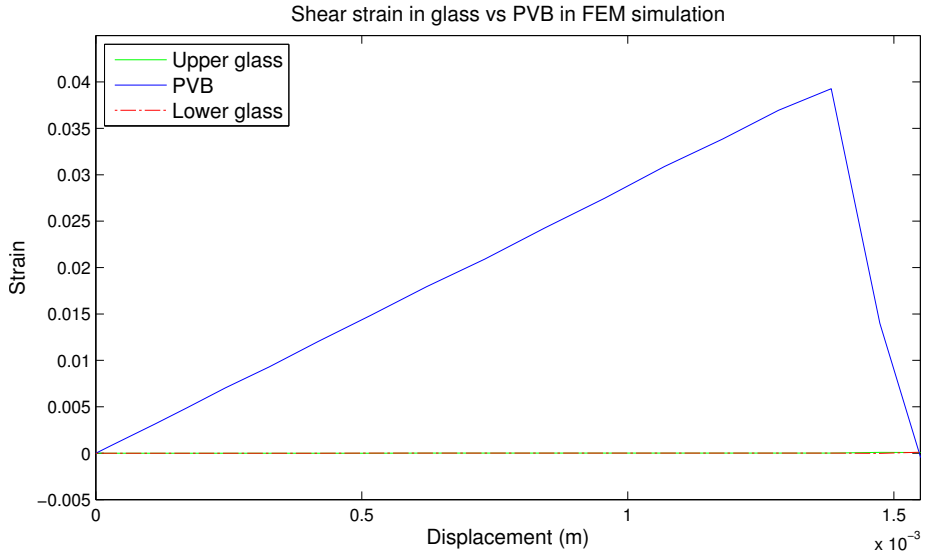

Figure 61: *Plot of shear strain (ϵ_{xz}) in glass and PVB from FEM simulation. Element location shown in "Element line B" in Figure 60. PVB strain drops when glass plies fail. Experimental results seen in Figure 38.*

7.3 Gas gun experiment

The glass behavior in the gas gun model was calculated for 5, 10, and 20 bar tank pressure. The resulting fracture pressures are listed in Table 16. Fracture was correctly predicted for 20 bar tank pressure, and incorrectly for 10 bar tank pressure. To avoid shattering of the glass, a 5 bar tank pressure had to be used in the numerical model. The reason for the numerical model to incorrectly predict fracture at 10 bar tank pressure can be due to errors in the applied pressure. The pressure was measured on a close to rigid frame leading to a higher pressure than what would effectively load a deformable plate. In addition, symmetric loading was assumed and there was an unphysical pressure discontinuity from one pressure zone to the other in the applied pressure.

Tank pressure	Experimental fracture	FEM Fracture pressure	FEM Peak pressure
5 bar	÷	÷	173 kPa
10 bar	÷	186 kPa	306 kPa
20 bar	√	175 kPa	293 kPa

Table 16: *Experimental vs numerical fracture point. Pressure data from sensor 1.*

Due to high computational cost and long loading period, the 5 bar model was stopped after the peak pressure was reached. Fracture of the pane can therefore still happen for longer simulation times, but based on the deformation histories shown in Figure 62 it is assumed not to. For 20 bar tank pressure the plate deformed in z-direction directly to failure. For 5 bar on the other hand, the mid-point of the plate had multiple elastic oscillations during the simulation.

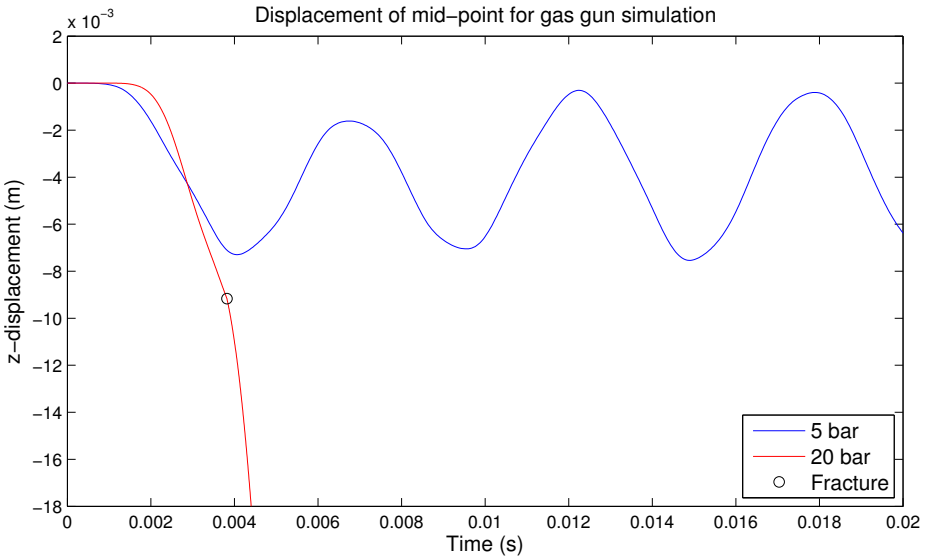

Figure 62: *Displacement history for mid-point with 20 bar and 5 bar tank pressure.*

Fracture pattern. Fracture pattern and time scale of crack growth for 20 bar tank pressure can be seen from Figure 63. Time from first crack initiation to fully fractured plate of 0.2 ms is in correspondence to the experimental results (see Figure 42). The symmetry seen in the experimental crack patterns was not captured in the numerical prediction.

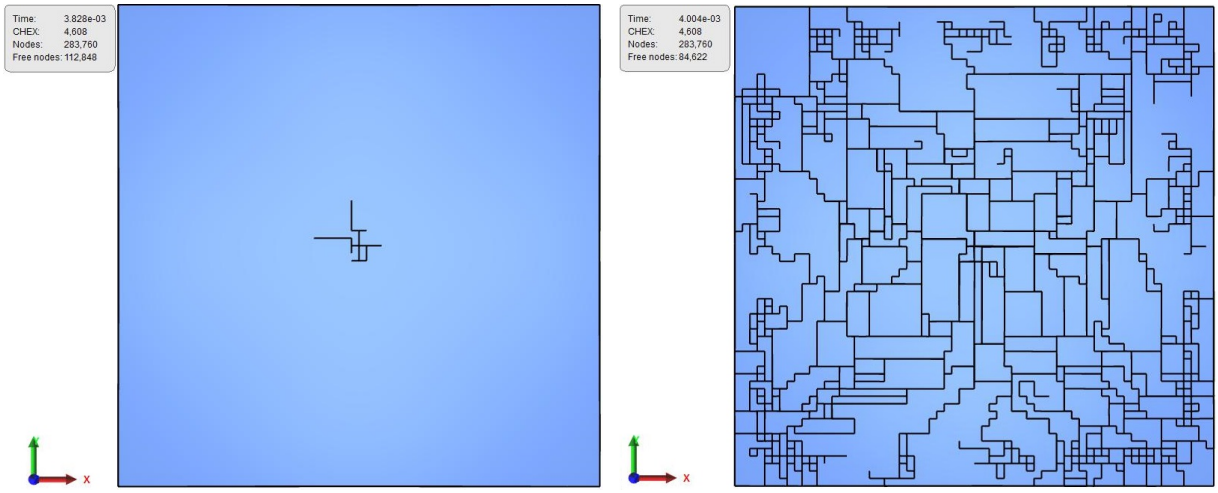

(a) *t=0* (b) *t=0.2 ms*

Figure 63: *Resulting crack pattern from numerical simulation. 20 bar tank pressure.*

7.4 Blast experiment

Due to high computational cost, all blast simulations were run in Sweden on the computers of IMPETUS Afea AS.

Pressure curve - Crack pattern

The crack patterns after the simulation time of 8 ms are shown in Figure 64. The results for pressure curve loading with 125 cm stand-off is seen in Figures 64a-64d, while 75 cm stand-off results are shown in Figures 64e-64h. For both load cases the introduction of node splitting in the interlayer leads to increased fracture in the glass plies. For 75 cm stand-off and no PVB cracking, the back glass pane (Figure 64f) has largest crack density in the central region of the plate. This is is contrast to the general observations from the experiments, where the largest crack density was along the borders of the frame.

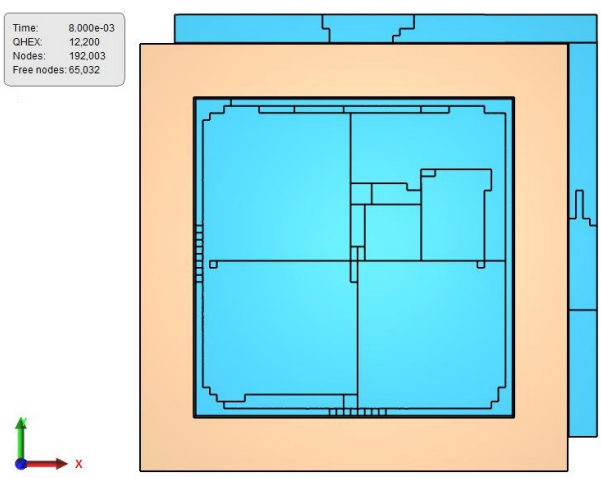

(a) *Pressure side 125 cm - No PVB cracking.*

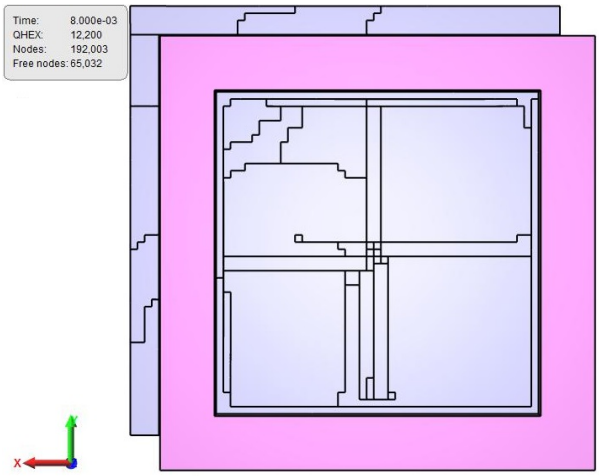

(b) *Back 125 cm - No PVB cracking*

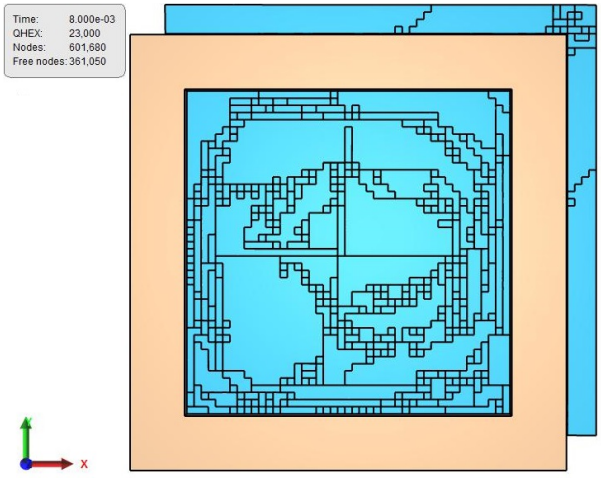

(c) *Pressure side 125 cm - PVB cracking*

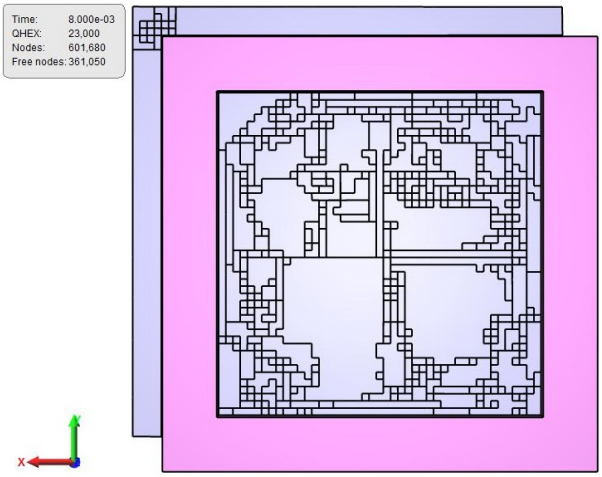

(d) *Back 125 cm - PVB cracking*

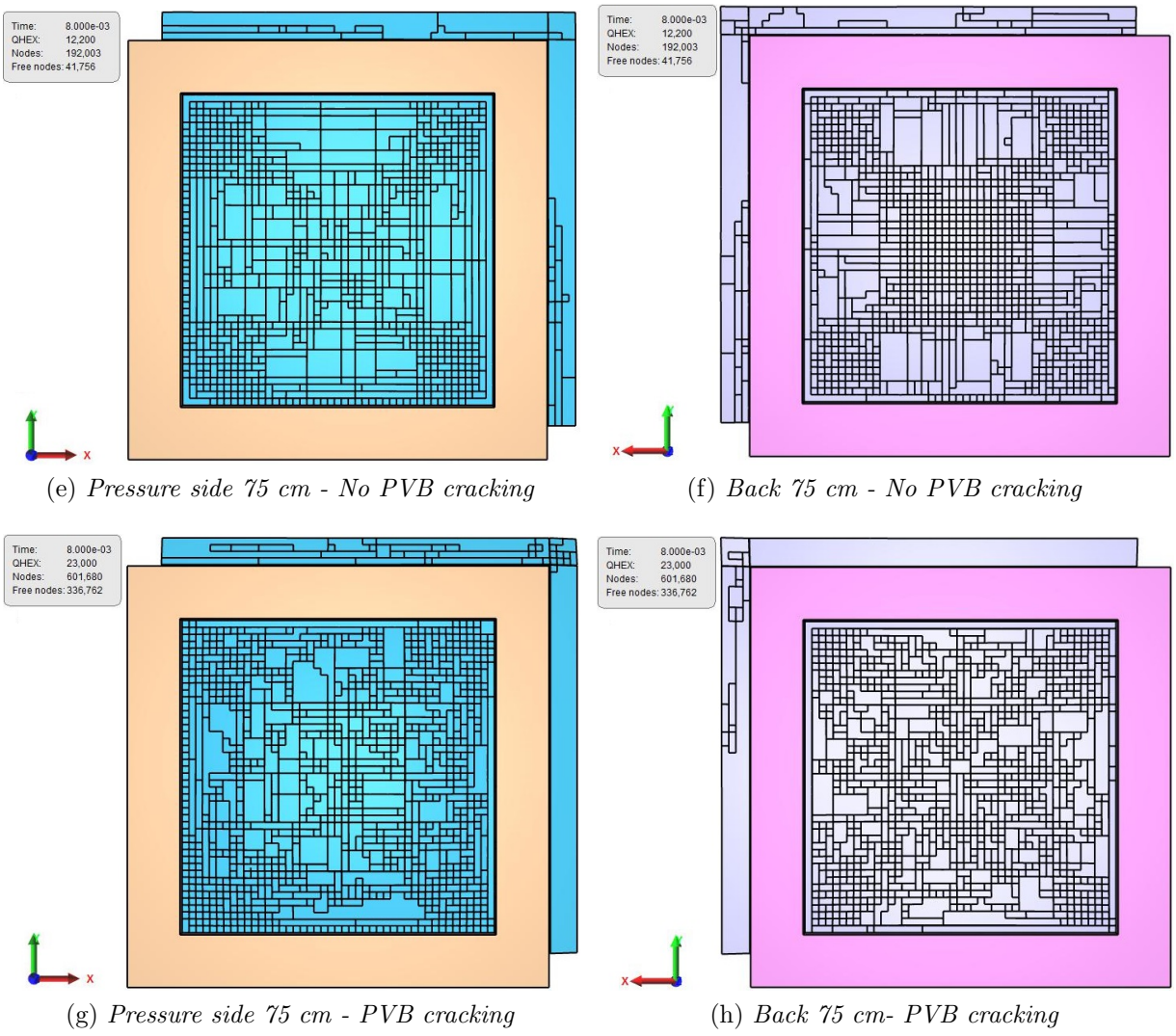

(e) *Pressure side 75 cm - No PVB cracking*

(f) *Back 75 cm - No PVB cracking*

(g) *Pressure side 75 cm - PVB cracking*

(h) *Back 75 cm- PVB cracking*

Figure 64: *Resulting crack pattern from numerical simulation with load curve for 75 and 125 cm stand-off. Results both with and without micro cracking in PVB can be seen.*

Pressure curve - z-displacement

The progress of z-displacement for the mid-point of the pane is shown in Figure 65 for all four simulations. It should be noted that no numerical damping was included in the simulations, and elastic deformations will therefore not be damped out. For both stand-off distances the enabled plastic straining of PVB leads to decreased oscillation frequency. For 75 cm stand-off the node splitting in the PVB layer also enables significantly larger z-displacement than the elastic situation. Its maximum displacement (including plastic and elastic deformation) of 0.01 m is still small compare to the experimental situation shown in Figure 45. Unfortunately the simulation is run to short to tell its level of constant plastic deformation (this would be the mean displacement of the purely elastic oscillation). A plastic strain level of approximately 0.0025 and 0.08 was obtained in the PVB layer for 125 and 75 cm stand-off respectively. As assumed no plastic straining occurred in the models without node splitting in PVB.

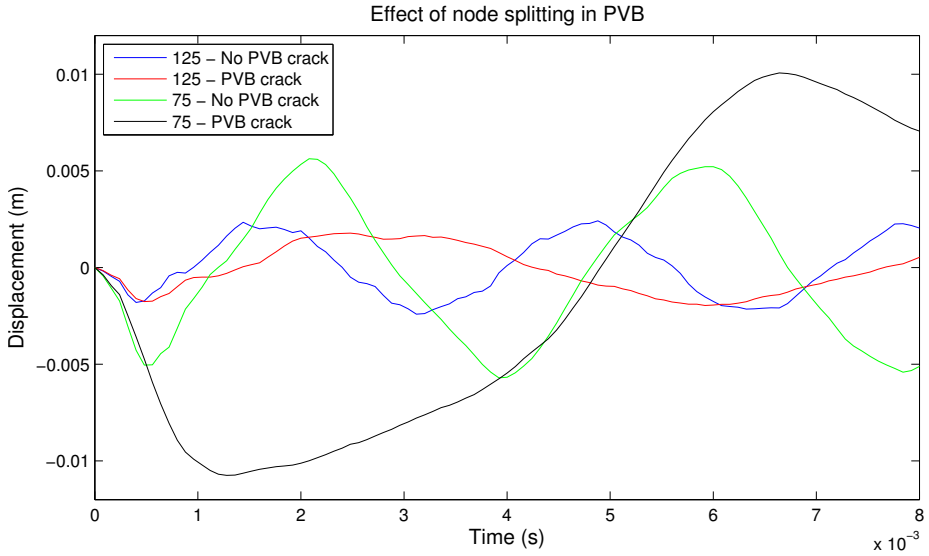

Figure 65: *Displacement history for mid-point in blast simulations, 125 cm stand-off.*

***PBLAST**

For the calculations with *PBLAST, the large scaled distance (small charge and large stand-off) combined with brittle material behavior resulted in dominating numerical noise. Therefore no useful results were obtained for the laminated glass plate. However, in combination with a rigid plate *PBLAST was used to find an estimate for the head-on pressure that would result from the explosion with 125 cm stand-off. From *BLAST the total positive impulse was found to be 168 Ns/m^2 compared to 51 Ns/m^2 for the measured pressure curve. This is a clear indication that the pressure measurements from 2009 is not truly representative for the pressure situation obtained in the blast experiments in this thesis. The presented results found with measured pressure curves on laminated panes should therefore be seen as a case study for the effect of node splitting in PVB, and not as a valid prediction of the experimental results.

8 Concluding remarks

In this thesis experimental and numerical investigations of laminated glass were performed. This section present concluding remarks from the two areas.

For the **4-point bend experiment** unreliable high and varying values for E were found. This led to an assumption that the calculated fracture stress was also biased with unphysical variations. The resulting Weibull fit for fracture strength was not in consistency with experimental results. The mean fracture strength increased from 84 to 93 MPa by increasing the deformation rate from 0.5 mm/min to 1.9 mm/min, indicating a rate dependency of glass strength.

The response of laminated glass exposed to quasi-static **3-point bending** was found to be close to the lower bound of beam behavior, indicating that the PVB interlayer transfers only small amounts of shear forces between the two glass plies.

Significant **delamination** between glass and PVB was found in quasi-static experiments. From dynamic gas gun experiments, no delamination could be found with DPI. This indicates a rate dependency of the PVB-glass adhesion.

In the **gas gun experiments** on pure glass the panes were intact at 10 bar tank pressure, while shattering for 20 bar tank pressure.

For the **blast experiments** on laminated glass, significant glass fracture was seen in all experiments. No PVB rupture or glass-PVB delamination could be found by visual inspection. Significant plastic deformation of PVB was observed for 75 and 60 cm stand-off distance.

The **3-point bend model** showed good resemblance of experimental stiffness for an elastic material behavior of PVB. Due to strong area dependence of the new initial damage criterion, the fracture stress of glass was lower from the 4-point bend result of 115 MPa to 70 MPa to obtain a reasonable fracture point. The first principal strain in PVB found from the DIC measurements was predicted in the FE model to be dominated by shear strain.

The **gas gun model** predicted fracture correctly for 20 bar tank pressure, and incorrectly for 10 bar tank pressure. To avoid shattering of the glass plate, a 5 bar tank pressure had to be used in the model.

In the **blast model** a JC material model for PVB was used to account for the large strain rate. Node splitting was introduced in the PVB layer to enable plastic deformation of the interlayer. Plastic deformation of PVB seemed to be vital to obtain a reasonable response of the laminated plate exposed to blast loading.

9 Further work

Blast loading on laminated glass panes is a complex problem, and many questions are still unanswered. More knowledge of material properties and component behavior is needed to be able of accurately simulate the behavior of laminated glass under blast loading. This section presents aspects the author thinks should be given priority in the further work with on laminated glass exposed to blast pressure.

- Redo fracture experiments on glass to find parameters for Weibull distribution with better fit to experimental data.
- Investigate rate dependency of fracture strength in glass.
- Investigate how the lamination process affects the mechanical properties of PVB. If mechanical properties are not affected by lamination, material testing of PVB would be simplified.
- Do blast experiments with DIC measurements to get pane deformation. Measurements of head-on pressure should also be performed. Stand-off distance should be increased to find an approximation of the critical distance where cracks occur in the glass panes.
- Do experiments to document how glass-PVB adhesion strength is influenced by loading rate.
- Examine plates from blast experiments to check physical validity of introducing micro cracks in PVB for numerical simulations.
- Improve the initial damage algorithm to reduce its strong area dependency.

References

[1] Anderson T.L., Fracture Mechanics, Fundamentals and Applications, Third Edition, *Taylor and Francis*, 2005.

[2] Ashby M.F., Jones D.R.H., Engineering Materials 1 - An Introduction to Properties, Applications, and Design (4th Edition), *Elsevier*, 2012.

[3] Bauchau O.A., Craig J.I., Structural Analysis, *Springer*, 2009

[4] Butchart C., Overend M., Delamination in fractured laminated glass, *International Conference at glasstec, Düsseldorf, Germany*, 2012.

[5] Børvik T., Hopperstad O.S., Langseth M., Malo K.A., Effect of target thickness in blunt projectile penetration of Weldox 460 E steel plates, *International Journal of Impact Engineering*, Vol.28, 431-464, 2003.

[6] Børvik T., Olovsson L., Hanssen A.G., Dharmasena K.P., Hansson H., Wadley H.N.G., A discrete particle approach to simulate the combined effect of blast and sand impact loading of steel plates, emphJournal of the Mechanics and Physics of Solids, Vol.59, 940-958, 2011.

[7] Cook R., Malkus D., Plesha M., Witt R., Concepts and Applications of Finite Element Analysis, Fourth edition, *Wiley*, 2002.

[8] C1161-02 Standard Test Method for Flexural Strength of Advanced Ceramics at Ambient Temperature, *ASTM International standard*, 2002.

[9] C1239-07 Standard Practice for Reporting Uniaxial Strength Data and Estimating Weibull Distribution Parameters for Advanced Ceramics, *ASTM International standard*, 2007.

[10] Engineering Design Handbook. Explosions in Air. Part one. *U.S Army Materiel Command,* 1974.

[11] Fagerholt E., Field measurements in mechanical testing using close-range photogrammetry and digital image analysis, *PhD Thesis NTNU* 2012

[12] Griffith A.A., The phenomena of rupture and flow in solids, *Philosophical Transactions of the Royal Society of London Series A*, Vol.221, 163-198, 1921.

[13] Iwasaki R., Sato C., Latailladeand J. L., Viot P., Experimental study on the interface fracture toughness of PVB/glass at high strain rates, *International Journal of Crashworthiness*, Vol.12, 293-298, 2007.

[14] Hooper P.A., Sukhram R.A.M., Blackman B.R.K., Dear J.P., On the blast resistance of laminated glass, *International Journal of Solids and Structures*, Vol.49, 899-918, 2012.

[15] Hopperstad O.S., Børvik T., Mechanics of Materials, *Lecture notes in TKT 4135 at NTNU*, 2012.

[16] *https://upload.wikimedia.org/wikipedia/commons/e/e7/Fracture_modes_v2.svg*, downloaded 6.4.2003.

[17] Kalstad S., Nord T.S., Fragmentation of Metallic Materials During Impact, *Master Thesis NTNU*, 2011.

[18] Karlsen T., Kjølseth A.B., Fragmentation of Metallic Materials During Impact, *Master Thesis NTNU*, 2012.

[19] Kranzer C., Gürke G., Mayrhofer C., Testing of Bomb Resistant Glazing Systems Experimental Investigation of the Time Dependent Deflection of Blast Loaded 7.5 mm Laminated Glass, *Glass Processing Days,* 2005.

[20] Larcher M., Solomos G., Casadei F., Gebbeken N., Experimental and numerical investigations of laminated glass subjected to blast loading, *International Journal of Impact Engineering*, Vol.39, 42-50, 2012.

[21] Larcher M., Solomos G., Laminated glass loaded by air blast waves - Experiments and numerical simulations, *JRC Technical Notes*, 2010.

[22] Larcher M., Pressure-Time Functions for the Description of Air Blast Waves, *JRC Technical Notes*, 2008.

[23] Larcher M., Simulation of the Effects of an Air Blast Wave, *JRC Technical Notes*, 2007.

[24] Mathisen K.M., Nonlinear finite element analysis, *Lecture notes in TKT 4197 at NTNU*, 2012.

[25] Morison C., The resistance of laminated glass to blast pressure loading and the coefficients of single degree of freedom analysis of laminated glass, *PhD Thesis, Cranfield University*, 2007.

[26] Norville, H., King K., Swofford J., Behavior and Strength of Laminated Glass.*Journal of Engineering Mechanics* , 124(1), 46-53, 1998.

[27] Pan B., Qian K., Xie H., Anand A., Two-dimensional digital image correlation for in-plane displacement and strain measure: a review, *Meas. Sci. Technol.* 20 062001, 2009.

[28] Peroni M., Solomos G., Pizzinato V., Larcher M., Experimental investigation of high strain-rate behaviour of glass, *Applied Mechanics and Materials*, Vol.82, 63-68, 2011.

[29] Product Information Bulletin, Saflex R series PVB Interlayer. *Architectural Technical Application Center, Saflex.*

[30] Rakvåg K.G., Combined Blast and Fragment Loading on Plates, *Master Thesis NTNU*, 2009.

[31] Sandven A.T., Blast Loaded Window Glasses, *Master Thesis NTNU*, 2009.

[32] Sewell R.G.S., Kinney G.F., Response of Structures to Blast: A New Criterion, *Annals of the New York Academy of Sciences*, 1968.

[33] Smith D.C., Glazing for injury alleviation under blast loading: United Kingdom practice, *Glass Processing Days Conference Proceedings*, 2001.

[34] Sun D., Andrieux F., Ockewitz A., Klamser H., Hogenmüller H., Modelling of the failure behavior of windscreens and component tests, *LS-DYNA Anwenderforum, Bamberg*, 2005.

[35] Timmel M., Kolling S., Osterrieder P., Du Bois P.A., A finite element model for impact simulation with laminated glass, *International Journal of Impact Engineering*, Vol.34, 1465-1478, 2007.

[36] Structures to resist the effects of accidental explosions, *Unified Facilities Criteria,* UFC 3-340-02, 2008.

[37] User Guide & Keyword Manual, IMPETUS Afea, version 3.0 beta. Downloaded from *http://manual.impetus-afea.com/solver/version/3.0b/overview*

[38] Wachtman J.B., Cannon W.R., Matthewson M.J., Mechanical Properties of Ceramics, Second edition, *Wiley*, 2009.

[39] Walpole R.E., Myers R.H., Myers S.L., Ye K., Probability & Statistics for Engineers and Scientists, eighth edition, *Pearson Prentice Hall*, 2007.

[40] Wei J., Dharani L., Response of laminated architectural glazing subjected to blast loading, *International Journal of Impact Engineering*, Vol.32, 2032-2047, 2006.

[41] Weibull W., A Statistical Theory of the Strength of Materials, *Ingenioervetenskapsakademiens Handlingar*, Vol.151, 1-45, 1939.

[42] Zhang X., Hao H., Ma G., Laboratory Test and Numerical Simulation of laminated Glass Window Vulnerability to Debris Impact,*International Journal of Impact Engineering*, Vol.55, 49-62, 2013.

A Force-displacement curves for tension test

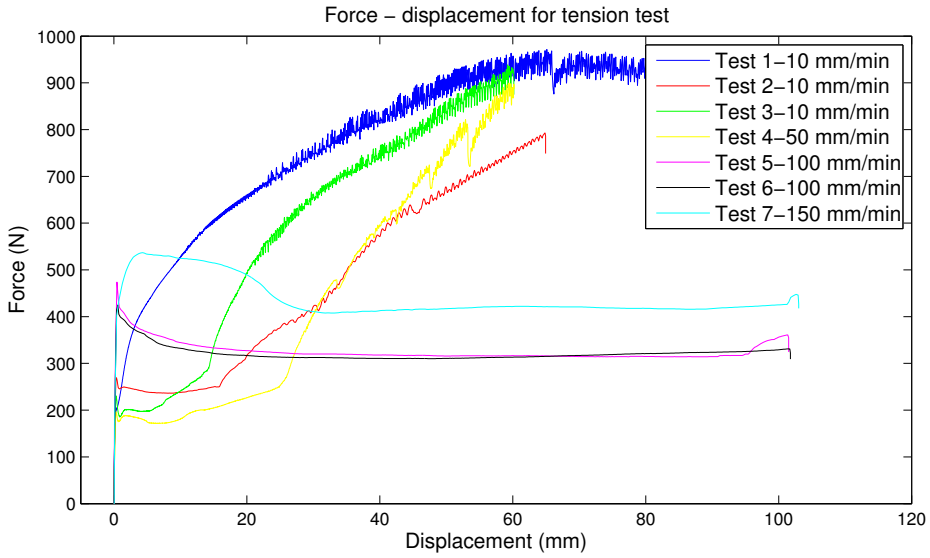

(a) *Test 1-7*

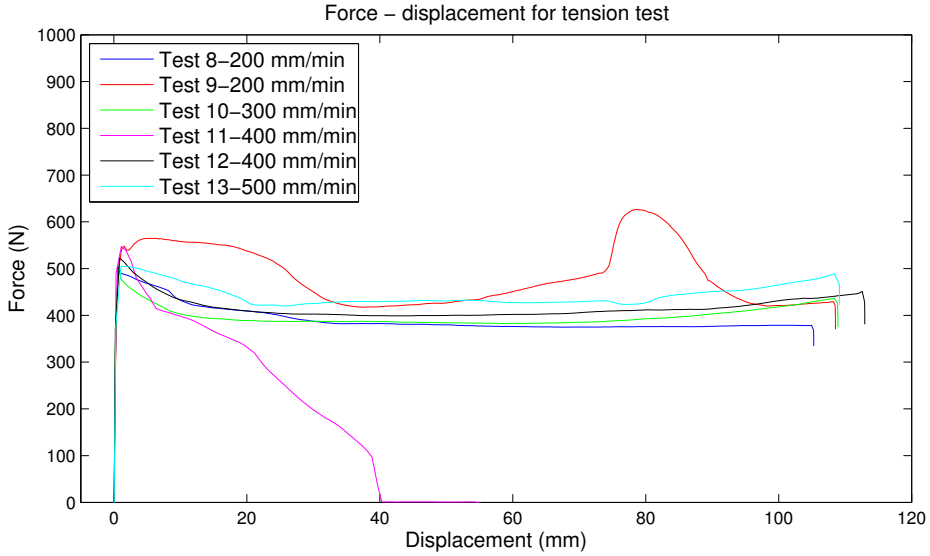

(b) *Test 8-13*

Figure 66: *All resulting force-displacement curves for tension test on precracked laminated glass. In test 11 the PVB layer tore, probably due to damage from precracking the glass.*

B Fractography, 4-point bend

Fractography on specimen number 14 was performed by Ida Westermann (SINTEF). Point of crack initiation is shown in figure 67. The initiation is likely to happen due to an inherent air bubble or a chemical impurity.

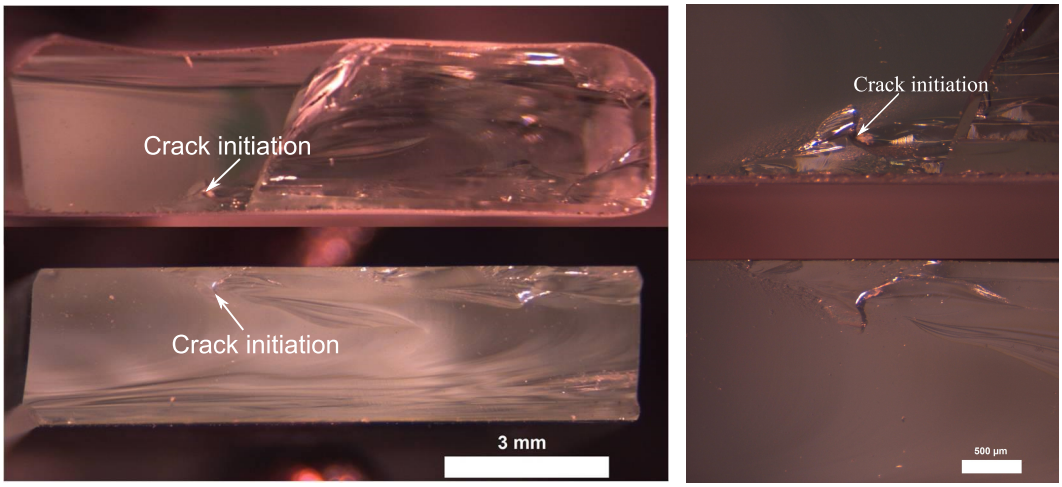

(a) (b)

Figure 67: *Crack initiation in 4-point bend sample. Specimen number 14.*

C Measured specimen dimensions

C.1 4-point bend test

Specimen	Length	Width	Thickness	Specimen	Length	Width	Thickness
1	45.93	11.15	2.86	31	45.06	10.22	2.05
2	45.93	11.11	2.87	32	44.94	9.61	2.05
3	45.93	11.50	2.86	33	45.75	11.69	2.06
4	45.93	11.15	2.86	34	45.93	11.35	2.86
5	45.93	10.85	2.05	35	45.80	11.40	2.86
6	45.93	11.05	2.06	36	45.84	11.30	2.86
7	45.72	11.65	2.86	37	45.65	11.51	2.87
8	45.93	11.08	2.86	38	45.70	11.23	2.86
9	45.91	11.72	2.86	39	45.75	11.57	2.87
10	45.46	11.45	2.86	40	45.66	11.09	2.86
11	45.56	11.60	2.86	41	45.82	11.31	2.87
12	45.72	11.28	2.86	42	45.65	11.70	2.87
13	45.85	11.22	2.86	43	45.52	11.43	2.87
14	45.82	11.24	2.86	44	45.66	11.39	2.87
15	45.78	11.52	2.86	45	45.80	11.55	2.86
16	45.65	11.42	2.86	46	45.74	11.39	2.06
17	45.68	11.26	2.86	47	45.72	11.43	2.06
18	45.68	11.24	2.86	48	45.70	11.90	2.07
19	45.70	11.48	2.86	49	45.60	11.41	2.06
20	45.77	11.40	2.86	50	45.61	11.27	2.07
21	45.72	11.40	2.86	51	45.74	11.41	2.07
22	45.56	11.14	2.86	52	45.43	11.63	2.06
23	45.73	11.22	2.86	53	45.75	11.75	2.07
24	45.65	11.80	2.87	54	45.77	11.24	2.06
25	45.73	11.32	2.86	55	45.71	11.70	2.06
26	45.81	11.41	2.86	56	45.68	11.29	2.06
27	45.68	11.28	2.86	57	45.79	11.46	2.07
28	45.78	11.43	2.86	58	45.61	11.21	2.07
29	45.79	11.30	2.86	59	45.75	11.51	2.06
30	45.91	11.55	2.86	60	45.68	11.21	2.06

Table 17: *Measured specimen dimensions for 4-point bend test, all measurements in mm.*

C.2 Tension test

		Thickness			Width precrack		
Test	Width	Glass1	PVB	Glass2	Point1	Point2	Point3
1	40.30	2.53	1.54	3.12	0.035	0.030	0.035
2	40.80	2.98	1.40	3.00	0.020	0.030	0.030
3	40.43	2.85	1.74	2.67	0.250	0.020	0.020
4	40.23	2.70	1.51	3.00	0.025	0.030	0.030
5	41.22	2.62	1.85	2.84	0.025	0.020	0.015
6	41.50	2.81	1.52	2.90	0.030	0.020	0.025
7	40.43	2.98	1.46	2.85	0.025	0.020	0.020
8	41.30	2.85	1.55	2.91	0.020	0.030	0.025
9	40.74	2.94	1.53	2.65	0.035	0.035	0.040
10	40.76	2.98	1.50	2.83	0.015	0.020	0.015
11	41.33	2.98	1.43	2.85	0.020	0.015	0.020
12	40.00	2.92	1.49	2.83	0.025	0.035	0.025
13	40.77	3.00	1.53	2.76	0.025	0.020	0.025

Table 18: *Measured specimen dimensions for tension test of precracked laminated glass. All measurements in mm. For width of precrack point 1 and 3 is close to the edge of specimen, while point 2 is in the midle of specimen.*

C.3 3-point bend test

			Thickness		
Test	Length	Width	Glass1	PVB	Glass2
1	200.11	41.36	2.83	1.48	2.97
2	200.28	40.57	2.93	1.50	2.84
3	199.16	40.32	2.85	1.54	2.86
4	199.15	40.00	2.91	1.44	2.85
5	198.68	40.86	2.84	1.54	2.88
6	198.77	40.70	2.94	1.50	2.85
7	198.67	40.56	2.90	1.37	3.00

Table 19: *Measured specimen dimensions for 3-point bend test, all measurements in mm.*

D IMPETUS Scripts

See [37] for information on how the keywords are defined.

D.1 IMPETUS script, 3-point bend

```
*PARAMETER
######################
### Set parameters ###
######################
seed=3#change distribution of initial damage
dist=1.8e-3#punch displacement
tend=15e-3#termination time
l=199e-3#specimen length
b=40.82e-3#specimen width
tglass=2.9e-3#thickness of glass
tPVB=1.37e-3#thickness of pvb
r=25.7e-3#radius of support dies
r2=16e-3#radius of punch
d=159.3e-3#distance between outer dies
nel=40#number of elements
nel_l=1#number of elements in thickness
Kc=75e4#fracture thoughness of glass
tc=1.0e-5#fracture parameter
ac=1.0#fracture parameter
s_min=58e6#min fracture stress
s_max=70e6#max fracture stress
S_0=46e6#weibull parameter
d_max=1-[%s_min]/[%s_max]#maximum damage
m=5.58#weibull parameter
############################
### Set time and output ###
############################
*TIME
[%tend]
*OUTPUT
[%tend/25], [%tend/500]
########################
### Create geometry ###
########################
*COMPONENT_BOX
"Glass tension side"
1,1,[%nel],[%nel/5],[%nel_t]
0,0,0,[%l],[%b],[%tglass]
*COMPONENT_BOX
"PVB layer"
2,2,[%nel],[%nel/5],[%nel_t]
0,0,[%tglass],[%l],[%b],[%tglass+%tPVB]
*COMPONENT_BOX
"Glass force side"
3,3,[%nel],[%nel/5],[%nel_t]
0,0,[%tglass+%tPVB],[%l],[%b],[2*%tglass+%tPVB]
*COMPONENT_CYLINDER
"die 1"
2,4,3,4
[(%l-%d1)/2],-0.001,[-%r1],[(%l-%d1)/2],[%b+0.001],[-%r1],[%r1]
*COMPONENT_CYLINDER
"punch"
3,5,3,4
[%l/2],-0.001,[%r2+2*%tglass+%tPVB],[%l/2],[%b+0.001],[%r2+2*%tglass+%tPVB],[%r2]
*COMPONENT_CYLINDER
"die 2"
5,4,3,4
[(%l-%d1)/2+%d1],-0.001,[-%r1],[(%l-%d1)/2+%d1],[%b+0.001],[-%r1],[%r1]
*CHANGE_P-ORDER
ALL,0,3
*SMOOTH_MESH
ALL,0,45
################################
### Set material parameters ###
################################
*MAT_ELASTIC
1, 2530.0, 72.0e9, 0.22, 1
*PROP_DAMAGE_BRITTLE
1,3
[%s_max],[%Kc],[%tc], [%ac]
*MAT_ELASTIC
3,1100,1.56e6,0.485
*INITIAL_DAMAGE_SURFACE_RANDOM
```

```
P, 1 , [%S_0/%s_max], [%m], [%d_max]
*INITIAL_DAMAGE_SURFACE_RANDOM
P, 3 , [%S_0/%s_max], [%m], [%d_max]
*MAT_RIGID
2,7800
*PART
"Glass 1"
1,1
"Glass 2"
3,1
"PVB"
2,3
"die"
4,2
"punch"
5,2
########################################
### Set load and boundary conditions ###
########################################
*BC_MOTION
P,4,XYZ,XYZ
*BC_MOTION
P,5,XY,XYZ
V,Z,2
*FUNCTION
2
-smooth_v([%disp],0,[%tend])
*CONTACT
1
ALL,0,ALL,0,0.1,-1e12
##########################
### Merge PVB to glass ###
##########################
*MERGE
P, 1, P, 2
*MERGE
P, 2, P, 3
*END
```

D.2 IMPETUS script, blast model

```
*PARAMETER
######################
### Set parameters ###
######################
seed          = 2                    #change distribution of initial damage
tend          = 8e-3                 #termination time
l_w           = 400e-3               #window dimension
l_f           = 400e-3               #length of frame
b_f           = 50e-3                #width of frame
t_f           = 10e-3                #thickness of frame
m_x           = 30e-3                #move glass in x
m_y           = 30e-3                #move glass plate in y
tglass        = 2.9e-3               #thickness of glass
tPVB          = 1.37e-3              #thickness of pvb
nel           = 60                   #number of solid elements
nel_rig       = 20                   #number of rigid elements
c4_length     = 130e-3               #length of charge
c4_radius     = 15e-3                #radius of charge
standoff      = 1.25                 #distance to charge
n_part        = 1e6                  #number of particels
Kc            = 75e4                 #frcture thoughness of glass
tc            = 1.0e-5               #fracture parameter
ac            = 1.0                  #fracture parameter
s_min         = 58e6                 #min fracture stress
s_max         = 115e6                #max fracture stress
S_0           = 46e6                 #weibull parameter
d_max         = 1-[%s_min]/[%s_max]  #maximum damage
m             = 5.58                 #weibull parameter
mass_c4       = 0.148
tnt_eq        = %mass_c4*1.34        # equivalent TNT charge mass
head_on_scale = 7
##########################
### Set time and output ###
##########################
*TIME
[%tend], 0, 1.0e-7
*INCLUDE
../../load_75cm.txt
*CHANGE_P-ORDER
ALL, 0, 2
```

```
*UNIT_SYSTEM
SI
#######################
### Create geometry ###
#######################
*COMPONENT_BOX
"Glass tension side"
1,1,[%nel],[%nel],1
[%m_x],[%m_y],0,[%m_x+%l_w],[%m_y+%l_w],[%tglass]
*COMPONENT_BOX
"PVB layer"
2,2,[%nel],[%nel],4
[%m_x],[%m_y],[%tglass],[%m_x+%l_w],[%m_y+%l_w],[%tglass+%tPVB]
*COMPONENT_BOX
"Glass force side"
3,3,[%nel],[%nel],1
[%m_x],[%m_y],[%tglass+%tPVB],[%m_x+%l_w],[%m_y+%l_w],[2*%tglass+%tPVB]
*COMPONENT_BOX
"Frame"
4,4,[2*%nel_rig],[%nel_rig/4],1
0,0,0,[%l_f],[%b_f],[-%t_f]
*COMPONENT_BOX
"Frame"
4,4,[%nel_rig/4],[1.5*%nel_rig],1
[%l_f-%b_f],[%b_f],0,[%l_f],[%l_f-%b_f],[-%t_f]
*COMPONENT_BOX
"Frame"
4,4,[2*%nel_rig],[%nel_rig/4],1
0,[%l_f-%b_f],0,[%l_f],[%l_f],[-%t_f]
*COMPONENT_BOX
"Frame"
4,4,[%nel_rig/4],[1.5*%nel_rig],1
0,[%b_f],0,[%b_f],[%l_f-%b_f],[-%t_f]
*COMPONENT_BOX
"Frame"
5,5,[2*%nel_rig],[%nel_rig/4],1
0,0,[2*%tglass+%tPVB],[%l_f],[%b_f],[2*%tglass+%tPVB+%t_f]
*COMPONENT_BOX
"Frame"
5,5,[%nel_rig/4],[1.5*%nel_rig],1
[%l_f-%b_f],[%b_f],[2*%tglass+%tPVB],[%l_f],[%l_f-%b_f],[2*%tglass+%tPVB+%t_f]
*COMPONENT_BOX
"Frame"
5,5,[2*%nel_rig],[%nel_rig/4],1
0,[%l_f-%b_f],[2*%tglass+%tPVB],[%l_f],[%l_f],[2*%tglass+%tPVB+%t_f]
*COMPONENT_BOX
"Frame"
5,5,[%nel_rig/4],[1.5*%nel_rig],1
0,[%b_f],[2*%tglass+%tPVB],[%b_f],[%l_f-%b_f],[2*%tglass+%tPVB+%t_f]
*MERGE_DUPLICATED_NODES
P, 2, P, 1, 1.0e-5
P, 2, P, 3, 1.0e-5
P, 4, P, 4, 1.0e-5
P, 5, P, 5, 1.0e-5
##############################
### Set material parameters ###
##############################
*MAT_ELASTIC
1, 2530.0, 72.0e9, 0.22, 1
*PROP_DAMAGE_BRITTLE
1, 3, 1
[%s_max], [%Kc], [%tc], [%ac]
*MAT_JC
3, 1100, 0.53e9, 0.485, 3
6.72e6, 10.6e6, 0.303, 0.248
*PROP_DAMAGE_CL
3, 3, 1
1.0e9
*INITIAL_DAMAGE_SURFACE_RANDOM
P, 1, [%S_0/%s_max], [%m], [%d_max]
*INITIAL_DAMAGE_SURFACE_RANDOM
P, 3, [%S_0/%s_max], [%m], [%d_max]
*MAT_RIGID
2, 7800
*PART
"Glass 1"
1, 1
"Glass 2"
3, 1
"PVB"
2, 3
"Frame 1"
4, 2
"Frame 2"
5, 2
#######################################
### Set load and boundary conditions ###
```

```
128 ######################################
129 *BC_MOTION
130 P, 4, XYZ, XYZ
131 *BC_MOTION
132 P, 5, XYZ, XYZ
133 ############################
134 ### Merge glass to frame ###
135 ############################
136 *MERGE
137 P, 1, P, 4, 1.0e-4
138 *MERGE
139 P, 3, P, 5, 1.0e-4
140 *LOAD_PRESSURE
141 ALL, 0, 1, 0, 0, 0, 1
142 *COORDINATE_SYSTEM_FIXED
143 1, [%l_f/2], [%b_f/2], [%standoff]
144 *END
```

E MATLAB Scripts

E.1 Processing of 4-point bend test data

```
% Script processing data from material test on glass
% 4-point bend test method. Unites used: m, N.
clear all; close all
%%%%%%%%%%%%%%%
%%%Load data%%%
%%%%%%%%%%%%%%%
% Data arranged  Force_test1 (N), disp_test1 (mm), force_test2(N), disp_test2(mm) .....
test=textread('glasstest.txt');
n=size(test);
w=286.8e-3; %Weight of upper fixture (kg)
test(:,1:2:end)=test(:,1:2:end)+w*9.81;
% Set dimension vectors
b=[11.15 11.11 11.5 11.15 10.85 11.05 11.65 11.08 11.72 11.45...
    11.6 11.28 11.22 11.24 11.52 11.42 11.26 11.24 11.48 11.40...
    11.4 11.14 11.22 11.8 11.32 11.41 11.28 11.43 11.3 11.55...
    10.22 9.61 11.69 11.35 11.40 11.3 11.51 11.23 11.57 11.09...
    11.31 11.7 11.43 11.39 11.55 11.39 11.43 11.9 11.41 11.27...
    11.41 11.63 11.75 11.24 11.70 11.29 11.46 11.21 11.51 11.21]*1e-3;

d=[2.86 2.87 2.86 2.86 2.05 2.06 2.86 2.86 2.86 2.86...
   2.86 2.86 2.86 2.86 2.86 2.86 2.86 2.86 2.86 2.86...
   2.86 2.86 2.86 2.87 2.86 2.86 2.86 2.86 2.86 2.86...
   2.05 2.05 2.06 2.86 2.86 2.86 2.87 2.86 2.87 2.86...
   2.87 2.87 2.87 2.87 2.86 2.06 2.06 2.07 2.06 2.07...
   2.07 2.06 2.07 2.06 2.06  2.06 2.07 2.07 2.06 2.06
   ]*1e-3;

l=[46 46 46 46 46 46 45.72 45.93 45.91 45.46...
    45.56 45.72 45.85 45.82 45.78 45.65 45.68 45.68 45.70 45.77...
    45.72 45.56 45.73 45.65 45.73 45.81 45.68 45.78 45.79 45.91...
    45.06 44.94 45.75 45.93 45.80 45.84 45.65 45.70 45.75 45.66...
    45.82 45.65 45.52 45.66 45.80 45.74 45.72 45.70 45.60 45.61...
    45.74 45.43 45.75 45.77 45.71 45.68 45.79 45.61 45.75 45.68]*1e-3;

L=39.98*1e-3; %Outer span
%%%%%%%%%%%%%%%%%%%%%%%%%%%%%%%%%
%%%Find max force and plot F-D%%%
%%%%%%%%%%%%%%%%%%%%%%%%%%%%%%%%%
%%
[f_max I]=max(test(:,1:2:end));
for i=1:length(f_max);
d_f_max(i)=test(I(i),2*i);
end
 figure(1)
 hold on
for i=1:n(2)/2
if d(i)>2.5e-3
 p1=plot(test(1:I(i),2*i),test(1:I(i),2*i-1));
elseif d(i)<2.5e-3
    p2=plot(test(1:I(i),2*i),test(1:I(i),2*i-1),'r');
end
end
 p3=plot(d_f_max,f_max,'ko');
axis([0 2.55e-4 0.5 400])
 legend([p1 p2 p3],'Thick specimens','Thin specimens'...
     ,'Fracture point','Location','NorthWest')
 set(gcf,'position',[507 346 956 437])
set(findobj(gcf,'Type','text'),'FontSize',12)
 xlabel('Displacement (m)'); ylabel('Force (N)');
title('Force - Displacement 4-point bend 60 tests')
%%%%%%%%%%%%%%%%%%%%%%%%%%%%%%%%%
%%%Calculate E, stress and strain%%%
%%%%%%%%%%%%%%%%%%%%%%%%%%%%%%%%%

%%
p=0.4; % Percent of data points not used for calculation of E
figure(2)
hold on
for i=1:n(2)/2 % Slipte stykker, ruller i ytre posisjon
E(i)=((11/64)*L^3/((d(i)^3)*b(i)))*...
((test(ceil(I(i)*(1-p/2)),2*i-1)-test(ceil(1+I(i)*p/2),2*i-1))...
/(test(ceil(I(i)*(1-p/2)),2*i)-test(ceil(1+I(i)*p/2),2*i)));
s(:,i)=3*L*test(:,2*i-1)/(4*b(i)*(d(i))^2); %Stress
e(:,i)=s(:,i)/E(i); %Strain
if d(i)>2.5e-3
p1=plot(e(1:I(i),i),s(1:I(i),i),'b');
elseif d(i)<2.5e-3
p2=plot(e(1:I(i),i),s(1:I(i),i),'r');
```

```
end
end
xlabel('Strain'); ylabel('Stress (MPa)');
title('Stress - Strain plot');
legend([p1 p2],'Thick specimens', 'Thin specimens')
%%%%%%%%%%%%%%%%%%%%%%%%%%%%%%
%%%Do weibull calculations%%%
%%%%%%%%%%%%%%%%%%%%%%%%%%%%%%
%%
use_test=[7:14 16 19:30 34:45]; %33 tests, 2.87 mm, grind edges
n_wei=size(use_test);

%Preallocate:
s_max_wei=zeros(n_wei); E_wei=zeros(n_wei); d_wei=zeros(n_wei);
b_wei=zeros(n_wei); f_max_wei=zeros(n_wei); d_f_max_wei=zeros(n_wei);

for i=1:n_wei(2);
s_max_wei(i)=s_max(use_test(i));
E_wei(i)=E(use_test(i));
d_wei(i)=d(use_test(i));
b_wei(i)=b(use_test(i));
f_max_wei(i)=f_max(use_test(i));
d_f_max_wei(i)=d_f_max(use_test(i));
end

log_s_max_wei=log(s_max_wei);
[log_s_max_wei ix]=sort(log_s_max_wei);
pf=zeros(n_wei);
    for i=1:n_wei(2)
        pf(i)=(i-0.5)/n_wei(2);
    end
    figure(8)
    log_pf=log((log(1./(1-pf))));
    loglog(log_s_max_wei,log_pf,'x')
  p1 = 5.5813;
  p2 = -102.24;
  y=p1*log_s_max_wei+p2;
  loglog([17.8 18.7],[-2.893 2.13],'r')
  xlabel('ln(\sigma_{max})','FontSize',12);
  ylabel('ln(ln($\frac{1}{1-p_f}$))','interpreter','latex','fontsize',12);
  legend('Experiment values','Linear estimate','Location','NorthWest')
  title('Linear regression - weibull estimate','FontSize',12)

A=2*L*(mean(d_wei)+mean(b_wei));
s_area_indep=s_null*(L*((mean(d_wei)/m+1)+mean(b_wei))...
    *((0.5*m+1)/(m+1)))^(1/m);

%%%%%%%%%%%%%%%%%%%%%%%%%%%%%%
%%% Weibull comparison plot %%%
%%%%%%%%%%%%%%%%%%%%%%%%%%%%%%
%%
x=[50e6:0.01e6:120e6];
bin=10;
figure(15)
hold on
%Make density funciton
f=zeros(length(x),length(m));
for i=1:length(x)
    for j=1:length(m)
    f(i,j)=((m(j)/s_null)*(x(i)/s_null)^(m(j)-1)*exp(-(x(i)/s_null)^m(j)));
    end
end
[func,bin]=hist(s_max_wei,bin);
bar(bin,func/trapz(bin,func));
plot(x,f,'r','LineWidth',2)
ylabel('f(\sigma_f)','FontSize',12); xlabel('\sigma_f (Pa)','FontSize',12);
title('Probability density function - weibull theory vs experiment','FontSize',12)
legend('Experimental results','m=5.58','Location','NorthEast');


%Cumulative distribution function
figure(17)
cdfplot(s_max_wei);
m2=3;
for i=1:length(x)
    for j=1:length(m)
    F(i,j)=1-exp(-(x(i)/s_null)^m(j));
    end
end
for i=1:length(x)
    for j=1:length(m2)
    F2(i,j)=1-exp(-(x(i)/s_null)^m2(j));
    end
end
plot(x,F,'r','LineWidth',2)
hold on
plot(x,F2,'g','LineWidth',2)
```

```
166 ylabel('F(\sigma_f)','FontSize',12);
167 xlabel('\sigma_f (Pa)','FontSize',12);
168 title('Cumulative distribution — weibull theory vs experiment','FontSize',12)
169 legend('Experimental results','m=5.58','Location','NorthWest');
```